# AN ABSTRACT OF THE THESIS OF

Suhail Alhejji for the degree of Master of Science in Geology presented on June 3, 2019.

Title: Timing and Composition of Volcanism at Harrat Ithnayn, Western Saudi Arabia.

Abstract approved: _____

Adam J.R. Kent

Western Saudi Arabia hosts a number of young volcanic fields, known as “Harrats”. Harrats cover a significant proportion of western Saudi Arabia and are associated with significant volcanic hazards. However, the ultimate cause of volcanic activity remains unclear. Younger volcanism (<12 Ma) is clearly represented by the north-south-trending region known as the Makkah-Madinah-Nafud (MMN) line, which consists of three moderate sized volcanic fields: Harrat Rahat, Harrat Khaybar, and Harrat Ithnayn. Harrat Ithnayn is the northern-most and the least studied volcanic field of the MMN line, and it has been suggested that Ithnayn represents the youngest field produced by age progressive volcanism along the MMN line. Harrat Ithnayn is thus a critical piece in the puzzle in determining the causes of the volcanic activity in the MMN line region. This research focuses primarily on investigating the age and composition of the volcanic activity at Harrat Ithnayn and how it changes through time. I apply geochronological, geochemical, and petrological methods to understand the origin and tectonic controls on volcanism in this region.

I report new age determinations on 10 lava flows, one sample from the northern part of Harrat Khaybar and 9 samples from Harrat Ithnayn, by the $^{40}Ar$-$^{39}Ar$ laser step heating method. All ages are younger than 2 Ma and most of these lavas range in age between ~500 and 120 Ka. These ages constrain the timing and chemical variations of volcanic activity at Harrat Ithnayn.

Unlike older Harrats Rahat and Khaybar, the volcanism at Harrat Ithnayn has also undergone less magmatic evolution, suggesting a lack of shallow crustal magma bodies. Similar to Harrat Hutaymah and other younger volcanic fields peripheral to the MMN line, olivine ± clinopyroxene dominated crystal fractionation at a range of upper mantle and crustal pressures, with some evidence of crustal assimilation. The new age constraints agree with the hypothesis of south-to-north volcanic progression of volcanism along the MMN line. In addition, active mantle upwelling, decompression melting and possible asthenospheric flow from the Afar mantle plume, appears to have been the source of this volcanic activity, produced from ~ 2-14% partial melting of a shallow garnet peridotite mantle source for magmas.

# Timing and Composition of Volcanism at Harrat Ithnayn, Western Saudi Arabia

by
Suhail Alhejji

A THESIS

submitted to

Oregon State University

in partial fulfillment of
the requirements for the
degree of

Master of Science

Presented June 3, 2019
Commencement June 2019

Master of Science thesis of Suhail Alhejji presented on June 3, 2019

APPROVED:

Major Professor, representing the Geology

Dean of College of Earth, Ocean, and Atmospheric Sciences

Dean of the Graduate School

I understand that my thesis will become part of the permanent collection of Oregon State University libraries. My signature below authorizes release of my thesis to any reader upon request.

Suhail Alhejji, Author

# ACKNOWLEDGEMENTS

I would first like to express my sincere thanks to my major professor advisor Dr. Adam Kent for his great support and help throughout my master's degree journey. I would also like to thank my committee members, Dr. Robert Duncan, Dr. David Graham, and Dr. Clare Reimers for their encouragement and guidance. My sincere thanks also go to Dr. Abdullah Al-Amri for his helpful academic advising and funding a part of the fieldwork expanse. I also greatly thank the Saudi Arabian Cultural Mission (SACM) for the fully funding of my graduate school expanses. I am grateful to the National Science Foundation (NSF) and King Abdulaziz City for Science and Technology (KACST) for supporting this research. Also, I would like to thank King Saud University (KSU) and the Saudi Society for Geosciences (SSG) for funding a major part of the fieldwork expense. I thank Dr. Victor Camp for kindly providing the geochemical data of lavas from Harrat Ithnayn, Dr. Dan Miggins provided valuable assistance with $^{40}Ar$-$^{39}Ar$ age analysis, Dr. Saeed Al-Shaltoni for his field assistance, Mr. Mufleh Aldossari for his valuable academic advising and his assistance in shipping the rock samples from Saudi Arabia to OSU. Last but not least, my special thanks to my parents, my wife, and my friends for being there when I need them and their support throughout this experience.

TABLE OF CONTENTS

TABLE OF CONTENTS (Continued)

Page

# LIST OF FIGURES

Figure Page

# LIST OF TABLES

# LIST OF APPENDICES

# LIST OF APPENDIX FIGURES

Figure Page

# LIST OF APPENDIX TABLES

## 1- Introduction:

Volcanic lava fields, locally known as Harrats, cover a large area (about 180,000 km$^2$) in the western part of the Arabian plate. Half of these Harrats, ~90,000 km$^2$, occur in Saudi Arabia. The Arabian Harrats are Oligocene (>30 Ma) to Recent intra-continental basaltic volcanic fields constructed on the stable Precambrian Arabian Shield and are the only volcanism within the Arabian plate that remains potentially active. Volcanism at the Arabian Harrats can be divided into two distinct phases. Camp and Roobol (1992) classified the volcanism in western Arabia into two phases of volcanic activity based on the geochemical and geochronological evidence that was available at that time. This classification of western Arabian volcanism still exists, but it has also been further developed since the time of publication due to improvement in the geophysical and geochemical constraints (e.g. Hansen et al., 2006; Pik et al., 2006; Daradich et al., 2003). Volcanism in Western Arabia started in the Oligocene, about 30 million years ago, and continued for 10 million years, followed by a quiescent period (Camp and Roobol, 1992; Ilani et al., 2001). This lack of volcanism lasted for 7 million years, then volcanic activity started again about 12 million years ago and has continued up to the present (Camp and Roobol, 1992). The two periods of volcanic activity are associated with different styles of volcanism.

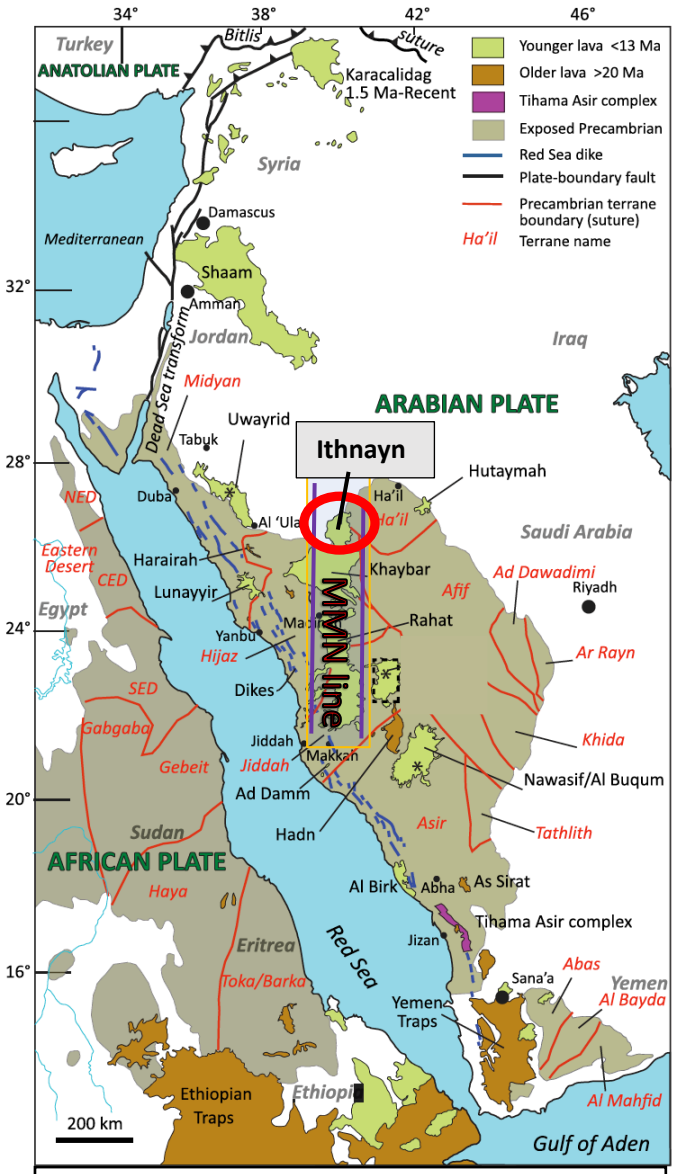


Figure 1: this map illustrates the western volcanism in western Arabia, the dark brown color indicates the older volcanism while the light the green shows the younger volcanism. (modified after Ahmed et al, 2016)

The older phase of volcanism is concentrated in the southwest of the Arabian plate and has a structural trend defined by dike orientations that is parallel to the Red Sea, in the NW-SE direction (fig.1).

The early volcanism (30 - 20 Ma) includes relatively small volcanic fields, which are Harrats Uwaynd, Hadan, Sirat, Harairah and Ishara in Saudi Arabia, and Yemen Traps in the northwest part of the Republic of Yemen (Coleman et al., 1983; Chandarasekharam et al., 2014). These Harrats produced lavas that compositionally are tholeiitic (quartz-normative) to transitional (nepheline-normative and hypersthene-normative) basalts (Camp and Roobol, 1992; Konrad et al., 2016). The volcanism in that period is attributed to a passive mantle upwelling associated with crustal extension during the opening of the Red Sea (Camp and Roobol, 1992). Interestingly, the opposite side of the Red Sea, eastern Egypt and Sudan, does not show evidence of an equivalent distribution and volume of volcanism during this period of Africa-Arabia separation (Bohannon et al., 1989; Duncan et al., 2016).

The younger phase of western Arabia volcanism (> 12 Ma) has erupted more lavas and formed a larger number of volcanic fields (Harrats Rahat, Kura, Khaybar, Ithnayn, Lunayyir, Hutaymah, and Kishb) (Coleman et al., 1983; Camp et al., 1991). The volcanism in this phase started 12 million years ago, and produced harrats that have a north-south trend, creating the linear volcanic vent system, called the Makkah-Madinah-Nufud (MMN) volcanic line (Camp and Roobol, 1992). A number of historical volcanic events have occurred during this phase. Camp et al. (1987) determined that approximately twenty-one volcanic eruptions occurred in western Arabia during the past 1500 years, including eruptions of Harrat Lunayyir (1000 AD), Khaybar (650 AD), Rahat (1256 AD, known as the Madinah eruption), and an uncertain volcanic eruption at Harrat Ithnayn (1800 AD) (Coleman et al., 1983; Camp et al., 1987; Camp et al., 1991; Chandarasekharam et al., 2014). The latest activity in western Arabia happened in the period between April and June of 2009, at Harrat Lunayyir. There were no lavas erupted, but a swarm of about 30,000 earthquakes have been attributed to intrusion of magma along a

north-south dike that rose to approximately 1-2 km depth beneath the volcanic field (Pallister et al., 2010).

Compositionally, this phase has generated transitional to strongly alkali basaltic rocks (Camp and Roobol, 1992; Konrad et al., 2016). Camp and Roobol (1992) attribute the younger volcanism in western Arabia to an active mantle upwelling, but the cause of this mantle upwelling is still unknown. Evidence of mantle upwelling in the younger phase of volcanism is seen clearly in those volcanic fields that are located along the MMN volcanic line, where these magmas are generated by a high degree of partial melting, at a shallower depth of source melting, but Harrats from the same age and located to the east or the west of the MMN line do not show the same shallow magmatic sources (Camp and Roobol, 1992). Konrad et al. (2016) summarized the three possible models for the mantle upwelling during the younger phase of volcanism: 1) Reactivation of old "fossilized" mantle plume materials beneath the lithosphere of western Arabia (Stein and Hofmann, 1992); 2) West-East extensional thinning of the lithosphere causing decompression melting and mantle upwelling (Bertrand et al., 2003; Moufti et al., 2012; Shaw et al., 2003); 3) Mantle plume material coming from the Afar mantle plume in East Africa through sub-lithospheric channels beneath the Arabian plate (Chang and Van der Lee, 2011). It is possible that one or more of these models combined caused what it is now called the younger phase of volcanism. In my point of view, the best model is the model that can explain the age progressive nature of volcanism along that MMN line.

Harrat Ithnayn is the northernmost volcanic field in the MMN line, and the least studied. This research primarily focuses on investigating the timing and erupted compositions of the volcanic activity at Harrat Ithnayn. I apply geochronological, geochemical, and petrological methods to understand the origin and tectonic controls on volcanism in this region. Harrat Ithnayn represents the most recent episode of the northern progression of volcanism along the MMN line. Volcanism started from Harrat Rahat (> 10 Ma), then moved to Harrat Khaybar (> 6 Ma), finally beginning at Harrat Ithnayn (> 2 Ma) (Camp and Roobol, 1991; Camp and Roobol,1992; Shaw et al., 2004, etc.). The lavas

of the volcanic field of Harrat Ithnayn cover an area of about 4,000 $km^2$ with thickness average of about 50 m (Roobol and Camp, 1991a). These lavas lie in part on the older lavas erupted from the northern portion of Harrat Khaybar just to the south. They also buried part of the older rocks of the Arabian-Nubian Shield (ANS) beneath "Hijaz and Afif terranes, ~700 – 800 Ma" (Roobol and Camp, 1991a; McGuire and Stern, 1993). Although the north-south trend of the MMN line includes Harrat Ithnayn, it has also been noticed that there are distinct morphological differences between Ithnayn and the other harrats central to the MMN line. The vents on Harrat Ithnayn are more scattered than what it is found on Khaybar and Rahat (Camp et al., 1991) which occur as relatively thick sequences of bedded lavas, with younger volcanic edifices on the surface. In contrast, Harrat Ithnayn shows morphological and compositional evidence that resemble peripheral harrats of MMN line (e.g. Hutaymah and Lunayyir).

Comparing the geochemical and geochronological results at Harrat Ithnayn with the available data on the other volcanic fields on the MMN axial line, Harrat Rahat and Harrat Khaybar, helps us to construct a model of melting processes in the underlying lithospheric mantle. In particular, the major and trace element compositional data provide insights into whether regional crustal thinning played a major role in the magmatic processes which led to these lavas being erupted. Harrats Rahat and Khaybar have experienced magmatic differentiation processes and their volcanic production changed in the latest volcanic activity of their lifespan (Camp and Roobol, 1989; Camp et al., 1991). However, the volcanism at Harrat Ithnayn appears to represent magmas that have undergone less magmatic differentiation. I investigate this issue further with new geochemical data to constrain the magmatic processes that resulted in the compositions of these lava flows and how these processes evolved through time. Understanding the timing and composition of volcanism at Harrat Ithnayn is a critical piece in the puzzle to determine the causes of the volcanic activity in the MMN line region. In addition, the three volcanic lava fields on the axis of the MMN line are located near cities with relatively high populations and high cultural and religious significance. Therefore, understanding the causes of

volcanism in this region can provide insight into the timing and scale of volcanic hazards along the MMN line.

Previous work has defined the stratigraphy of Harrat Ithnayn. The geologic map of Roobol and Camp (1991a), the most recent geologic map of the area, used an integrated volcanic stratigraphic classification for both Khaybar and Ithnayn. They divided the stratigraphy of Harrats Khaybar and Ithnayn into four main volcanic units, from the oldest to the youngest: Kura, Jarad, Mukrash, and Abyad Basalts, respectively (Roobol and Camp a, 1991). Each of these units was divided into subunits. The older two units, Kura and Jarad Basalts are not found at Harrat Ithnayn. Disconformities among these units were determined using the false-color band of LandSat imagery, degree of surface erosion, and field observations (Roobol and Camp, 1991a). Prior to this work there were no published radiometric dates (K/Ar and/or $^{40}$Ar-$^{39}$Ar methods) for Harrat Ithnayn lavas; all stratigraphic ages are based on numbers of K-Ar isotopic age determinations for units that was taken place exclusively at Harrat Khaybar, then Camp and Roobol (1991) applied the integrated stratigraphy to infer ages of Harrat Ithnayn lavas. Also, defining the ages of Harrat Ithnayn is largely based on morphologic criteria: flow erosion, weathering and dust-pond development. Based on this evidence, relatively young lavas flows are present, including some flows with surface textures equivalent to post-Neolithic lavas, but there are no clearly historic flows that have the distinct unweathered appearance and lack of dust ponds. Geochronological results, using the technique of $^{40}$Ar-$^{39}$Ar age incremental heating determinations, provide an important temporal framework for geochemical data, allowing us to evaluate changes in magmatic processes at Harrat Ithnayn through time.

One of the most accepted interpretations of the cause of active mantle upwelling in the younger phase of volcanism in western Arabia is the influence of the Afar mantle plume. It has been thought that the upwelling of the Afar plume from depth causes the regional west-east crustal extension by generating uplift and extensional tectonic stress (Konrad et al., 2016). Also, the counterclockwise toroidal motion of the large-scale region of Arabia-Anatolia-Aegean (AAA) region may be caused by

the Afar plume upwelling to the south, asthenospheric flow beneath the Arabia plate, coupled with a slab pull to the north beneath the Aegean area (Faccenna et al., 2013). The possible presence of the Afar mantle plume material has been identified by the anomalous low seismic velocity channels within the upper mantle beneath western Arabia (Chang and Van der Lee, 2011). *However, there is no consensus on how the Afar plume influences the younger phase of volcanism geochemically.* Therefore, the use of helium isotopes and trace element ratios is suggested because they are one of the best tools that indicate deep mantle plume sources, and the Afar plume is distinguished by its high values of $^{3}He/^{4}He$, as high as $21R_A$ (Stuart, 2013; Konrad et al., 2016). Elevated values of $^{3}He/^{4}He$ have been found in Harrat Rahat (Murcia et al.,2013) and the Kura formation of Harrat Khaybar (Kent et al., unpublished), signaling Afar plume influence, but more study of rocks from the other harrats is needed.

**1.1 Regional Background:**

Understanding the modern volcanism in western Saudi Arabia requires knowledge of the plate tectonic evolution of the region. About 25 million years ago, the Arabian plate separated from the African plate, accelerating the closing the Tethys Sea to the northeast of the new tectonic plate (Stern and Johnson, 2010). This resulted in the opening of the Red Sea and the Gulf of Aden to the west and the south, respectively. On the other side of the Arabian plate, continent-continent collision between the Arabian plate and the Eurasian plate produced the Zagros Mountain fold belt (Johnson and Stern, 2010). The Arabian plate has been rotated counterclockwise due to the toroidal mantle flow

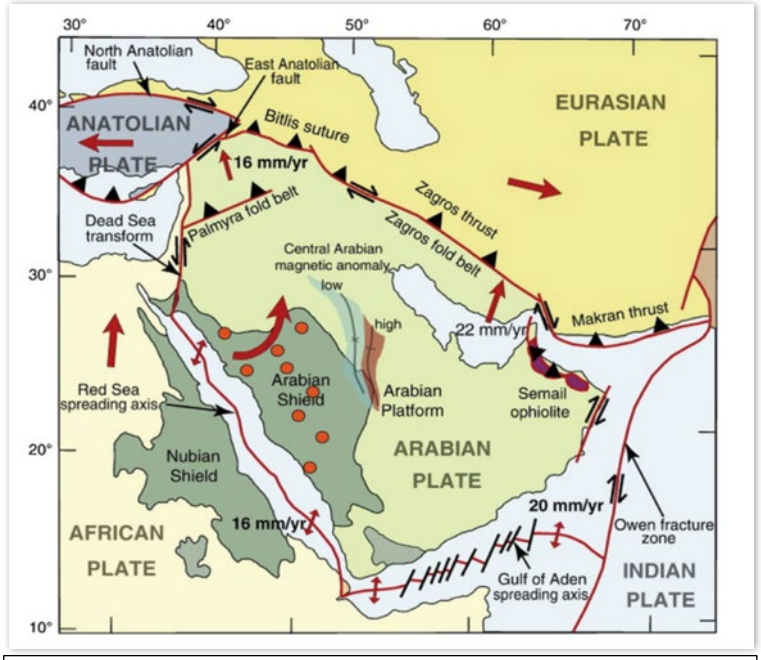


Figure 2: The geologic and tectonic setting of the Arabian plate. The red dots represent the distribution of the Arabian Harrats (modified from: Stern and Johnson, 2010).

and the role of slab rollback (fig.1) (Coleman et al., 1983; Reilinger and McClusky, 2011; Faccenna et al., 2013).

The geology of the Arabian plate is divided into three main geological units: The Arabian-Nubian Shield (the basement rocks), the Arabian Shelf or Platform (the sedimentary formations), and the Arabian Harrats (the Cenozoic intra-plate volcanism) (Fig.1). The Arabian-Nubian Shield (ANS) is exposed on the west side of the Arabian plate, and the other two thirds of the plate is covered by the Cambrian to Holocene sedimentary formations of the Arabian Platform. About fifteen volcanic fields of the Arabian Harrats lie on the top of the Precambrian basement of ANS and cover an area of about 180,000 $km^2$ (Coleman et al., 1983). Half of this volcanism occurs in Saudi Arabia, about 90,000 $km^2$ (Coleman et al., 1983; Camp and Roobol, 1991). The volcanism in western Arabia has been divided into two distinct phases (Camp and Roobol, 1992; Shaw et al., 2004). Each of these phases is characterized by its volcanic compositions, tectonic origin, and spatial and temporal extent of volcanic activity.

**1.2 Makkah-Madinah-Nufud (MMN) line volcanism:**

The north-south-trending region known as the Makkah-Madinah-Nafud (MMN) line is a linear volcanic vent system that extends 600 kilometers (Camp and Roobol, 1989; Roobol and Camp, 1991a). The MMN line consists of three moderate to large sized volcanic fields: Harrat Rahat, Harrat Khaybar, and Harrat Ithnayn. Total area of volcanic exposure and estimated volume of volcanism of these three Harrats are summarized in (Table 1). This shows that how Harrat Ithnayn is a much smaller volcanic field compared to the other harrats of the MMN line (e.g. Rahat, and Khaybar). These numbers are based on previous work done by Camp and Roobol (1989), Camp et al. (1991), and Mufti et al. (2013). Camp et al. (1991) include only the basalt vents and flows of Kura that are exposed at the southern part of Harrat Khaybar in the estimated area of Khaybar, but the rest of the Kura formation was treated as a separate lava field, not as the oldest unit of Harrat Khaybar. Harrat Rahat has been studied extensively (e.g. Camp et al., 1987; Camp and Roobol, 1989; Moufti et al., 2013; Murcia et al., 2015,

2017; Downs et al., 2018), and there are a couple of ongoing studies of Harrat Khaybar (Kent et al., in preparation). However, the northern-most volcanic field at MMN axis line, Harrat Ithnayn, has not been studied in detail, although it is a critical piece of the puzzle in understanding the volcanism in this region.

Table 1: The estimated area and volume of volcanism in MMN volcanic fields. (Camp et al., 1991)

| **Harrat** | **Area of Exposure ($km^2$)** | **Average Thickness (m)** | **Estimated Volume ($km^3$)** |
|---|---|---|---|
| **Rahat** | 19,830 | 100 | 2,000 |
| **Khaybar*** | 14,064 | 100 | 1,400 |
| **Ithnayn** | 4,000 | 50 | 200 |

The MMN line is defined by a north-south trend of volcanic fields and vent alignments. The volcanic lava field of Harrat Rahat to the south is the oldest and largest volcanic field of the three (fig.3). Harrat Rahat is divided into three main stratigraphic units: the oldest unit is Shawahit (10 – 2.5 Ma), then Hammah (2.5 – 1.7 Ma), and Madinah (1.7 Ma – Present) (Camp and Roobol, 1989; Moufti et al., 2010). These units can be easily identified on aerial photographs because they are not substantially eroded (Camp and Roobol, 1989). *The oldest unit is located in the south and the youngest unit occupied the northernmost of Harrat Rahat (Fig. 3)*. Some volcanologists (e.g. Moufti et al., 2010 and Murcia et al., 2015) suggest that the Madinah unit is a separate volcanic field; however, others (e.g. Camp and Roobol, 1989; Murcia et al., 2017; Downs et al., 2018) keep the three units together based on their petrologic similarity. Harrat Rahat also contains more than 644 scoria and other pyroclastic cones and experienced two recent volcanic eruptions at 641 AD and 1256 AD (Camp and Roobol, 1989). The rock compositions of this volcanic field have a wider compositional range from

alkali-basalt to phonolite and trachyte, exclusively in the Madinah unit (Fig. 4). The tectonic discrimination plot of Cabanis and Lecolle (1991) "La/10, Nb/8, and Y/15" exhibits a typical continental basaltic composition (Murcia et al., 2016, 2017; Downs et al., 2018). The first period of volcanism at Rahat (10-2.5 Ma), which produced about 70 % of the lavas, generated the least differentiated rocks due to the short crustal residence time, whereas the most recent two periods of volcanism (< 2.5 Ma) exhibit heterogeneous lava compositions as a result of magmas that have undergone mixing and longer periods of fractional crystallization within the crust (Camp and Roobol, 1989; Murcia et al., 2017).

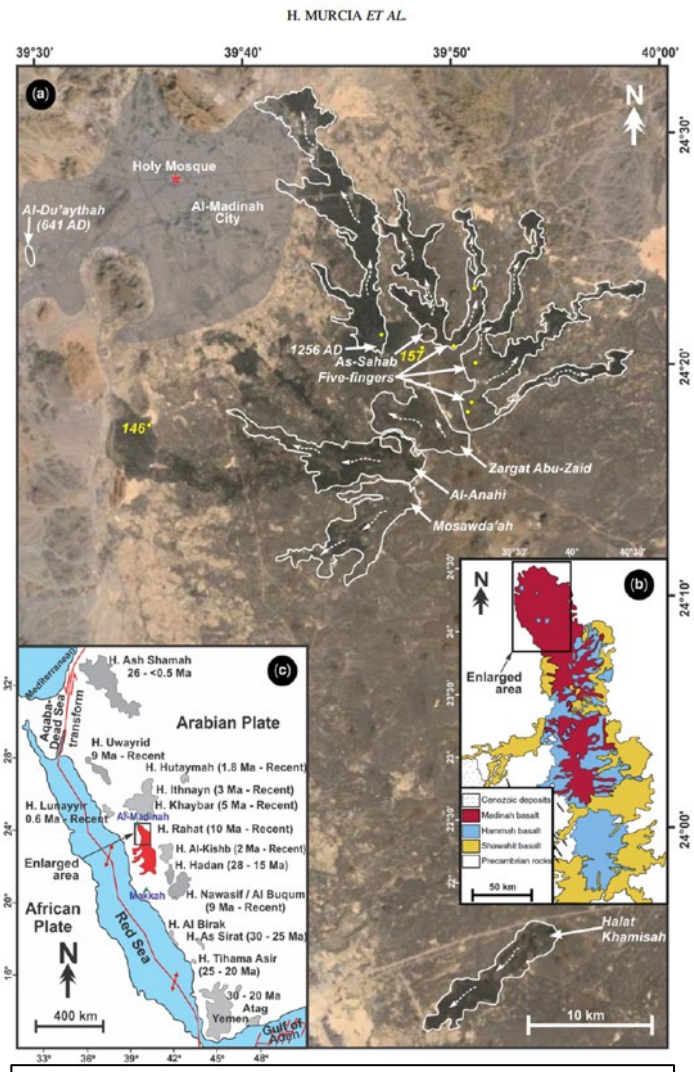


Figure 3: (A) Distribution of youngest volcanic units of the Madinah unit with flow direction shown in dashed white arrows in white-bordered lavas (B) map for Harrat Rahat, the red unit is Madinah unit. (C) ages and distributions of the Arabian harrats. Harrat Rahat follows the N-S trend (from: Murcia et al., 2017).

Harrats Khaybar and Ithnayn together form the largest volcanic lava province in the Arabian Peninsula, covering an area of about 2,500 $km^2$ and have produced a huge volume of volcanic materials of about 1,850 $km^3$, including the earliest stage of Kura formation (Camp et al., 1991; Kent et al., in progress). More than 326 scoria cones and 45 shield volcanic cones have been identified in the two harrats (Camp et al., 1991). The range of ages in these harrats is relatively wide from Pliocene (~ 10 Ma) to Recent (Camp et al., 1991). Based on previous K-Ar age determinations, the volcanism at Harrat Khaybar started > 5 million years ago, while the volcanism at Harrat Ithnayn began later, approximately 3 million years ago (Camp et al., 1991). Stratigraphically, these integrated two harrats

are constituted of four stratigraphic volcanic units, which are from oldest to youngest are: Kura (> 5 Ma), Jarad (5-3 Ma), occurring only in Harrat Khaybar, Mukrash (3-1 Ma), and Abyad basalts (< 1 Ma), occurring in both Khaybar and Ithnayn (Camp et al., 1991). Recent $^{40}Ar$-$^{39}Ar$ age determinations suggest that all volcanism at Harrat Khaybar started at 2.3 Ma, not including the Kura formation (Kent et al., unpublished data). Camp et al. (1991) suggested that Harrat Khaybar that formed in three stages: Kura stage, which was formed by lower degree of melting (10-5%) and fast ascending of magmas from a deeper magmatic source; Jarad and Mukrash Stage which formed by higher degree of melting (15-10%)and developed a crustal level magmatic chamber; finally, the Abyad Stage occurred in two phases, one in Khaybar which exhibits the most evolved rocks and highest degree of melting (>15%), and another phase in Harrat Ithnayn which shows a similar characteristics to the oldest stage of Kura, where there is a lower degree of melting (~5%).

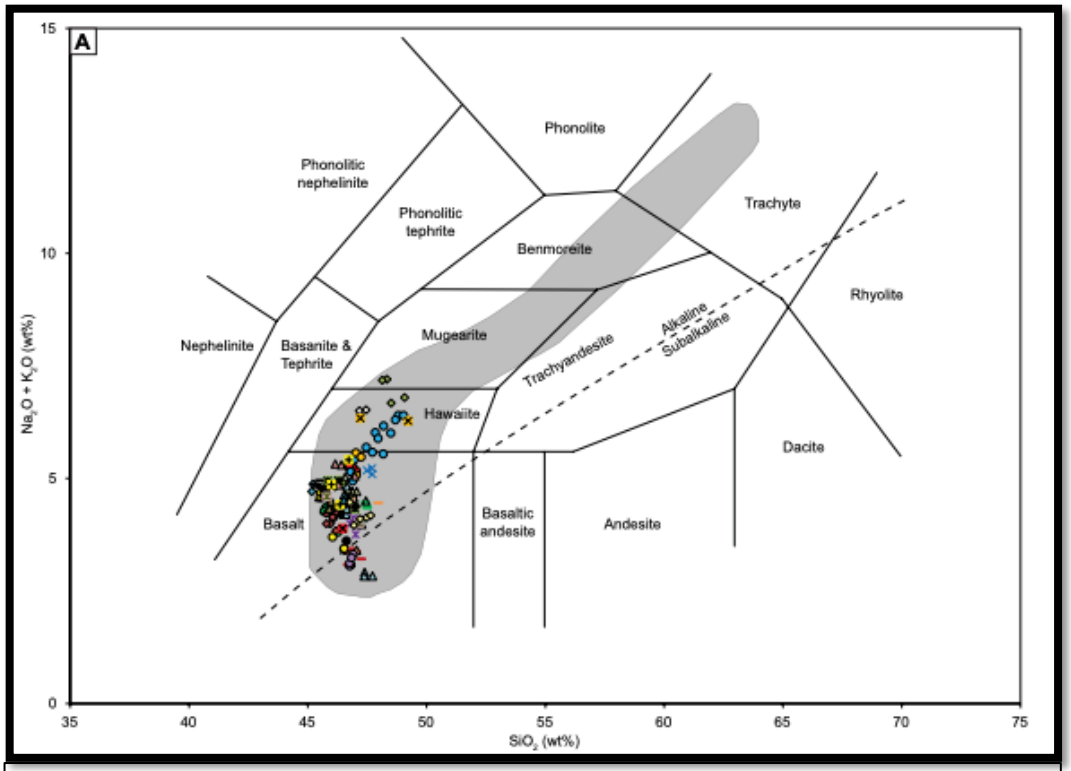


Figure 4: Composition of Harrat Rahat units on a TAS from: Downs et al (2018). It shows the narrow range of rock compositions of most of Harrat Rahat lavas from alkali-basalt to hawaiite; although the northern part of Rahat exhibits a significantly wider range of compositions from sub-alkali basalts to trachyte, showing in the gray shaded region.

Similar to Harrats Rahat and other Harrats, the oldest basaltic unit in Khaybar and Ithnayn is the most extensive and voluminous unit among these volcanic units (Camp et al., 1991; Camp et al., 1992). Also, younger units of Harrat Khaybar are more evolved rocks, especially the Abyad unit, which show evidence of extensive fractional crystallization in crustal level magma chambers. As a result, volcanism at Harrat Khaybar includes evolved felsic rocks types such comendite and trachyte (Camp et al., 1991). Similar evolved lavas have occurred in Harrat Rahat, although Harrat Khaybar shows a greater degree of magmatic differentiation (Camp and Roobol, 1989). However, there is no evidence of differentiated rocks having been produced in Harrat Ithnayn. Camp et al. (1991) interpret the strong fractionation at the end of the previous volcanism at Harrat Rahat and Khaybar to result from open-system magmatic processes involving shallow crustal magma storage beneath these two volcanic fields. This suggests that Harrat Ithnayn is yet to experience this phase.

**2- Research Problems/Specific aims:**

The primary objective of this research is to investigate the timing and composition of the volcanic activity at the Ithnayn volcanic lava field in western Saudi Arabia and place this harrat within the broader context of magmatism in the Arabian Peninsula and along the MMN line. I wish to specifically investigate the following hypotheses:

1) That there is a time progressive trend in volcanism from south to north along the MMN line. Existing evidence suggests a time progressive trend exists, although this is limited by lack of robust $^{40}$Ar-$^{39}$Ar dates for Harrat Ithnayn (e.g. Camp et al. 1991; Moufti et al., 2010). This research aims to evaluate this proposed volcanic age progression by studying the geochronology of Harrat Ithnayn using the technique of $^{40}$Ar-$^{39}$Ar age incremental heating age determinations.

2) Harrat Ithnayn has experienced relatively little stalling and fractionation of magma within the shallow crust. Harrats Rahat and Khaybar have experienced magmatic differentiation processes and their volcanic production changed in the latest volcanic activity of their lifespan (Camp and Roobol; 1989; Camp et al., 1991). However, the volcanism at Harrat Ithnayn appears more youthful and thus shallow level magma chambers may not have been established, consistent with the early phases of Rahat and Khaybar. This research investigates the magmatic processes that lead to the narrow range of compositions by looking at the role of the lithosphere and magmatic sources.

## 3- Materials and Methods:

In this research project, I follow a two-pronged strategy. The first part focuses on applying geochronological, geochemical, and petrological methods to volcanic samples that have been collected from Harrat Ithnayn. The second part uses the resulting data from Harrat Ithnayn and the published (and unpublished) results from the other harrats in the MMN line to provide further context and insight into the lithospheric and upper mantle geodynamic setting expressed by the north-trending volcanic axis of MMN line.

### 3.1 Sampling Collection and Categorization:

The fieldwork team collected twenty whole rock samples from lava flows in the Harrat Ithnayn volcanic field during fieldwork conducted in September of 2017. Based on the geologic map of Roobol and Camp (1991), the sampling coverage includes most of the subunits of Mukrash and Abyad Basalt units that were identified at Harrat Ithnayn. The only two subunits that were difficult to collect are Qb2 and Qb3[1], located in the center of the volcanic field and formed from two volcanic vents (Fig. 5). Most of the lava flows of these two subunits are covered by younger subunits of Abyad Basalt from Qb4 to Qb6 and make them isolated to one location. I excluded sample (HI-20) from my age and chemical interpretations since it appears geographically and compositionally to be from the unit of Jarad Basalt, a unit of Harrat Khaybar that is not found in Harrat Ithnayn.

Roobol and Camp (1991) distinguished volcanic units based on stratigraphic position, severity of weathering and erosion, and degree of dust-pond development. The age range of these volcanic units was thought to be 0-3 Ma, according to a limited number whole rock K-Ar radiometric age determinations (Roobol and Camp, 1991). Based on the field evidence, even the oldest stratigraphic

[1] Camp and Roobol (1991) identified 8 volcanic subunits of Mukrash and Abyad Basalts at Harrat Ithnayn, from QTm1(Mukrash) to Qb6 (Abyad). QTm1 is the oldest subunit, and QT6 is the youngest. This classification is based on field relations and erosional evidence. Samples were collected from all volcanic units at Harrat Ithnayn except Qb2 and Qb3 due to the difficulty of access to their mapped locations.

units were suggested to be younger than the previous K-Ar age estimates (Camp et al., 1991). It is likely in this dry and desert environment that qualitative age estimated based on minimal apparent weathering may be misleading; however, the fieldwork team focused on collecting the least weathered and unaltered samples for geochronological and compositional studies.

The samples were collected are compact, fine-to-medium grained alkali olivine basalts, trachy-basalts, and tephrite basanites, which show aphyric to coarse phyric texture and a few of them are vesicular. The main phenocrysts are olivine with some plagioclase. The size range of these phenocrysts is 800 to 150 μm. Groundmasses are mainly composed of glass and micro- to cryptocrystalline plagioclase, and augite with minor olivine. After examining texture and mineralogy, and based on the spatial distribution, I categorized samples and divided them into groups for geochronological and geochemical analyses. I culled samples that, in petrographic inspection, are more altered or exhibited xenolithic/xenocrystic fragments, but I chose instead dense samples with crystalline groundmass which lack interstitial glass. These characteristics are known to potentially affect the accuracy of $^{40}Ar$-$^{39}Ar$ age determinations.

**3.2 Whole-rock XRF and ICP-MS Geochemistry:**

I analyzed whole rock major and minor element concentrations for my samples at the GeoAnalytical Laboratory at Washington State University (WSU) in Pullman, Washington using the method of X-ray fluorescence (XRF) (Table 3), following the procedures outlined in Johnson et al. (1999). Also, I obtained trace element concentrations for all samples at the GeoAnalytical Laboratory (WSU) using the method of inductively coupled plasma-mass spectrometry (ICP-MS), following the procedures described in Knaack et al. (1994). Concentrations of trace and rare earth elements are reported in parts per million (ppm) and detection limits are sub-ppm (Table 3). I prepared whole rock samples by first cutting them into pieces less than 5mm in size, and removed pieces showing visible weathering or alteration.

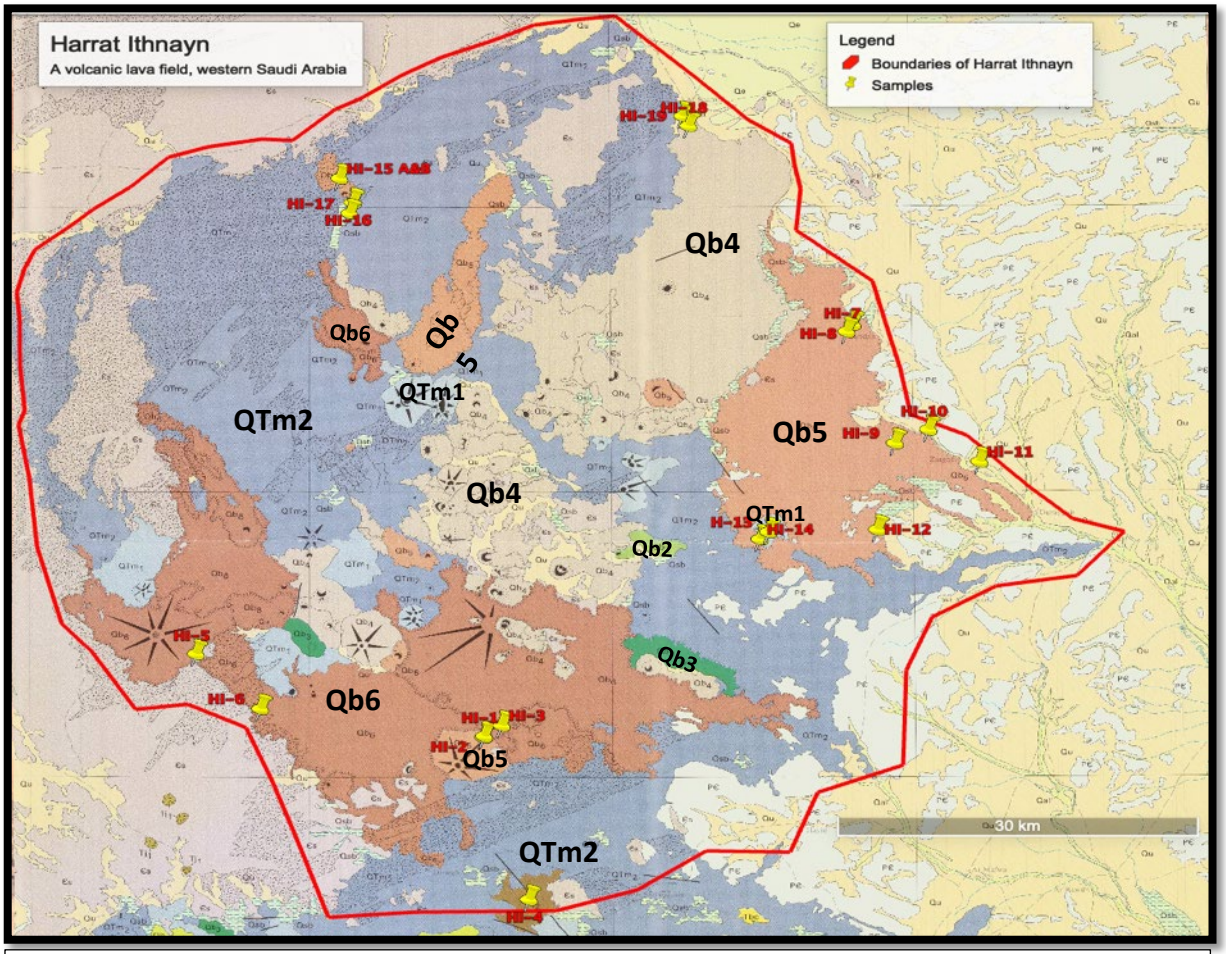


(Figure 5): This map shows locations of samples collected during the field work during the summer of 2017. Samples geographically cover Harrat Ithnayn and represent all units except Qb2 and Qb3.

Alteration is usually found in rare vesicles that contained some zeolites, carbonates, clays, and loess materials. Total sample weights were each about 50 mg. For the analyses fused, beads were produced by mixing an amount of the rock powder with a dilithium tetraborate flux (2:1 ratio for XRF; and 1:1 ratio for ICP-MS). Replicate analyses were used to estimate uncertainties (at ± 2s). For analysis by XRF, I estimated uncertainties (± 2s) for all major element measurements which are less than 0.5% for all elements. Johnson et al. (1999) described the accuracy and precision of the major-element XRF analyses, and Kelly (2006) did some modifications that shows improvement in accuracy in some elements (Wall et al., 2018). Also, I estimated uncertainties (at ± 2s) for trace element concentrations measured by XRF using duplicate analysis that showed lower precision for some elements such as U and La <60%, Ce and Pb <27%, and Sc, Nd, Rb, and Ni all are <7% (2s). For trace element

concentrations measured by ICP-MS, the estimated uncertainties (± 2s) using the duplicate analyses are less than 5% for all elements except Cs <10% and Sm <6% (2s). Further details on precision and detection limits are reported in Knaack et al. (1994) and updated in Steenberg et al. (2017).

**3.3 $^{40}$Ar/$^{39}$Ar Geochronology:**

I prepared and analyzed groundmass separates of Harrat Ithnayn lavas at Oregon State University Argon Geochronology Laboratory, using the standard method of $^{40}$Ar/$^{39}$Ar laser step heating. Ten dense samples with a holo-crystalline groundmass were crushed and sieved to 150-355 μm, washed, and ultrasonicated. I isolated groundmass separates from phenocryst phases using a Frantz magnetic separator. I followed this separation procedure with an acid leaching procedure with HCl and $HNO_3$ acids with different acidic strength and triple-distilled water. Some samples were subjected to 3% HF leaching for about 8 min to remove any attached glass or volcanic matrix, followed by triple-distilled water washing and an hour of ultrasonic bath, then leached separated groundmasses were dried in an oven (~70 °C). I examined the cleaned groundmass separates under a binocular microscope for a final handpicking to remove any remaining phenocrysts and/or altered materials. About 50 mg of each prepared groundmass separate wrapped in aluminum foil was loaded with flux monitor FCT sanidine (FCT-NM; 28.201 Ma; Kuiper et al., 2008) in evacuated quartz vials, then irradiated for 6 hours in the 1 MW TRIGA (Training, Research, Isotopes, General Atomics) nuclear reactor at Oregon State University. After the neutron irradiation and ~20 days cooling, I then loaded these irradiated samples in a high vacuum sample chamber, and incrementally heated each (in 15 to 39 steps) using a 25W laser beam resulting in a release of the Ar (and active gases that were removed by metal-metal oxide getters in the extraction line). Compositions of the argon isotopes were detected and analyzed using the ARGUS VI multi-collector mass spectrometer at Argon Geochronology Laboratory, Oregon State University. I used the decay constant of 5.530 ±0.097 $\times 10^{-10} yr^{-1}$ as proposed by Min et al. (2000) along with other reactor interference corrections reported in Koppers et

al. (2003) for my age calculations. I preformed the calculation of my $^{40}Ar/^{39}Ar$ ages (documented at 2σ uncertainty) using the ArArCALC v2.6.2 software package from Koppers (2002).

**3.4 Conditions and Compositions Modelling:**

I used the MELTS software package from Ghiorso and Sack (1995) to model conditions of parental melt generation and evolution. I used the most primitive lava compositions reported from Harrat Ithnayn that have the highest value of Mg# (> 66) as the initial parental magma composition. This included one primitive lava composition from this study (HI-7, from Qb5), and another composition from Camp and Roobol (1991) (sample number 4947, from Qb4) (Table 2). The Mg# was calculated as = {(molar MgO/ MgO + FeO) * 100}. Following the procedure of Duncan et al. (2016) I ran models with a small amount of water present (0.2 wt.%) and buffered at the quartz-fayalite-magnetite (QFM) for oxygen fugacity.

In addition, I used the REEBOX MATLAB modeling program (Brown and Lesher, 2014) that employs a polybaric non-modal melting after Fram and Lesher (1993) for REE contents in basalts to estimate the melt distribution as a function of depth in a mantle melting column. The final depth of melting is interpreted to be thickness of the lithosphere. In this model, I used the partition coefficient calibrations from McKenzie and O'Nions (1991), and I chose the mantle source composition as 5% depleted garnet peridotite to model the depth, range, and degree of melting. The REEBOX model uses observed REE contents to constrain the pressures of the beginning and ending of mantle melting and their equivalent melt fractions.

**(Table 2): Parental magma for Harrat Ithnayn lavas. All compositions are in wt.% unless otherwise noted.**

| Oxide, element | This study (wt., ppm) | Camp et al. (1991) Study* (wt., ppm) |
|---|---|---|
| **SiO2** | 47.93 | 45.89 |
| **TiO2** | 1.36 | 1.49 |
| **Al2O3** | 15.61 | 15.05 |
| **FeO*** | 10.37 | 10.23 |
| **MnO** | 0.17 | 0.18 |
| **MgO** | 10.71 | 11.62 |
| **CaO** | 9.93 | 10.33 |
| **Na2O** | 3.01 | 3.79 |
| **K2O** | 0.66 | 0.96 |
| **P2O5** | 0.24 | 0.59 |
| **Ni (µg/g)** | 294.25 | 301.00 |
| **Cr (µg/g)** | 500.60 | 392.00 |
| **Mg#** | 66.93 | 66.70 |

***The most primitive lava composition in Harrat Ithnayn from Camp et al. (1991) study. The Mg# was calculated as = {(molar MgO/ MgO + FeO) * 100}.**

## 4- Results:

### A) Geochemistry:

I report in Table 3 concentrations of major, trace, and rare earth element for 19 new samples collected from Harrat Ithnayn along with previous published compositions from Camp et al. (1991) which are reported in the Appendices Section under "Geochemical Data". Also, chemical data of one sample from the northern part of Khaybar (HI-20) is reported in Table 3. I compare compositions of Harrat Ithnayn lavas with those from other harrats lava in western Saudi Arabia using a total alkalis vs. silica (TAS) diagram (Fig. 6). This diagram shows that my new data from Harrat Ithnayn are comparable to the previous data from Camp et al. (1991), although the previous data have slightly higher total alkalis. The range of $SiO_2$ for Ithnayn lavas is between 46.8 and 50.1 wt.%, while the range of the total alkalis ($Na_2O+K_2O$) is from 3.4 to 5.3 wt.%. This shows that Harrat Ithnayn has a narrow range of compositional variation, from alkali basalt to trachy-basalt. MgO contents have a moderately restricted range from 10.71 to 6.53 wt.%. The Mg# was calculated as = {(molar MgO/ MgO + FeO) * 100}, with the assumption that the total ratio of $Fe_2^+/Fe$ is 0.895, and ranges between 66.9 and 55.8. This indicates that lavas from Harrat Ithnayn exhibit only a small range of rather primitive basaltic compositions. The absence of more evolved compositions at Harrat Ithnayn makes it more similar to those harrats located off the MMN line such as Harrat Hutaymah and Lunayyir, rather than to those larger volcanic fields that are to the south of Ithnayn and on the MMN (Rahat and Khaybar) (Duncan et al., 2016; Duncan and Alamri, 2013). Also, I use bivariate (Harker) diagrams to compare major and selected trace element ratios with MgO contents (see Figures 7-10). Major element ratios of $P_2O_5$, $Na_2O$, and $K_2O$ seem to systematically exhibit three different trends with MgO, indicating either different magmatic sources or degree of partial melting (Fig. 7). On the other hand, $TiO_2$ and FeO contents are broadly scattered with MgO, and $SiO_2$ and $Al_2O_3$ contents showing a slightly negative correlation with the increase of MgO (Fig. 8), while CaO shows a notable increase with the increase in MgO contents, illustrating consistency with crystal fractionation (Fig. 9). The latter can be also

explained by lower pressure fractionation of clinopyroxene and plagioclase, indicated by both petrographic study and modelling of the chemical data.

Concentrations of compatible trace elements, such as Ni and Cr, range from 68 to 294 ppm, and from 195 to 501 ppm, respectively (Fig. 10). They also show a simple trend that demonstrates a decrease in these compatible element concentrations with decreasing MgO, indicating a significant olivine and clinopyroxene fractionation. These values agree with the major element concentrations in which none of Harrat Ithnayn samples depicts a primary magma. Incompatible element concentrations and ratios (e.g. Ba, La, Nb/Zr etc.), on the other hand, do not show any systematic change with MgO, although it typically should show an increase with MgO decreasing. Similar to most of the Arabian Harrats (e.g. Camp et al., 1991; Moufti and Hashad, 2005; Duncan et al., 2016; Duncan and Alamri, 2013) Harrat Ithnayn lavas demonstrate an enrichment in light REE and a depletion in heavy REE (Fig. 11).

**Table 3**: Geochemical Data for lava flows, Harrat Ithnayn, Western Saudi Arabia (major elements in wt.%, trace elements in µg/g)

| **Sample ID** | **ADK HI-4** | **ADK HI-20** | **ADK HI-7** | **ADK HI-8** | **ADK HI-9** | **ADK HI-10** | **ADK HI-11** | **ADK HI-12** | **ADK HI-14** | **ADK HI-18** |
|---|---|---|---|---|---|---|---|---|---|---|
| **Latitude, N** | 26° 8'0.90" | 25°58'35.00" | 26°37'43.20" | 26°38'5.60" | 26°31'50.50" | 26°32'32.50" | 26°30'50.10" | 26°27'18.20" | 26°26'51.00" | 26°48'37.10" |
| **Longitude, E** | 40°10'27.01" | 40°27'46.10" | 40°26'32.00" | 40°26'49.60" | 40°28'52.80" | 40°30'33.50" | 40°33'5.30" | 40°27'57.00" | 40°22'5.20" | 40°18'44.10" |
| **Unit** | **QTm2** | **Tj2** | **Qb5** | **Qb5** | **Qb5** | **Qb5** | **Qb5** | **Qb5** | **QTm2** | **Qb4** |
| **SiO2** | 45.96 | 47.01 | 47.50 | 47.97 | 46.75 | 48.05 | 48.13 | 46.97 | 46.00 | 48.36 |
| **TiO2** | 1.77 | 1.49 | 1.35 | 1.59 | 1.58 | 1.74 | 1.77 | 1.64 | 2.02 | 1.40 |
| **Al2O3** | 15.54 | 15.24 | 15.47 | 16.01 | 16.07 | 16.22 | 16.29 | 15.41 | 15.22 | 15.77 |
| **FeO*** | 11.21 | 10.89 | 10.28 | 10.31 | 9.90 | 10.35 | 10.48 | 9.99 | 10.81 | 10.50 |
| **MnO** | 0.177 | 0.171 | 0.170 | 0.170 | 0.160 | 0.162 | 0.171 | 0.171 | 0.172 | 0.176 |
| **MgO** | 8.06 | 9.44 | 10.71 | 8.39 | 7.03 | 8.02 | 6.83 | 10.10 | 7.25 | 8.92 |
| **CaO** | 11.97 | 10.45 | 9.84 | 10.37 | 11.61 | 9.82 | 10.96 | 9.87 | 12.50 | 10.10 |
| **Na2O** | 3.01 | 2.82 | 2.98 | 3.38 | 3.36 | 3.71 | 3.54 | 3.71 | 2.97 | 3.20 |
| **K2O** | 0.34 | 0.57 | 0.65 | 0.74 | 0.61 | 0.81 | 0.67 | 1.01 | 0.82 | 0.62 |
| **P2O5** | 0.224 | 0.188 | 0.242 | 0.326 | 0.288 | 0.382 | 0.315 | 0.508 | 0.364 | 0.213 |
| **Total** | 98.09 | 98.08 | 99.10 | 99.19 | 97.16 | 99.19 | 99.09 | 99.31 | 97.97 | 99.18 |
| **Mg#** | 58.04 | 62.48 | 66.93 | 61.26 | 57.49 | 60.10 | 55.87 | 66.30 | 56.28 | 62.29 |
| **µg/g** | | | | | | | | | | |
| **Ni** | 131 | 231 | 294 | 174 | 100 | 157 | 94 | 267 | 117 | 210 |
| **Cr** | 291 | 356 | 501 | 334 | 213 | 281 | 210 | 423 | 224 | 372 |
| **Ga** | 18 | 16 | 17 | 18 | 19 | 18 | 19 | 18 | 18 | 17 |

| | | | | | | | | | | |
|---|---|---|---|---|---|---|---|---|---|---|
| **Cu** | 80 | 78 | 93 | 92 | 85 | 81 | 89 | 79 | 102 | 100 |
| **Zn** | 85 | 80 | 76 | 79 | 78 | 83 | 83 | 76 | 79 | 80 |
| **La** | 8.47 | 10.19 | 14.60 | 19.84 | 15.04 | 21.14 | 17.34 | 35.89 | 17.91 | 15.16 |
| **Ce** | 21.60 | 22.52 | 29.75 | 39.15 | 31.70 | 43.62 | 36.41 | 65.82 | 38.42 | 31.37 |
| **Pr** | 3.11 | 3.03 | 3.78 | 4.86 | 4.11 | 5.50 | 4.76 | 7.40 | 4.94 | 3.96 |
| **Nd** | 14.51 | 13.80 | 15.92 | 20.30 | 17.84 | 22.80 | 20.44 | 28.31 | 21.71 | 16.78 |
| **Sm** | 3.87 | 3.65 | 3.89 | 4.73 | 4.54 | 5.28 | 5.10 | 5.82 | 5.22 | 4.24 |
| **Eu** | 1.50 | 1.33 | 1.40 | 1.70 | 1.62 | 1.88 | 1.83 | 2.00 | 1.78 | 1.48 |
| **Gd** | 4.39 | 4.07 | 4.05 | 4.82 | 4.63 | 5.18 | 5.16 | 5.44 | 5.38 | 4.48 |
| **Tb** | 0.75 | 0.68 | 0.69 | 0.82 | 0.77 | 0.83 | 0.84 | 0.88 | 0.88 | 0.77 |
| **Dy** | 4.61 | 4.19 | 4.26 | 5.00 | 4.66 | 4.79 | 5.12 | 5.13 | 5.32 | 4.92 |
| **Ho** | 0.91 | 0.85 | 0.90 | 0.97 | 0.92 | 0.91 | 1.03 | 1.00 | 1.04 | 0.99 |
| **Er** | 2.39 | 2.24 | 2.44 | 2.66 | 2.46 | 2.37 | 2.68 | 2.67 | 2.82 | 2.69 |
| **Tm** | 0.33 | 0.31 | 0.34 | 0.38 | 0.34 | 0.32 | 0.37 | 0.36 | 0.39 | 0.38 |
| **Yb** | 2.04 | 1.92 | 2.07 | 2.29 | 2.05 | 1.96 | 2.30 | 2.24 | 2.38 | 2.34 |
| **Lu** | 0.30 | 0.30 | 0.32 | 0.35 | 0.32 | 0.29 | 0.35 | 0.36 | 0.37 | 0.37 |
| **Ba** | 102 | 179 | 210 | 250 | 212 | 249 | 230 | 335 | 282 | 208 |
| **Th** | 0.50 | 0.95 | 2.01 | 2.79 | 1.85 | 2.62 | 2.20 | 5.07 | 2.18 | 1.56 |
| **Nb** | 7.22 | 12.87 | 16.82 | 24.76 | 18.79 | 26.59 | 21.89 | 42.94 | 18.70 | 14.73 |
| **Y** | 22.67 | 20.92 | 21.92 | 24.83 | 22.64 | 22.67 | 25.13 | 24.88 | 26.06 | 24.50 |
| **Hf** | 2.82 | 2.47 | 2.95 | 3.75 | 3.46 | 4.13 | 3.85 | 4.74 | 3.33 | 2.92 |
| **Ta** | 0.50 | 0.85 | 1.09 | 1.59 | 1.22 | 1.69 | 1.42 | 2.64 | 1.20 | 0.90 |
| **U** | 0.38 | 0.26 | 0.52 | 0.77 | 0.63 | 0.86 | 0.73 | 1.36 | 0.83 | 0.43 |
| **Pb** | 0.92 | 1.19 | 1.82 | 2.34 | 3.23 | 2.40 | 2.22 | 3.15 | 2.43 | 1.63 |
| **Rb** | 2.0 | 7.1 | 11.7 | 12.4 | 9.2 | 13.0 | 9.9 | 21.0 | 14.3 | 13.1 |
| **Cs** | 0.01 | 0.04 | 0.16 | 0.19 | 0.12 | 0.19 | 0.14 | 0.31 | 0.22 | 0.15 |
| **Sr** | 380 | 378 | 394 | 500 | 490 | 624 | 510 | 655 | 457 | 455 |
| **Sc** | 29.4 | 27.6 | 30.3 | 31.7 | 29.7 | 26.6 | 31.9 | 27.0 | 32.4 | 31.3 |
| **Zr** | 120 | 100 | 138 | 180 | 159 | 201 | 177 | 247 | 139 | 129 |
| **Nb/Zr** | 0.06 | 0.13 | 0.12 | 0.14 | 0.12 | 0.13 | 0.12 | 0.17 | 0.13 | 0.11 |
| **La/Sm** | 2.19 | 2.79 | 3.75 | 4.19 | 3.31 | 4.01 | 3.40 | 6.17 | 3.43 | 3.58 |
| **K/Nb** | 397 | 376 | 326 | 251 | 276 | 255 | 255 | 197 | 372 | 352 |
| **Dy/Yb** | 2.25 | 2.18 | 2.05 | 2.18 | 2.28 | 2.45 | 2.23 | 2.28 | 2.24 | 2.10 |
| **Sm/Yb** | 1.90 | 1.90 | 1.87 | 2.07 | 2.22 | 2.69 | 2.22 | 2.59 | 2.20 | 1.81 |
| **Zr/Y** | 5.30 | 4.80 | 6.30 | 7.25 | 7.03 | 8.88 | 7.03 | 9.95 | 5.33 | 5.25 |

**Table 3** *(continue)*

| Sample ID | ADK HI-19 | ADK HI-6 | ADK HI-1 | ADK HI-2 | ADK HI-16 | ADK HI-17 | ADK HI-3 | ADK HI-13 | ADK HI-15 | ADK HI-5 |
|---|---|---|---|---|---|---|---|---|---|---|
| Latitude, N | 26°49'8.20" | 26°18'5.60" | 26°16'36.40" | 26°16'32.50" | 26°44'40.70" | 26°44'6.30" | 26°17'10.00" | 26°27'13.10" | 26°45'57.70" | 26°20'58.90" |
| Longitude, E | 40°18'26.00" | 39°57'10.30" | 40° 8'17.80" | 40° 8'15.40" | 40° 1'52.90" | 40° 1'44.00" | 40° 9'9.90" | 40°22'30.90" | 40° 1'13.60" | 39°53'58.20" |
| Unit | Qb4 | Qb6 | Qb5 | Qb5 | QTm2 | QTm2 | Qb4 | QTm1 | Qb5 | Qb6 |
| SiO2 | 47.18 | 49.46 | 47.18 | 46.02 | 47.47 | 47.71 | 49.05 | 46.98 | 47.02 | 49.70 |
| TiO2 | 1.27 | 1.53 | 1.51 | 1.44 | 1.48 | 1.43 | 1.63 | 1.54 | 1.93 | 1.75 |
| Al2O3 | 15.49 | 16.70 | 16.35 | 15.65 | 15.60 | 15.94 | 16.63 | 15.10 | 15.07 | 16.87 |
| FeO* | 10.32 | 10.00 | 10.34 | 9.96 | 10.82 | 10.52 | 10.07 | 10.02 | 10.14 | 9.47 |
| MnO | 0.17 | 0.17 | 0.17 | 0.16 | 0.18 | 0.17 | 0.16 | 0.17 | 0.18 | 0.15 |
| MgO | 9.59 | 6.55 | 7.62 | 7.96 | 8.89 | 8.56 | 7.35 | 10.55 | 9.83 | 6.53 |
| CaO | 10.18 | 10.70 | 11.43 | 11.96 | 11.09 | 11.18 | 10.25 | 9.99 | 9.13 | 9.18 |
| Na2O | 2.94 | 3.41 | 3.17 | 3.03 | 2.87 | 2.88 | 3.39 | 3.35 | 4.18 | 4.14 |
| K2O | 0.59 | 0.75 | 0.47 | 0.46 | 0.52 | 0.51 | 0.67 | 0.96 | 1.26 | 1.08 |
| P2O5 | 0.19 | 0.29 | 0.27 | 0.25 | 0.25 | 0.22 | 0.27 | 0.43 | 0.62 | 0.44 |
| Total | 97.70 | 99.54 | 98.38 | 96.62 | 99.09 | 99.04 | 99.44 | 99.00 | 99.29 | 99.28 |
| Mg# | 64.03 | 56.10 | 58.69 | 60.23 | 61.47 | 61.22 | 58.73 | 67.14 | 65.36 | 57.29 |
| µg/g | | | | | | | | | | |
| Ni | 233 | 69 | 109 | 113 | 177 | 161 | 120 | 293 | 258 | 98 |
| Cr | 401 | 195 | 234 | 241 | 349 | 328 | 253 | 468 | 395 | 216 |
| Ga | 17 | 18 | 18 | 17 | 16 | 18 | 18 | 17 | 17 | 19 |
| Cu | 87 | 76 | 83 | 73 | 69 | 73 | 74 | 81 | 80 | 42 |
| Zn | 78 | 80 | 92 | 77 | 82 | 81 | 82 | 78 | 79 | 84 |
| La | 13.73 | 15.82 | 16.22 | 15.41 | 11.60 | 11.17 | 15.48 | 29.85 | 41.79 | 24.24 |
| Ce | 28.19 | 33.22 | 32.79 | 30.96 | 25.45 | 24.79 | 33.97 | 55.17 | 77.68 | 50.31 |
| Pr | 3.61 | 4.31 | 4.06 | 3.87 | 3.49 | 3.33 | 4.44 | 6.36 | 8.80 | 6.34 |
| Nd | 14.92 | 18.41 | 16.96 | 16.01 | 15.43 | 14.67 | 19.10 | 24.64 | 33.54 | 25.80 |
| Sm | 3.66 | 4.68 | 4.26 | 4.03 | 4.04 | 3.74 | 4.77 | 5.29 | 6.83 | 5.94 |
| Eu | 1.35 | 1.64 | 1.56 | 1.44 | 1.42 | 1.43 | 1.69 | 1.82 | 2.21 | 1.99 |
| Gd | 4.04 | 4.74 | 4.42 | 4.21 | 4.30 | 4.22 | 4.91 | 4.99 | 6.10 | 5.48 |
| Tb | 0.69 | 0.83 | 0.78 | 0.72 | 0.72 | 0.70 | 0.82 | 0.81 | 0.96 | 0.86 |
| Dy | 4.42 | 5.01 | 4.64 | 4.38 | 4.50 | 4.46 | 4.98 | 4.75 | 5.48 | 4.84 |
| Ho | 0.89 | 1.01 | 0.93 | 0.90 | 0.90 | 0.89 | 0.99 | 0.95 | 1.05 | 0.91 |
| Er | 2.39 | 2.74 | 2.46 | 2.36 | 2.48 | 2.38 | 2.66 | 2.48 | 2.66 | 2.39 |
| Tm | 0.34 | 0.37 | 0.35 | 0.33 | 0.35 | 0.34 | 0.37 | 0.35 | 0.37 | 0.32 |
| Yb | 2.11 | 2.30 | 2.11 | 2.06 | 2.09 | 2.06 | 2.25 | 2.15 | 2.21 | 1.99 |
| Lu | 0.32 | 0.34 | 0.33 | 0.30 | 0.32 | 0.31 | 0.35 | 0.33 | 0.34 | 0.30 |
| Ba | 189 | 225 | 226 | 200 | 173 | 183 | 171 | 315 | 346 | 247 |
| Th | 1.36 | 2.32 | 2.17 | 2.02 | 0.97 | 0.94 | 1.90 | 4.33 | 6.09 | 2.83 |

| | | | | | | | | | | |
|---|---|---|---|---|---|---|---|---|---|---|
| **Nb** | 13.34 | 18.24 | 18.69 | 17.88 | 9.67 | 9.42 | 17.07 | 35.00 | 60.11 | 27.93 |
| **Y** | 22.41 | 24.97 | 23.42 | 22.17 | 23.26 | 22.09 | 24.81 | 23.48 | 25.49 | 22.48 |
| **Hf** | 2.59 | 3.45 | 3.03 | 2.90 | 2.51 | 2.42 | 3.85 | 4.35 | 6.13 | 4.60 |
| **Ta** | 0.81 | 1.19 | 1.15 | 1.09 | 0.60 | 0.60 | 1.14 | 2.19 | 3.93 | 1.78 |
| **U** | 1.27 | 0.68 | 0.58 | 0.82 | 0.18 | 0.18 | 0.55 | 1.17 | 1.66 | 0.85 |
| **Pb** | 1.43 | 2.30 | 1.62 | 1.86 | 1.47 | 1.31 | 2.10 | 2.73 | 3.41 | 2.86 |
| **Rb** | 8.9 | 13.0 | 7.7 | 7.8 | 6.3 | 6.8 | 10.5 | 20.0 | 25.5 | 15.9 |
| **Cs** | 0.08 | 0.21 | 0.13 | 0.12 | 0.04 | 0.06 | 0.18 | 0.31 | 0.37 | 0.25 |
| **Sr** | 608 | 425 | 474 | 557 | 359 | 373 | 468 | 575 | 712 | 645 |
| **Sc** | 29.0 | 32.2 | 31.0 | 29.6 | 29.5 | 30.9 | 31.1 | 27.2 | 24.5 | 24.6 |
| **Zr** | 108 | 157 | 139 | 135 | 103 | 100 | 173 | 220 | 323 | 217 |
| **Nb/Zr** | 0.12 | 0.12 | 0.13 | 0.13 | 0.09 | 0.09 | 0.10 | 0.16 | 0.19 | 0.13 |
| **La/Sm** | 3.75 | 3.38 | 3.81 | 3.82 | 2.87 | 2.98 | 3.25 | 5.65 | 6.12 | 4.08 |
| **K/Nb** | 375 | 341 | 212 | 219 | 452 | 451 | 325 | 231 | 176 | 324 |
| **Dy/Yb** | 2.09 | 2.18 | 2.20 | 2.13 | 2.15 | 2.16 | 2.21 | 2.21 | 2.48 | 2.44 |
| **Sm/Yb** | 1.74 | 2.03 | 2.01 | 1.96 | 1.94 | 1.82 | 2.11 | 2.46 | 3.09 | 2.99 |
| **Zr/Y** | 4.84 | 6.31 | 5.93 | 6.08 | 4.42 | 4.54 | 6.99 | 9.38 | 12.67 | 9.66 |

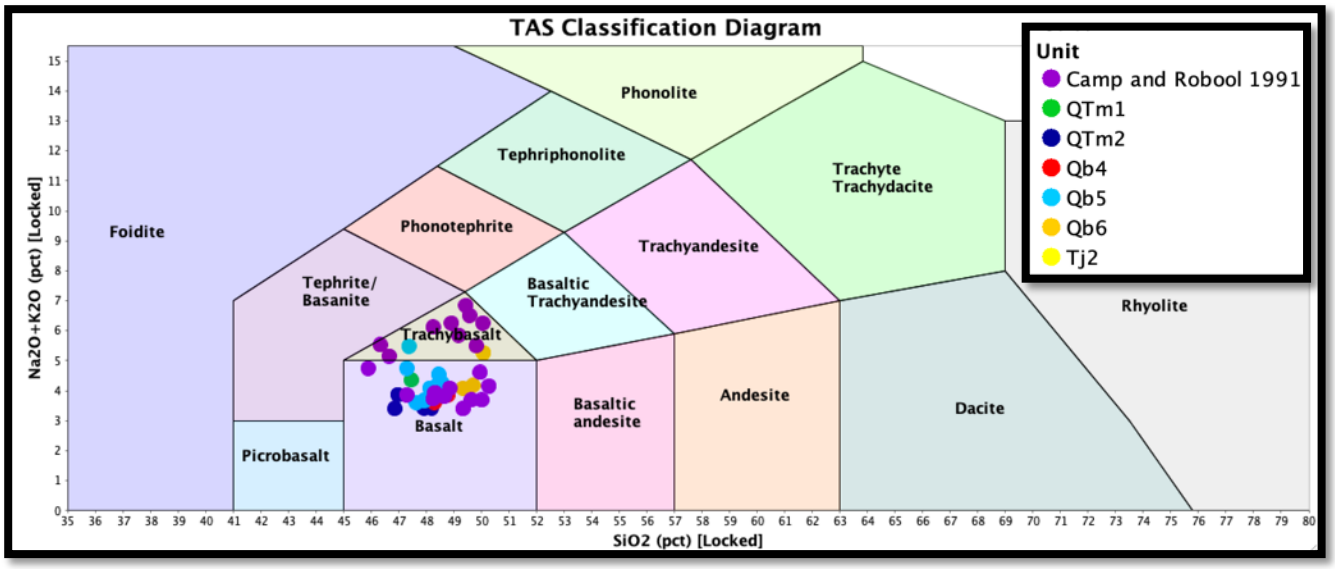


Figure 6: Total alkali vs. silica (TAS) diagram showing the range of composition of lavas from Harrat Ithnayn. Samples collected for this study have been divided into 6 units based on Rooboland Camp geologic map (1991). Samples from Camp and Roobol(1991) have been labeled as purple circle. (TAS formatting modified from: Le Maitre et al, 1989).

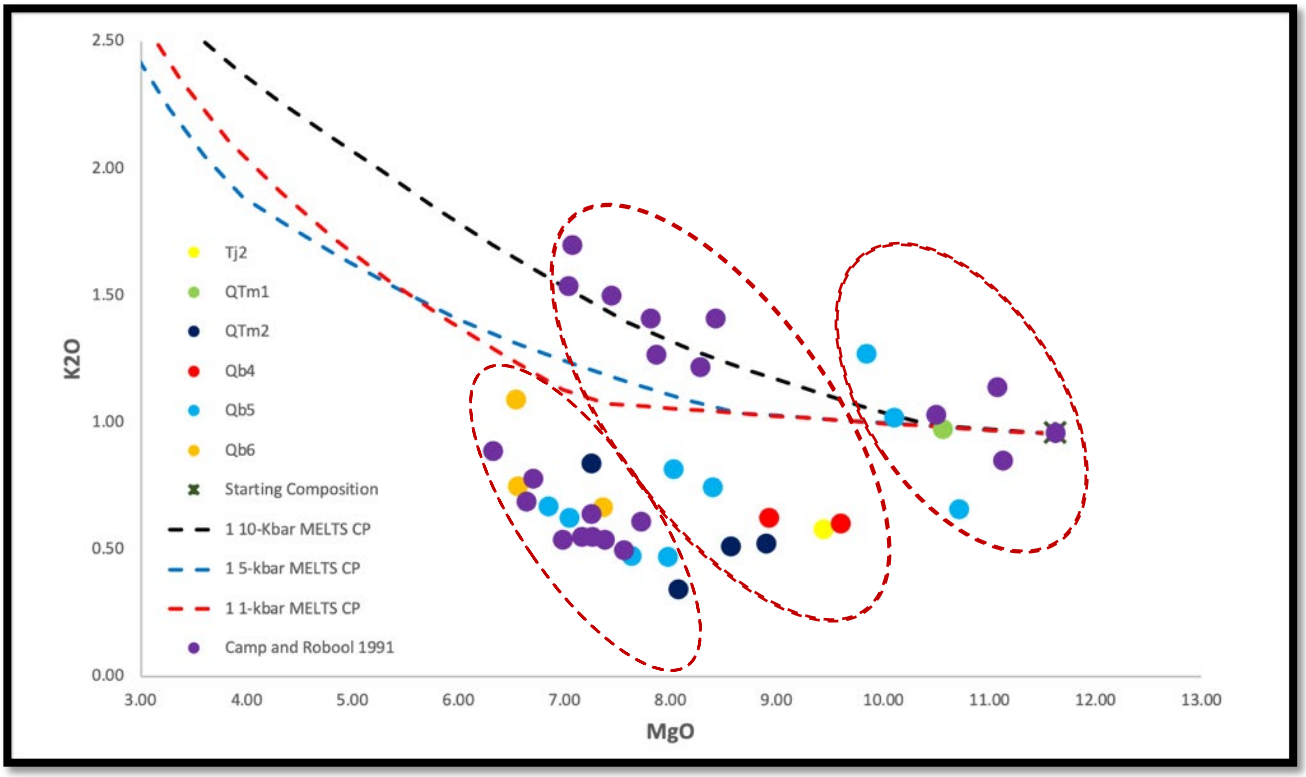


Figure 7: The bivariate diagram of MgO vs. $K_2O$ wt. % shows three different clusters of samples, which it can be explained by differences in magmatic sources and/or degree of melting. Also, it shows calculated liquid lines of descent for fractional crystallization of a representative primary liquid (see Table 2) determined using MELTS (Ghiorso and Sack, 1995).

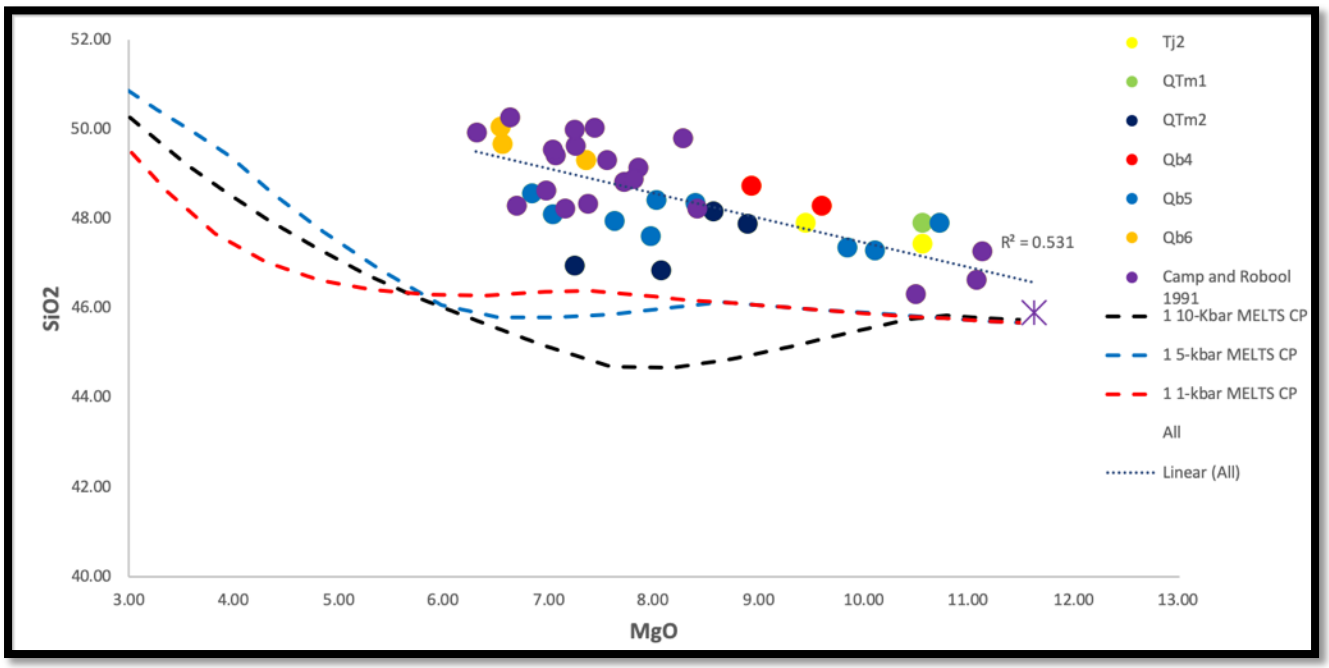


Figure 8: The bivariate diagram of MgO vs. $SiO_2$ wt. % shows a negative correlation between them. Also, it shows calculated liquid lines of descent for fractional crystallization of a representative primary liquid (see Table 2) determined using MELTS (Ghiorso and Sack, 1995). Red: 1-Kbar, Blue: 5-Kbars, and Black: 10-Kbars.

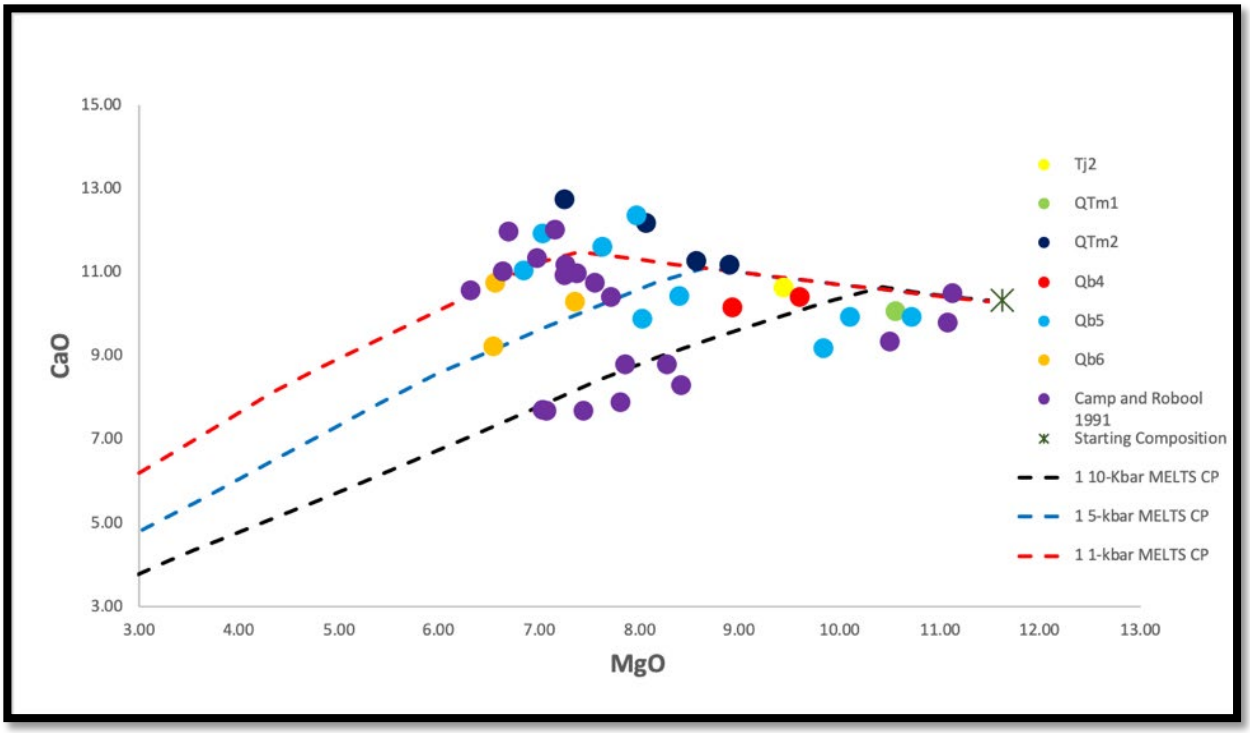


Figure 9: The bivariate diagram of MgO vs. CaO wt. % shows the effect of crystal fractionation at different pressures. Also, it shows calculated liquid lines of descent for fractional crystallization of a representative primary liquid (see Table 2) determined using MELTS (Ghiorso and Sack, 1995). Red: 1-Kbar, Blue: 5-Kbars, and Black: 10-Kbars.

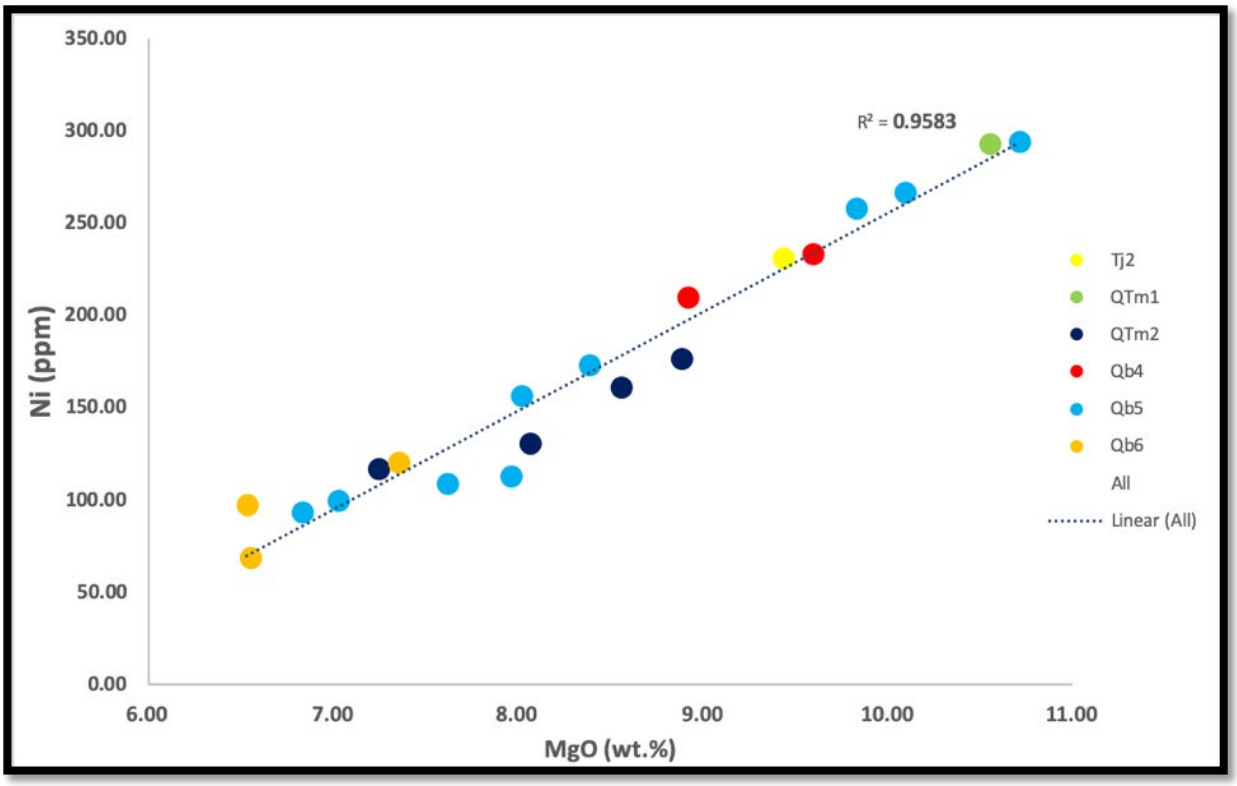


Figure 10: The bivariate diagram of MgO wt.% vs. Ni (ppm) shows the effect of olivine crystal fractionation which is illustrated by the strongly positive correlation.

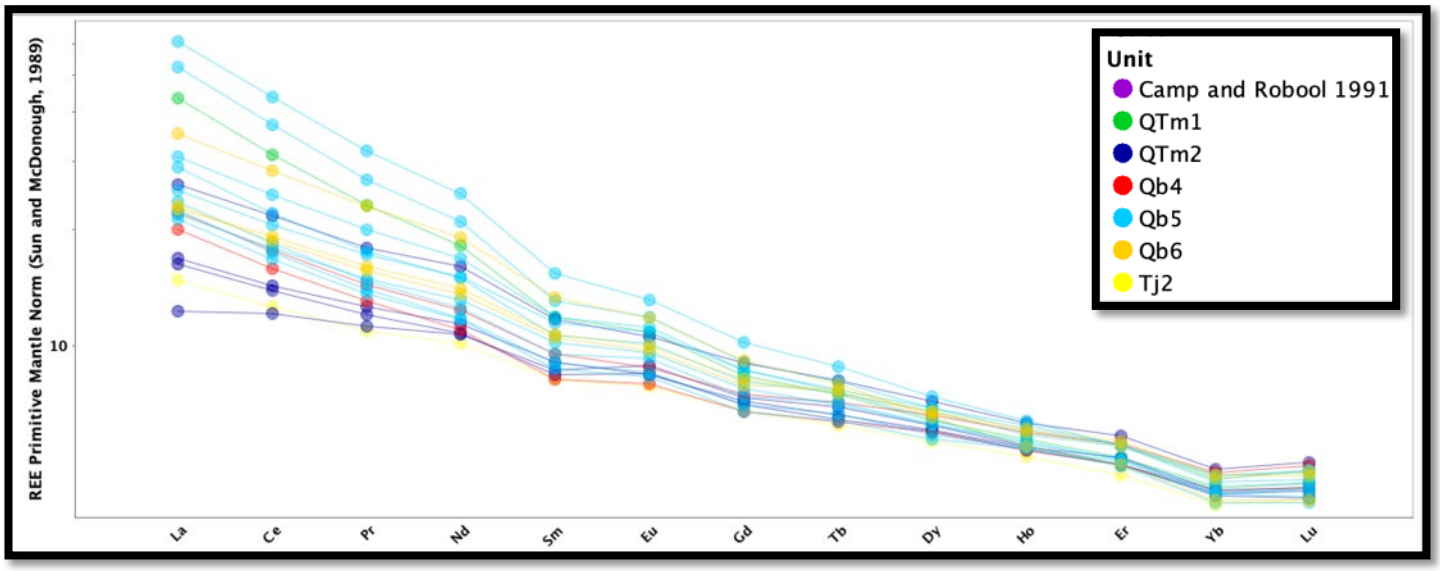


Figure 11: Primitive normalized REE profiles for lava flows from Harrat Ithnayn. Normalized using REE primitive mantle compositions from McDonough and Sun (1989). Symbols as for Fig.5.

**Geochronology:**

In Table 4, I summarize my new $^{40}Ar$-$^{39}Ar$ age data for 9 samples from Harrat Ithnayn and one sample that I interpret is from the northern boundary of Harrat Khaybar **(HI-20)**. The complete geochronological data files for all samples are available in the Appendices Section. I did 13 age experiments: 3 samples (HI-15, 13, and 12) were analyzed twice because either the first run resulted a significant atmospheric argon $^{40}Ar$ or/and there were enough materials to be re-analyzed in an effort to improve precision and to check reproducibility. I obtained reliable plateau ages for 12 experiments, and these ages range from 33.8 to 467.3 Ka. Most of these plateau ages have congruent isochron ages with intercepts of the atmospheric ratio of $^{40}Ar/^{36}Ar$. The second run of HI-15 sample is the only experiment that did not produce a reliable plateau age, and in this case, I use the isochron age as the more reliable indication of crystallization age (Table 4). Also, only three experiments (HI-15, 12, and 4) have isochron ages that are not consistent with plateau ages. These three samples (and the second run of HI-13) are the only ones that show evidence of significant excess $^{40}Ar$ (Fig. 12). Excess $^{40}Ar$ in the age spectra of these samples is most likely due to undetected xenolithic and/or olivine fragments in the groundmass separate (Duncan and Alamri, 2013; Duncan et al., 2016). Fine grain size textures are seen in groundmasses of many of my thin sections, which can lead to $^{39}Ar$ and $^{37}Ar$ recoil effects (re-distribution of these isotopes from high-concentration to low-concentration minerals). Evidence of the recoil effect was noticed in the HI-7 sample age spectrum, especially in the first two steps (Fig. 13). Nonetheless, using the ArArCALC program (Koppers, 2002) allows us to eliminate this problem by removing the steps that show evidence of $^{40}Ar$ excess and/or the $^{39}Ar$ recoil effect to calculate a more statistically reliable age plateau and isochron. In addition, I compared between ages of total fusion and plateau ages and found that total fusion ages are slightly older by an average of about 3%, indicating that excess $^{40}Ar$ is a minor problem. However, the precision in the plateau ages, measured by 2s error, was improved by an average of ~27%. The duplicate age analyses of the three samples (HI-15, 13, and 12) show that the range of 2s error of the plateau ages was significantly reduced in the

second run by an average of about 50%. The second run of these samples produced plateau ages slightly older than the initial determinations (by an average of ~10%), but all of the ages are consistent within 2s errors.

These new $^{40}Ar$-$^{39}Ar$ age are considerably younger and less variable than the previously reported K/Ar ages of Camp and Roobol (1991) (0.04 to 3 Ma). Also, my new age determinations are consistent with the volcanic stratigraphy of the geologic map of the Cenozoic lava fields of Harrats Khaybar, Ithnayn, and Kura (Roobol and Camp, 1991) rather than the earlier Fairer (1986) geologic map of the Harrat Ithnayn quadrangle, Sheet 26D. The interpretation of the sample ages and stratigraphy is further assessed in the Discussion Section under the sub-section of "Timing of magmatism at Harrat Ithnayn". $^{40}Ar$-$^{39}Ar$ age spectra and isochron plots of all experiments are in the Appendices Section (see the Geochronological data section, page 59)

**(Table 4): A summary table for my new $^{40}Ar$-$^{39}Ar$ determinations for lava flows from Harrat Ithnayn, western Saudi Arabia**

| Sample # | Unit based on 1986 Map | Unit based on 1991 Map | Total fusion (Ka) | 2s error (Ka) | Plateau age (Ka) | 2s error (Ka) | N | MSWD | Isochron age (Ka) | 2s error (Ka) | MSWD | 40Ar/36Ar initial | 2s error | Comment |
|---|---|---|---|---|---|---|---|---|---|---|---|---|---|---|
| **HI-15** | **QTb5** | **Qb5** | 215.2 | 110.6 | 205 | 70.6 | 31 | 0.1 | 135 | 142.4 | 0.1 | 298 | 9 | Excess 40Ar |
| **HI-15 *** | **QTb5** | **Qb5** | n/a | n/a | n/a | n/a | n/a | n/a | 10.2 | 3.5 | 1.04 | 290 | 4 | Plateau age is not reliable |
| **HI-3A** | **QTb5** | **Qb6** | 172.8 | 70.8 | 171.5 | 60 | 36 | 0.25 | 172.8 | 87.7 | 0.32 | 297 | 2 | |
| **HI-13** | **QTb4** | **QTm1** | 110.9 | 47.6 | 93.5 | 40.4 | 35 | 0.09 | 93.3 | 56.9 | 0.12 | 296 | 4 | |
| **HI-13 *** | **QTb4** | **QTm1** | 101.2 | 22.7 | 105.6 | 24.5 | 37 | 2 | 108.4 | 35.4 | 7.07 | 316 | 8 | Excess 40Ar |
| **HI-7** | **QTb1** | **Qb5** | 30.6 | 8.4 | 33.8 | 8.3 | 18 | 1.27 | 34.8 | 12.1 | 1.99 | 299 | 4 | |
| **HI-12** | **QTb1** | **Qb5** | 127.2 | 86.7 | 108.9 | 54 | 34 | 0.14 | 10.9 | 13.1 | 0.1 | 303 | 14 | significant error |
| **HI-12 *** | **QTb1** | **Qb5** | 127.1 | 19.8 | 117.4 | 18.9 | 37 | 1.14 | 118.4 | 30.3 | 1.51 | 302 | 4 | |
| **HI-19** | **QTb1** | **Qb4** | 127.8 | 8.3 | 125.2 | 7.6 | 36 | 1.06 | 123 | 13.3 | 1.43 | 302 | 7 | |
| **HI-11** | **QTb1** | **Qb5** | 109.7 | 28.4 | 113.3 | 16.4 | 18 | 1.15 | 112.7 | 24.5 | 1.45 | 297 | 1 | |
| **HI-14** | **QTb1** | **QTm2** | 456.9 | 23.5 | 467.3 | 22.6 | 18 | 1.5 | 487.7 | 42.9 | 1.49 | 295 | 2 | |
| **HI-20** | **QTb3 (KHB ?)** | **Tj2** | 2110 | 30 | 2110 | 20 | 36 | 0.35 | 2110 | 50 | 0.44 | 296 | 3 | |
| **HI-4** | **QTb3 (KHB ?)** | **QTm2** | 291.4 | 27.2 | 280.8 | 19.6 | 37 | 0.77 | 239.3 | 36.2 | 0.62 | 289 | 3 | Excess 40Ar |

I used sanidine monitor FCs (28.201 Ma) and the total decay constant $\lambda$ = 5.530E-10/yr in my age calculation. N is the number of heating steps (defining plateau/total); MSWD is an F-statistic that compares the variance within step ages with the variance about the plateau age.

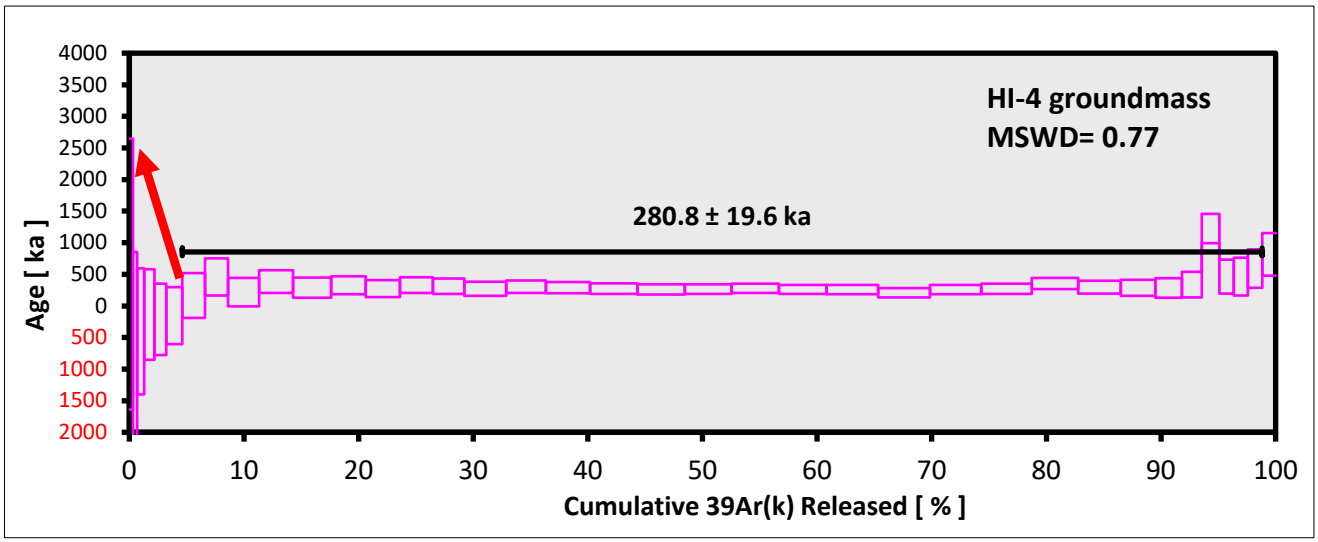


Figure 12: Evidence of excess 40Ar is shown in the 40Ar-39Ar age spectrum of sample HI-4.

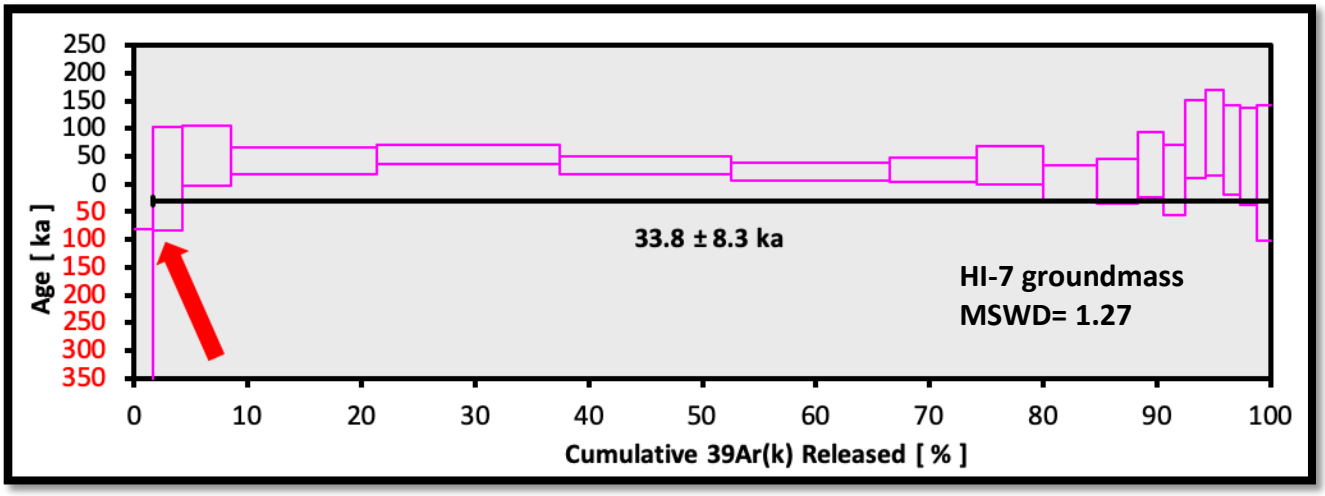


Figure 13: Evidence of Ar loss is shown in the 40Ar-39Ar age spectrum of sample HI-7.

## 5- Discussion:

### 5.1 Timing of magmatism at Harrat Ithnayn:

The new $^{40}Ar$-$^{39}Ar$ plateau age determinations for lava flows from Harrat Ithnayn range from 33.4 to 467 Ka. Overall, ages are younger and the duration of activity shorter than the previous age determinations of Camp and Roobol (1991), using the K/Ar total fusion technique (0.04 – 3Ma). It is worth mentioning that the previous ages were determined on lava flows from the Khaybar volcanic field only (Appendices Section, Figure 10), and inferring for Harrat Ithnayn based on common volcano-stratigraphic units. Because Camp and Roobol (1991) and the geologic map of Roobol and Camp (1991a) treated Harrats Khaybar and Ithnayn as two integrated lava fields and used the same volcanic stratigraphic classification for both harrats, they applied their age analyses of Harrat Khaybar to the stratigraphy of Harrat Ithnayn. The fieldwork team tried to collect samples from the oldest volcanic subunits of Mukrash Basalt, QTm1 and QTm2, based on the latest geologic map of Roobol and Camp (1991a), and all of these samples revealed ages < 500 Ka (Table 3), which is considerably younger than the previous interpreted age range of 3.29 Ma to 0.41 Ma (Camp and Roobol, 1991). The fieldwork team also collected one sample from the northern part of Harrat Khaybar, specifically from **Tj2**, a subunit of Jarad Basalt that had a previous K/Ar total fusion age range from 3.14 – 4.18 Ma (Table 3). The new age determination by the$^{40}Ar$-$^{39}Ar$ laser step heating technique is significantly younger than this range by about 1.3 Ma, and was 2.11 ± 0.03 Ma.

I assume that the dissimilarity between the two age determinations of Camp and Roobol(1991) and this study is caused by two reasons: (1) units and subunits classification at Harrat Ithnayn on the previous study and map (Camp et al., 1991; Roobol and Camp, 1991a); (2) un-degassed “excess” $^{40}Ar$ that is carried by the abundant fragments of olivine and clinopyroxene xenoliths that more likely were undetected during the previous K/Ar age analyses, possibly leading to older and erroneous total fusion

age results. The latter reason was responsible for age dissimilarity between the newer and older age determinations at Harrat Hutaymah and Lunayyir (Duncan and al-Amri, 2013; Duncan et al., 2016).

Although the previous studies did not make any age determinations on any samples from Harrat Ithnayn, using the integrated stratigraphic classification of units and subunits of Harrat Khaybar and Ithnayn in the Camp et al. (1991) study and the Roobol and Camp (1991a) map to determine ages of lava flows in Harrat Ithnayn seems a reasonable solution because of what they have in common regarding their compositions and volcanic characteristics. However, many volcanic events are also potentially neglected by this approach. Hence, a separate and specific age study on samples from Abyad and Mukrash basalts of Harrat Ithnayn was required to determine the actual span of volcanic activity. This also provides a better assessment of the hypothesis of volcanic progression along the MMN line since the new age determination shows that even Mukrash Basalt subunits, the older unit at Harrat Ithnayn, exhibit an age range that is less than 500 Ka (Table 3). This means that Harrat Ithnayn has formed in a significantly shorter time span, making it the youngest of the harrats along the MMN line. Also, I suggest that a re-mapping of the stratigraphic units and subunits at Harrat Ithnayn is needed using the available age data, coupled with other surface exposure (cosmogenic) dating techniques such as $^{36}Cl$ to construct a high-resolution geologic map, similar to the work done at Harrat Al-Madinah in the northernmost part of Harrat Rahat (Downs et al., 2018).

An additional reason why I believe that the new age determinations are not compatible with the previous age determinations of Camp and Roobol (1991) study and the Roobol and Camp (1991a) map is that the field observations and petrographic analysis of Ithnayn lava flows show evidence of high abundance of olivine and clinopyroxene xenolithic fragments which they more likely carry mantle-derived "excess" $^{40}Ar$. Harrat Ithnayn is a well-known site for xenolithic materials in which many researchers have chosen the volcanic field to pursue answers for their specific research questions (e.g. Stoeser and Camp, 1985; McGuire and Stern, 1993; Konrad et al., 2016). The size of these xenoliths can reach more than 10 cm in size (McGuire and Stern, 1993). Many believe that the

xenolithic “nodules” are fragments of upper and lower crust that have ages of ~ > 750 Ma, which is compatible with ages from the buried part of the Arabian shield beneath Harrat Ithnayn “Hijaz and Afif terranes” 700 – 800 Ma (McGuire and Stern, 1993). I believe this is more likely to be the cause of many of the older previously reported K/Ar ages. Also, this might explain the cause of the appearance of $^{40}$Ar “excess” in $^{40}$Ar-$^{39}$Ar age spectra of a few samples such as (Fig. 12). However, having the ability of evaluating the effect of xenolithic materials in $^{40}$Ar-$^{39}$Ar age spectra from the non-concordance of step ages makes the new ages more reliable than previous K/Ar ages.

The oldest lava flow measured (HI-14, 468 Ka) was collected near Al-Nub’wan village, and from the older subunit of Mukrash Basalt (QTm2) which is located between the youngest subunits of Abyad Basalt (Qb5 and Qb6) (Fig. 5), while the youngest lava flow (HI-7, 33.4 Ka) measured was collected near Al-Masa’a village, about 20 miles away from the oldest sample’s location. It erupted from a fissure-like structure where its lava flows cover a large area and based on the geologic map of Roobol and Camp (1991a) it should be under the (Qb5) subunit of Abyad basalt. However, this range of ages appears to be incompatible with the overall time-space variation of volcanism throughout the area of Harrat Ithnayn, but the coverage and consistency of age determinations most likely indicates that Ithnayn volcanism was confined to late Quaternary time (> 500 Ka). This finding also agrees with the hypothesis of volcanic progression along the MMN line, where the volcanic activity started at Harrat Rahat (10.0 Ma), then Khaybar (2.3 Ma), and finally began at Harrat Ithnayn (467 Ka) (Fig. 14) (Moufti et al., 2013; Kent et al., in progress; this study).

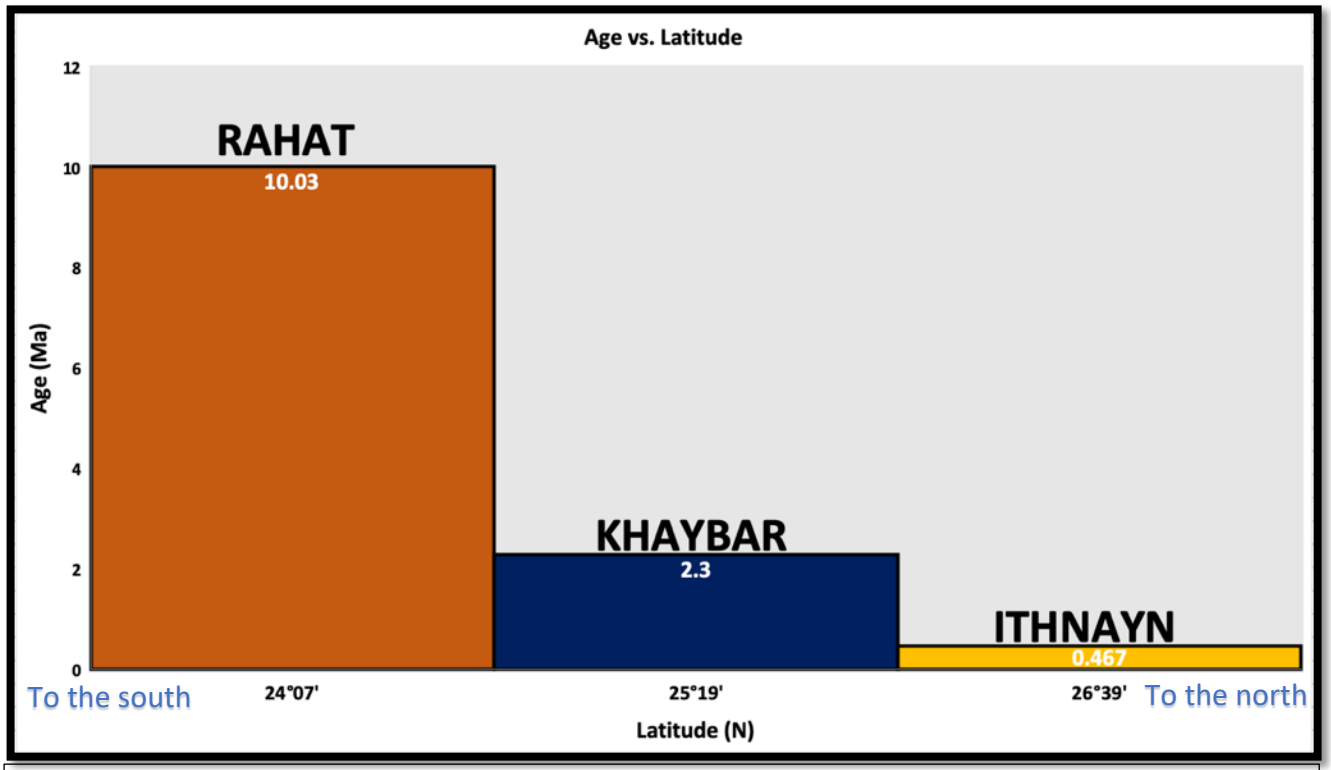


Figure 14: This bar chart shows the most recent $^{40}Ar$-$^{39}Ar$ age data from the three harrats along the MMN line. These ages and latitudes represent the oldest lava dated for each of these harrats (Moufti et al., 2013; Kent et al., in progress; this study). This illustrates the South-to-North volcanic progression along MMN line.

### 5.2 Causes of Chemical Variations in Harrat Ithnayn Lavas:

Although there is a narrow range of rock types present at Harrat Ithnayn lavas (from alkali basalt to trachybasalt), Ithnayn lavas exhibit important variations in their chemical composition. Chemical variations among major elements (see Figure. 5-9) are less variable than those data of trace elements. I suggest that there are three possible sources that lead to this variability in chemical composition. These three possible causes of chemical variations that I examine below are: (1) crystal fractionation, (2) variations in mantle sources and degree of melting, and (3) crustal assimilation. The order of the suggested causes is based on the importance of their roles.

### 5.2.1 Crystal fractionation:

Based on the petrographic evidence and forward MELTS modeling of the crystallization path (liquid line of descent) for a representative primary magma from Harrat Ithnayn (Table 2), I observe that most chemical variations in major element and compatible trace elements compositions and are controlled by the polybaric crystal fractionation, which took place over a different range of upper mantle and crustal pressures. This suggests that the erupted lavas of Harrat Ithnayn are from similar primary magma compositions and underwent similar crystal fractionation processes. The dominating abundance of olivine in phenocryst and groundmass phases of Harrat Ithnayn rocks, and the clear decrease of compatible elements such as Ni and Cr with MgO (Fig. 9), indicate that the crystal fractionation of olivine plays a key role in the earliest stages of fractionation. The following stages of crystal fractionation are dominated by clinopyroxene and plagioclase crystallization, as it is evidenced by their presence in some of phenocryst phases and dominance in groundmass phases. The low contents of CaO (Fig. 8) and $CaO/Al_2O_3$ ratio at lower MgO contents (Fig. 15) in a large number of Ithnayn lava compositions also can provide evidence of clinopyroxene and plagioclase fractionation. It is observed that at a given MgO content lavas from Harrat Ithnayn show a range of CaO and $CaO/Al_2O_3$ contents that move to lower CaO and $CaO/Al_2O_3$. These shifts to lower CaO and $CaO/Al_2O_3$ contents appear from higher MgO lava compositions (~10.4 wt.%) to lower MgO lava composition (~7.40 wt.%) (see Fig. 9 and 15). Also, the liquid lines of descent (crystallization path) for clinopyroxene and plagioclase removal is significantly sensitive to pressure; therefore, this provide constraints on pressure(s) of crystal fractionation (Duncan et al., 2016). Accordingly, the MELTS models show that Ithnayn lava compositions come across are compatible with crystal fractionation of clinopyroxene that occurred from higher pressures that is a slightly over 10 kbar to lower pressures about 1 kbar. This range of pressures, corresponding to depths of about 40 – 4 km, illustrated by olivine and clinopyroxene fractionation in CaO, FeO, and other major elements are equivalent to depths of the top part of the upper mantle continuing to lower crust. This range of depths correspond with off-MMN-

axis harrats where the depth ranges are almost identical (Duncan et al., 2016). In addition, the appearance of some minor euhedral plagioclase phenocrysts in some of Ithnayn lavas should not be neglected because it might provide some evidence for the depth of crystal fractionation (Appendices Section, page 51). I agree with Camp et al. (1991) on the depth of crystal fractionation that the occurrence of minor plagioclase phenocrysts and its association with spinel-free olivine observed indicate that some of these magmas fractionated at moderate crustal pressures within the stability field of plagioclase peridotite, above the spinel zone ~ < 28 km (Camp et al., 1991). On the other hand, high abundances of the transported upper and lower crustal xenoliths that are found in many of Harrat Ithnayn lavas (e.g. McGuire and Stern, 1993; Konrad et al., 2016) could indicate a relatively rapid ascent of magmas from the uppermost mantle or lower crust to the surface. Overall, these chemical variations in lavas from Harrat Ithnayn do not indicate that crystal fractionation processes occurred in high-level magma chambers, which make Ithnayn lavas different from those older MMN line lavas to the south (e.g. Khaybar and Rahat).

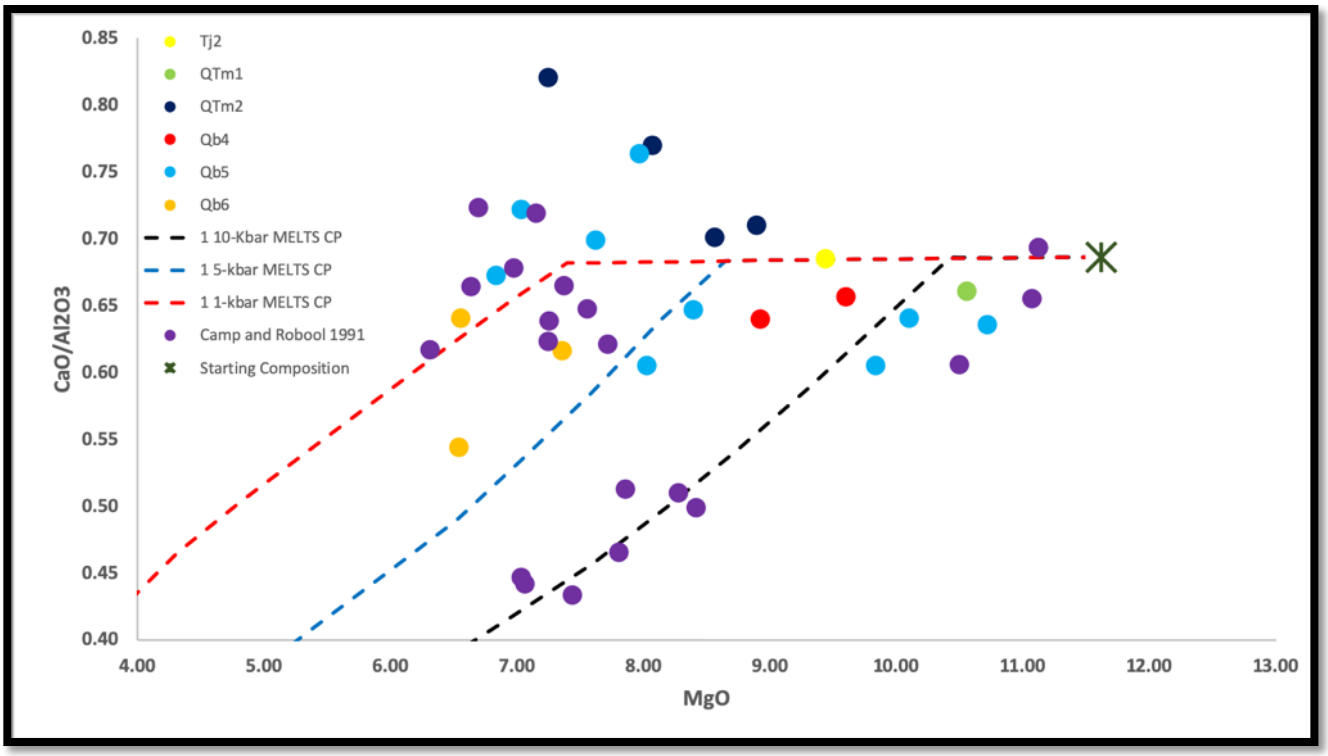


Figure 15: The bivariate diagram of MgO vs. $CaO/Al_2O_3$ (wt.%) illustrates the effect of clinopyroxene crystal fractionation at different pressure zone, especially those lavas of lower MgO contents. Also, it shows calculated liquid lines of descent for fractional crystallization of a representative primary liquid (see Table 2) determined using MELTS (Ghiorso and Sack, 1995). Red: 1-Kbar, Blue: 5-Kbars, and Black: 10-Kbars.

### 5.2.2 Variations in mantle sources and degree of melting:

The chemical variations in major, trace element, and more importantly REE compositions can provide insight into mantle sources and conditions of melting. Variations in major element concentrations and REE patterns can be correlated to depth of mantle sources since they are produced from mantle mineralogy (plagioclase-spinel-garnet stability fields) that is depth dependent (Ellam, 1992; Duncan and Al-Amri, 2013). Also, REE distributions are sensitive to mantle melt sources, and in the case of continental volcanism, these mantle sources are significantly influenced by solidus pressures (melting points), melt productivity (how much melt is produced per unit of decompression), and the pressure where melting ceases, which is affected by lithosphere thickness (Farm and Lesher, 1992; Duncan et al., 2016). Incompatible element concentrations in residual mantle minerals, on the other hand, can be strongly affected by the degree of partial melting, and as a rule of thumb, incompatible element concentrations decrease as the degree of partial melting increases (White, 2013). Therefore, variations in degree of melting can be detected by using incompatible element data, and mantle sources can be indicated by REE patters.

Concentrations of incompatible elements for Ithnayn lavas indicate that variations in degree of partial melting and/or mantle sources play a key role along with crystal fractionation in the chemical variability. I notice significant incompatible element assemblages at a given value of MgO (e.g. La, Rb, and Nb/Zr), similar to what it is noted above with some major elements, $K_2O$, $Na_2O$, and $P_2O_5$ (Fig. 6 and 7). This more likely an indication of variations in degree of partial melting, from higher to lower partial melting. However, these assemblages of incompatible element concentrations do not correlate well with the volcanic stratigraphy, in general, the younger lavas (HI-15, 12) have higher values of incompatible element contents (La > 30 ppm, Rb > 20 ppm, Nb/Zr > 0.15) which can indicate lower degree of melting.

I did a simple batch melting calculation of REE distributions, suggesting that Ithnayn lavas can be produced by garnet lherzolite melting of a primitive mantle source. Also, relatively high values of

heavier REE concentrations and ratios such as (Ce/Yb up to ~ 35.2, $[Sm/Yb]_N$ 2 – 3.4) that are sensitive to the occurrence of garnet in the mantle melting indicate greater depth of mantle melt separation from residual (> 60 km) (Ellam, 1992; Duncan and Al-Amri, 2013). LREE concentrations are slightly less enriched (i.e. $[La/Sm]_N$ ~ 1.4 – 3.8) (see fig. 7), suggesting that lavas of Harrat Ithnayn can be produced from higher degree of partial melting, greater than those lavas from Harrat Hutaymah, located off-MMN line, which show relatively higher enriched LREE (i.e. $[La/Sm]_N$ ~ 2.5 – 4.5) (Duncan et al., 2016). In addition, the strongly enriched and less variable LREE patterns of some off-MMN harrats (e.g. Harrat Lunayyir) is mainly attributed to fractional crystallization processes rather than variations in degree of partial melting (Duncan and Al-Amri, 2013). Unpublished data from Khaybar lava (Kent et al., in preparation) show a wider range of LREE concentrations from relatively less enriched to strongly enriched (i.e.$[La/Sm]_N$ ~ 1.4 – 5.2), which agrees with the data from Harrat Ithnayn in that MMN line lavas over all seen to be generated by higher degrees of partial melting (e.g. Camp et al., 1991; Duncan and Al-Amri, Duncan et al., 2016).

In order to constrain the melting conditions beneath Harrat Ithnayn, I have used the approach of Fram and Lesher (1993) and Brown and Lesher (2014). The ultimate goal of this approach is to define the pressure (depth) at which the mantle melts start and cease, and to estimate the degree of melting through a more sophisticating forward modeling of non-modal incremental batch melting in an upwelling mantle melting column, using the computed REE contents (Fram and Lesher, 1993; Brown and Lesher, 2014). Duncan and Al-Amri (2013) and Duncan et al. (2016) applied this modeling method to magmas from Harrat Lunayyir and Hutaymah, and I continue their work to understand the melting conditions beneath Harrat Ithnayn and other the younger volcanism phase in Western Saudi Arabia, especially those located along the rifting zone of MMN line. This will also test the hypothesis of the higher degree of melting and thinning of lithospheres beneath the MMN-line harrats (e.g. Camp and Roobol, 1989; Camp et al., 1991).

I have used the MATLAB script "REEBOX" to do the calculation for this forward modeling (Brown and Lesher, 2014). This a polybaric non-modal fractional melting model used to describe the upwelling mantle melting conditions. I applied the same parameters of the mantle source that Duncan et al. (2016) used in the REEBOX model (i.e. partition coefficients for REE from McKenzie and O'Nions (1991); melt productivity sets at 1.0% per 0.1 GPa) to reproduce the higher values of REE contents and to make comparing between those harrats data achievable. I also use a primitive mantle source starting composition in this model. In addition, sensitivity analysis that compares between input and output values was done, showing that an incorrect estimation of mantle source can produce a higher uncertainty (Appendices Section, page 56) (Brodie et al., 1994).

The REEBOX uses the two rare earth element ratios of $[Dy/Yb]_N$ and $[La/Sm]_N$. The $[Dy/Yb]_N$ ratio is in the Y axis and it is more sensitive to depth, whereas the ratio of $[La/Sm]_N$ is in the X axis and is more sensitive to the degree of melting. Therefore, the low $[Dy/Yb]_N$ means a shallower depth and lower solidus pressure, while a low $[La/Sm]_N$ means a higher degree of melting and vice versa. REEBOX also allows estimation of the pressure at which melting ceases, which is interpreted to reflect the thickness of the lithosphere, as this controls the extent of melting in an upwelling mantle column.

The result of the REEBOX modeling is shown in (Fig. 17). It is suggested that mantle melts beneath Harrat Ithnayn started at pressures that are approximately between 2.3 and 2.8 GPa, and ceased at pressures from about 1.4 to 2.3 GPa, which is equivalent to lithospheric thickness "lid" of 45 – 75 km. Also, mantle melts of Harrat Ithnayn were produced by relatively higher degrees of partial melting from ~ 2 – 14% (most of magmas have degree of melting ~> 5%). This illustrates that most of the mantle melts beneath Ithnayn have similar characteristics to mantle melts beneath those located along the MMN line (e.g. Rahat ~ > 7% and up to 15% of partial melting, Khaybar ~ > 4% and up to 16%), although the range of lithospheric thickness beneath is relatively thicker according to this model (Duncan et al., 2016; Kent et al., unpublished data). On the other hand, harrats that are peripheral to the MMN line (e.g. Lunayyir, Hutaymah) exhibit lower ranges of partial melting (2 – 10%, 1 -7%,

respectively) with considerably thicker lithosphere "lid" 50 – 80 km (Duncan et al., 2013; Duncan et al., 2016).

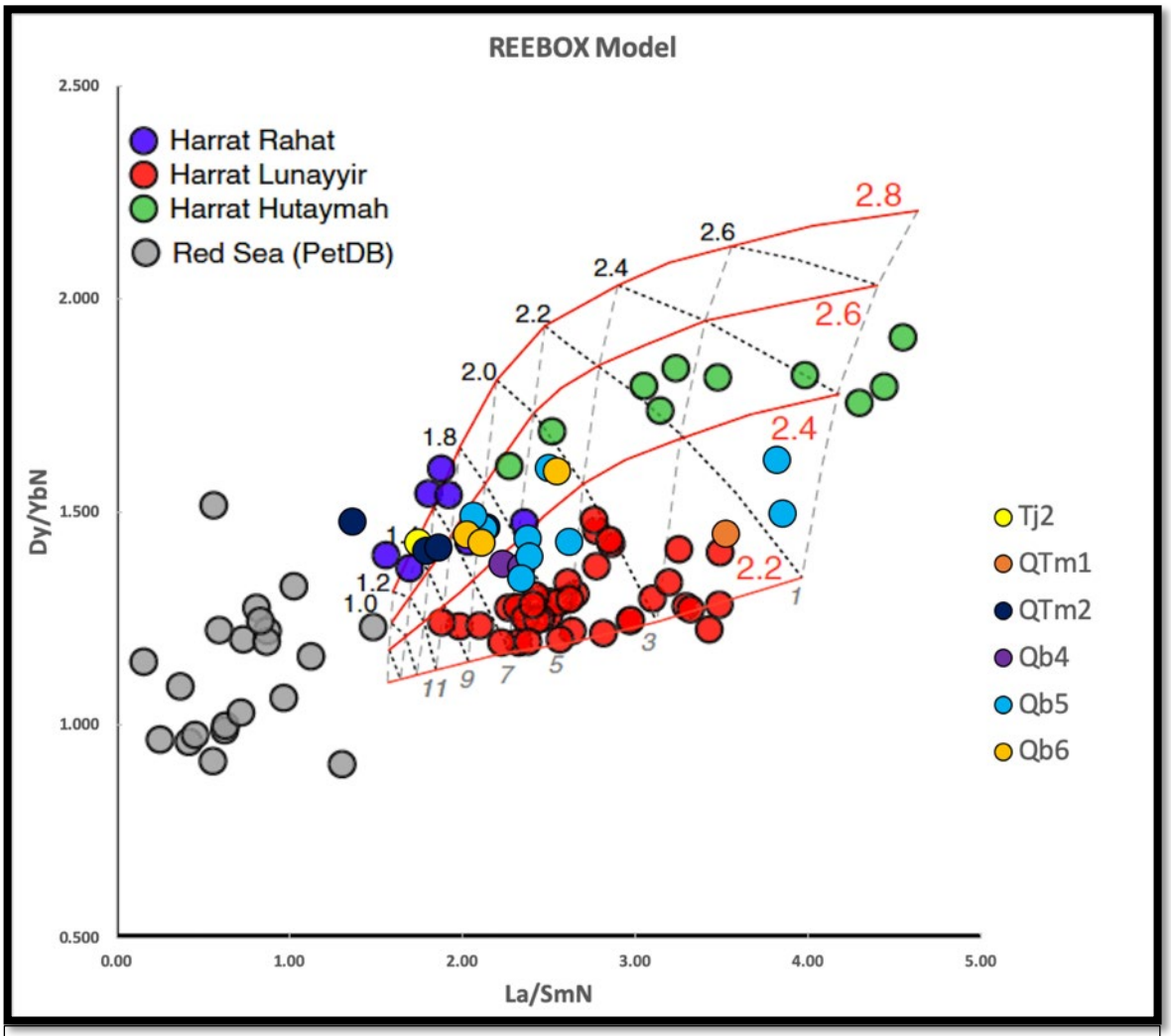


Figure 17: The result of the MATLAB script "REEBOX" calculations (Lesher and Brown, 2014). The thick red lines show the solidus pressure, and the dashed black lines illustrate the pressures of cessation of melting, while fine gray dashed lines and numerals exhibit the melt fraction as percent. It is worth noting mention that the Red Sea values (gray) are not modeled because they are from very shallow and depleted mantle source. (After Duncan et al., 2016). Red dots are values of Harrat Lunayyir (peripheral to the MMN line), whereas blue dots represent values of Harrat Rahat (on-MMN line) (Moufti and Hashad, 2005). Pressures are in GPa unit (1 GPa = 10 Kbar).

### 5.2.3 Crustal assimilation:

I also investigate whether addition of continental crustal material can cause the chemical variations in lavas from Harrat Ithnayn. It is common in continental volcanism settings that lavas compositions are influenced by crustal material, especially in a thick crust setting such as the Arabian-

Nubian Shield (ANS) (~ up to 85 km thick) (Kent et al, 2002). However, based on the previous strong evidence of chemical variation causes (i.e. polybaric fractionation, degree and depth of melting variation), and relatively homogenous compositions of Ithnayn lavas suggest that crustal contamination remains remarkably minor, and little chemical variability by crustal assimilation can be justified. A couple of incompatible element concentrations and ratios are sensitive to crustal assimilation (e.g. K/Nb, Ba/Nb, and K contents). Ithnayn lavas show relatively greater range of K contents and K/Nb (2,800 – 12,000 μg/g and 120 – 450, respectively), compared to other harrats such as Harrat Hutaymah (Duncan et al., 2016). Nonetheless, comparing these values to the average upper crustal values of potassium and K/Nb (28,000 μg/g and 500 – 1500, respectively, from Kent et al. (2002) shows agrees that crustal contamination does not play a key role in chemical variability in Ithnayn lavas.

However, I did a further investigation for the role of crustal assimilation, as I have calculated assimilation fractional crystal trends (AFC) for K and K/Nb similar to what it is used in Duncan et al. (2016) (Fig. 18, and Appendices Section, page 58). This shows that significant rapid increases in K contents and K/Nb ratios with decrease in MgO contents are caused by an increase in crustal assimilation during progressive crustal fractionation. Lava compositions from Harrat Ithnayn exhibit a wider range of crustal assimilations that occur at mass ratio of assimilated to crystallized material ($r$) < 0.1 to 1 (Kent et al., 2002; Duncan et al., 2016). Thus, this greater range of $r$ ratios suggests a greater role of crustal assimilation in causes of chemical variations for Ithnayn lavas. Hence, I recommend an isotopic compositions study (Sr, Nd, Pb, and O) for these lavas to investigate any compositional modification caused by crustal contamination.

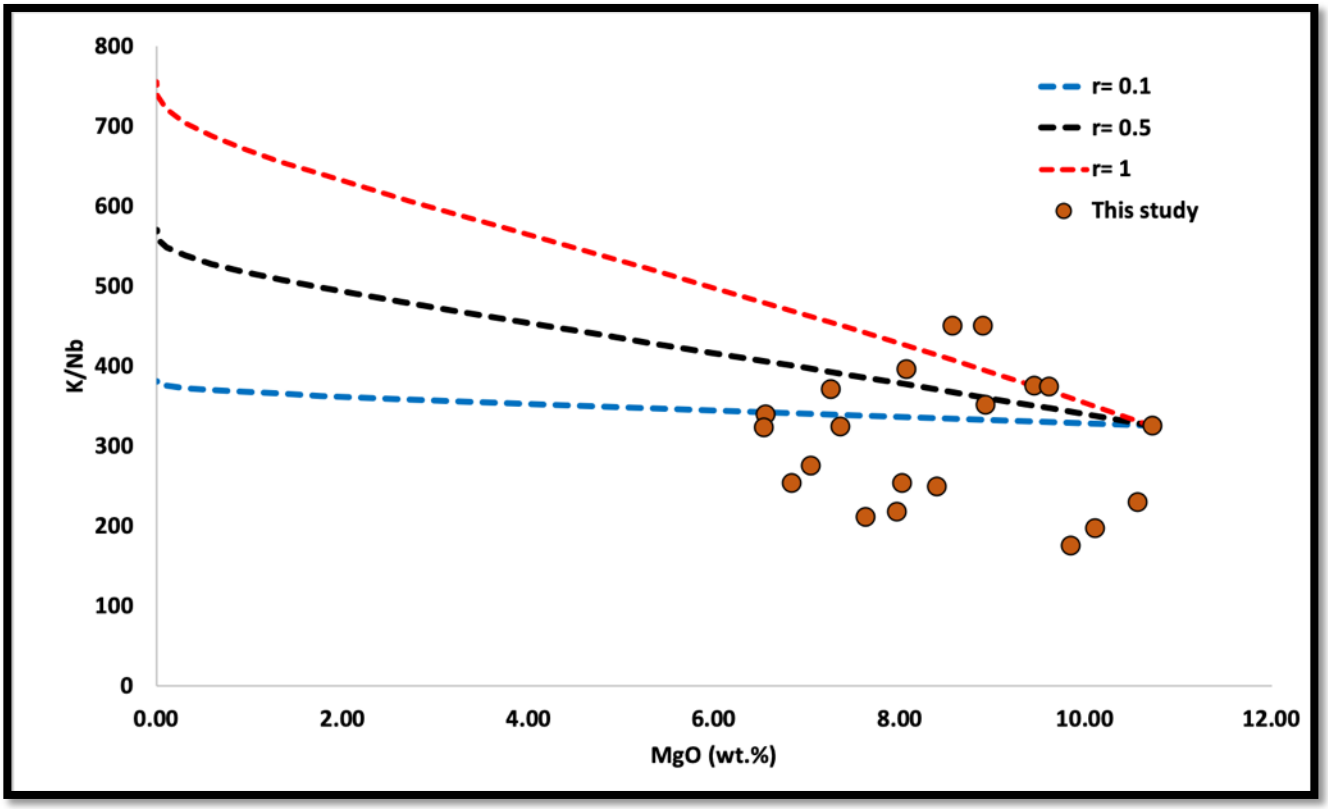


Figure 18: This is a scatter diagram of K/Nb ratio vs. MgO concentrations. Data shown here are only from this study, Camp and Roobol (1991) are excluded because of the lack of trace element concentrations (i.e. Ba and Nb). Lines are the assimilation fractional crystallization (AFC) trends for mass ratio of assimilated to crystallized material ( r ) (blue: 0.1, black: 0.5, and red: 1). Background data of the average upper continental used in this model are from Kent et al. 2002.

### 5.3 Regional Implications:

Harrat Ithnayn is the latest episode of the volcanism in the MMN line volcanic system. The new $^{40}Ar$-$^{39}Ar$ age determinations (467 – 33.4 Ka) show that Ithnayn is the youngest volcanic field of the three harrats that constitute the MMN volcanic line system (Rahat > 10 Ma, Khaybar > 2.3 Ma, and Ithnayn > 0.46 Ma) ((Moufti et al., 2013; Kent et al., in preparation; this study). It is worth mentioning that Kura Basalt in Harrat Khaybar show older ages (> 8 Ma), but still younger than the older lavas from Harrat Rahat (> 10 Ma) (Kent et al., unpublished). An age versus latitude diagram illustrates that the northward volcanic time progression does exist in the inception of volcanism along

MMN line (Fig. 19). Also, in this diagram, I added the latest measurement of $^{3}He/^{4}He$ ratios at the MMN line harrats (Murcia et al., 2013; Kent et al., unpublished). I notice that oldest harrats along MMN line are associated with the highest values of $^{3}He/^{4}He$, and a considerable decrease in values of $^{3}He/^{4}He$ with decrease in age, and thus with latitude (Rahat up to 11.8 $R_A$, Kura Basalt 12.7 $R_A$, Khaybar 8.3 $R_A$). This implies probably explained by that the older harrats along the MMN volcanic line system are the most influenced by the Afar mantle plume materials. The research team is aiming to investigate this hypothesis further with samples from Harrat Ithnayn to determine whether 3He/4He values decrease with time or not.

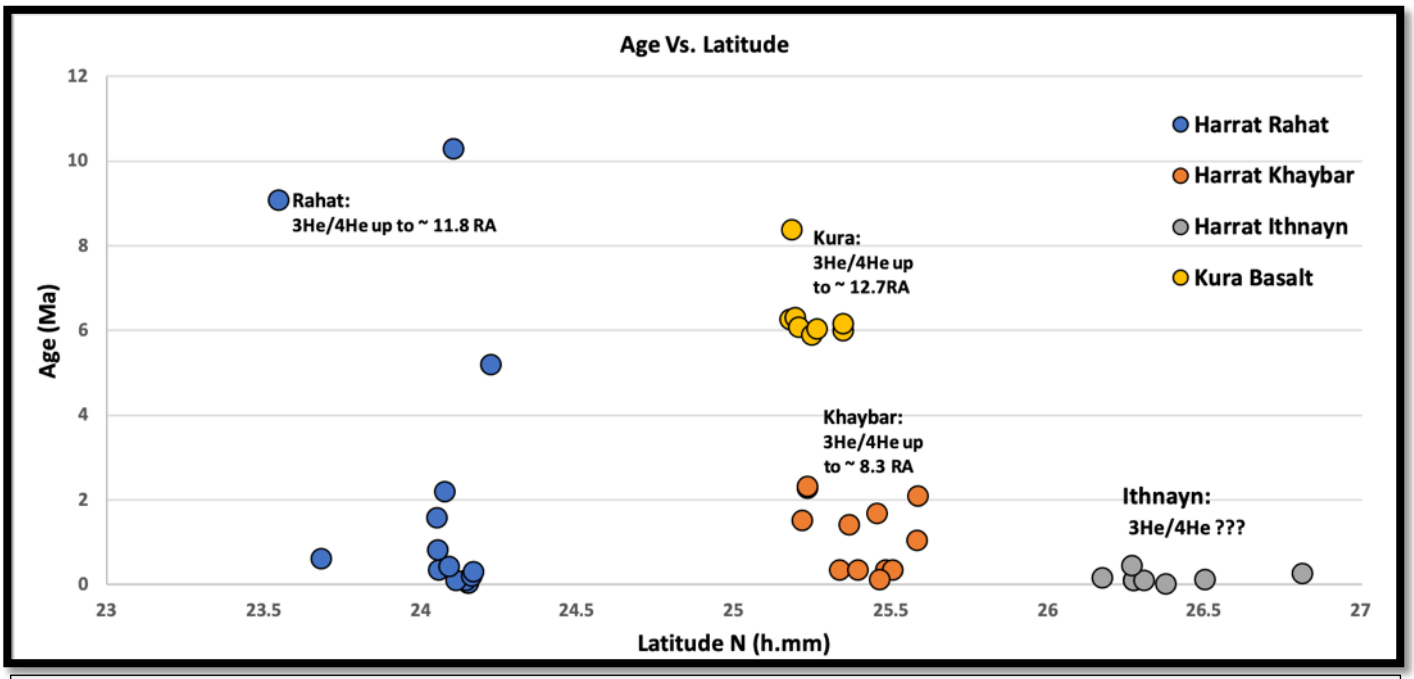


Figure 19: This scatter diagram (age vs. latitude) shows the most recent $^{40}Ar$-$^{39}Ar$ age data from the three harrats along the MMN line (Moufti et al., 2013; Kent et al., in preparation; this study). This illustrates the South-to-North volcanic progression along MMN line. I have treated Kura Basalt (yellow) as the oldest volcanic unit at Harrat Khaybar.

## 6- Conclusions:

Harrat Ithnayn is the northernmost and the least studied volcanic field in the Makkah-Madinah-Nafud (MMN) line. The new $^{40}Ar$-$^{39}Ar$ age determination ranges from 33.4 – 467 Ka, which suggests that Ithnayn lavas are much younger and formed in a shorter life span than previously thought (0.04 – 3Ma) (Camp et al., 1991). The considerably shorter life span of volcanism at Harrat Ithnayn compared to the previous ages is that the previously determined age was based on the K/Ar age determinations on lavas from Harrat Khaybar only followed by applying these ages on the integrated volcanic stratigraphy of the joint harrats (Khaybar and Ithnayn), which produced significantly older range of ages. This also makes Harrat Ithnayn the youngest volcanic lava field along the MMN line, indicating that the South-to-North volcanic progression does exist through using the most recent data of $^{40}Ar$-$^{39}Ar$ age determination (Moufti et al., 2013; Kent et al., unpublished; this study) (Figure, 13). However, northward volcanic progression within these volcanic fields has not been identified yet because this would require an intensive effort and wider sampling coverage. I suggest that a re-mapping of the stratigraphic units and subunits at Harrat Ithnayn is needed using the available age data, coupled with other surface exposure (cosmogenic) dating techniques such as $^{36}Cl$ to construct a high-resolution geologic map, similar to the work done at Harrat Al-Madinah in the northernmost part of Harrat Rahat (Downs et al., 2018).

Petrographic evidence and geochemical modelling indicate that chemical variations are mainly caused by crystal fractionation, predominantly of olivine (spinel-free and Cr spinel inclusion), clinopyroxene, and plagioclase. Crystal fractionation occurred over a range of crustal and mantle pressures, (~> 10 – less than 1 Kbar). On the other hand, incompatible trace element and REE concentrations imply that Ithnayn magmas were derived from mantle melts that vary in degree of partial melting (2 – 14%), and most magmas show evidence of primitive mantle source (garnet-field-stability) > 60 km. In an effort to better understanding the mantle melts beneath Harrat Ithnayn, I use the REEBOX forward model which suggests that melting under Ithnayn started at a pressures that are

approximately between 2.3 and 2.8 GPa, and ceased at pressures from about 1.4 to 2.3 GPa, which is equivalent to lithospheric thickness “lid” of 45 – 75 km. This illustrates that most of mantle melts beneath Ithnayn have similar characteristics to mantle melts beneath those located along the MMN line (e.g. Rahat ~ > 7% and up to 15% of partial melting, Khaybar ~ > 4% and up to 16%), although the range of lithospheric thickness beneath is relatively thicker according to this model. Finally, modeling of assimilation fractional crystallization (AFC) trends for incompatible element concentrations and ratios (e.g. K contents and K/Nb ratio) and mass ratio of assimilated to crystallized material ( r ) indicates that part of Ithnayn lavas modified via crustal assimilation ($r < 0.1 – 1$). Hence, further investigation for the role of crustal contamination in the chemical variability of Ithnayn lavas is recommended using isotopic compositions (Sr, Nd, Pb, and O).

**7- Bibliography:**

Bertrand, H., Chazot, G., Blichert-Toft, J., & Thoral, S. (2003). Implications of widespread high-μ volcanism on the Arabian Plate for Afar mantle plume and lithosphere composition. Chemical Geology, 198(1), 47-61.

Bohannon, R. G., Naeser, C. W., Schmidt, D. L., & Zimmermann, R. A. (1989). The timing of uplift, volcanism, and rifting peripheral to the Red Sea: A case for passive rifting? Journal of Geophysical Research: Solid Earth, 94(B2), 1683-1701.

Brown, E. L., & Lesher, C. E. (2014). North Atlantic magmatism controlled by temperature, mantle composition and buoyancy. Nature Geoscience, 7(11), 820.

Cabanis, B. (1989). Le diagramme La/10-Y/15-Nb/8: unoutil pour la discrimination des series volcaniques et la mise en evidence des processus de melande et/ou de contamination crustale. *CR Acad. Sci. Ser. II*, *309*, 2023-2029.

Camp, V. E., Hooper, P. R., Roobol, M. J., & White, D. L. (1987). The Madinah eruption, Saudi Arabia: magma mixing and simultaneous extrusion of three basaltic chemical types. Bulletin of Volcanology, 49(2), 489-508.

Camp, V. E., & Roobol, M. J. (1989). The Arabian continental alkali basalt province: Part I. Evolution of Harrat Rahat, Kingdom of Saudi Arabia. Geological Society of America Bulletin, 101(1), 71-95.

Camp, V. E., Roobol, M. J., & Hooper, P. R. (1991). The Arabian continental alkali basalt province: Part II. Evolution of Harrats Khaybar, Ithnayn, and Kura, Kingdom of Saudi Arabia. Geological Society of America Bulletin, 103(3), 363-391.

Camp, V. E., Roobol, M. John, & Saudi Arabia. Mudīrīyah al-ʻĀmmah lil-Tharwah al-Maʻdinīyah. (1991). Geologic map of the Cenozoic lava field of Harrats Khaybar, Ithnayn, and Kura, Kingdom of Saudi Arabia. Jiddah, Saudi Arabia]: Ministry of Petroleum and Mineral Resources, Directorate General of Mineral Resources.

Camp, V. E., Roobol, M. J., & Hooper, P. R. (1992). The Arabian continental alkali basalt province: PartI II. Evolution of Harrat Kishb, Kingdom of Saudi Arabia. Geological Society of America Bulletin, 104(4), 379-396.

Camp, V. E., & Roobol, M. J. (1992). Upwelling asthenosphere beneath western Arabia and its regional implications. Journal of Geophysical Research: Solid Earth, 97(B11), 15255-15271.

Chang, S. J., & Van der Lee, S. (2011). Mantle plumes and associated flow beneath Arabia and East Africa. Earth and Planetary Science Letters, 302(3), 448-454.

Chandarasekharam, D., & Aref, L. (2014). CO2 mitigation strategy through geothermal energy, Saudi Arabia. Renewable and Sustainable Energy Reviews, 38, 154-163.

Coleman, R. G., Gregory, R. T., and Brown, G. F., 1983, Cenozoic volcanic rocks of Saudi Arabia: Saudi Arabian Deputy Ministry for Mineral Resources Open-File Report USGS-OF-03-93, 82 p.

Daradich, A., Mitrovica, J. X., Pysklywec, R. N., Willett, S. D., & Forte, A. M. (2003). Mantle flow, dynamic topography, and rift-flank uplift of Arabia. Geology, 31(10), 901-904.

Duncan, R. A., & Al-Amri, A. M. (2013). Timing and composition of volcanic activity at Harrat Lunayyir, western Saudi Arabia. Journal of Volcanology and Geothermal Research, 260, 103-116.

Duncan, R. A., Kent, A. J., Thornber, C. R., Schlieder, T. D., & Al-Amri, A. M. (2016). Timing and composition of continental volcanism at Harrat Hutaymah, western Saudi Arabia. *Journal of Volcanology and Geothermal Research*, *313*, 1-14.

Downs, D. T., Stelten, M. E., Champion, D. E., Dietterich, H. R., Nawab, Z., Zahran, H., … Shawali, J. (2018). Volcanic history of the northernmost part of the Harrat Rahat volcanic field, Saudi Arabia. Geosphere (Boulder, CO), 14(3), 1253–1282. https://doi.org/10.1130/GES01625.1

Faccenna, C., Becker, T. W., Jolivet, L., & Keskin, M. (2013). Mantle convection in the Middle East: Reconciling Afar upwelling, Arabia indentation and Aegean trench rollback. Earth and Planetary Science Letters, 375, 254-269.

Fairer, George M. *Geologic Map of the Harrat Ithnayn Quadrangle, Sheet 26D, Kingdom of Saudi Arabia*. Vol. 26D. Jiddah: Directorate General of Mineral Resources, Ministry of Petroleum and Mineral Resources, 1986. Web.

Fram, M. S., & Lesher, C. E. (1993). Geochemical constraints on mantle melting during creation of the North Atlantic basin. Nature, 363 (6431), 712.

Ghiorso, M. S., & Sack, R. O. (1995). Chemical mass transfer in magmatic processes IV. A revised and internally consistent thermodynamic model for the interpolation and extrapolation of liquid- solid equilibria in magmatic systems at elevated temperatures and pressures. *Contributions to Mineralogy and Petrology*, *119*(2-3), 197-212.

Hansen, S., Schwartz, S., Al-Amri, A., & Rodgers, A. (2006). Combined plate motion and density-driven flow in the asthenosphere beneath Saudi Arabia: Evidence from shear-wave splitting and seismic anisotropy. Geology, 34(10), 869-872.

Ilani, S., Harlavan, Y., Tarawneh, K., Rabba, I., Weinberger, R., Ibrahim, K., ... & Steinitz, G. (2001). New K-Ar ages of basalts from the Harrat Ash Shaam volcanic field in Jordan: Implications for the span and duration of the upper-mantle upwelling beneath the western Arabian plate. Geology, 29(2), 171-174.

Johnson, D., Hooper, P., & Conrey, R. (1999). XRF Method XRF Analysis of Rocks and Minerals for Major and Trace Elements on a Single Low Dilution Li-Tetraborate Fused Bead. *Advances in X-ray Analysis*, *41*, 843-867.

Kent, A. J., Baker, J. A., & Wiedenbeck, M. (2002). Contamination and melt aggregation processes in continental flood basalts: constraints from melt inclusions in Oligocene basalts from Yemen. *Earth and Planetary Science Letters*, *202*(3-4), 577-594.

Knaack, C., Cornelius, S., & Hooper, P. R. (1994). Trace element analyses of rocks and minerals by ICP-MS. *GeoAnalytical Laboratory. Wash. State Univ*, *2*, 18.

Konrad, K., Graham, D. W., Thornber, C. R., Duncan, R. A., Kent, A. J., & Al-Amri, A. M. (2016) Asthenosphere–lithosphere interactions in Western Saudi Arabia: Inferences from 3 He/4 He in xenoliths and lava flows from Harrat Hutaymah. Lithos, 248, 339-352.

Koppers, A. A., Staudigel, H., & Duncan, R. A. (2003). High-resolution 40Ar/39Ar dating of the oldest oceanic basement basalts in the western Pacific basin. *Geochemistry, Geophysics, Geosystems*, *4*(11).

Koppers, A. A. (2002). ArArCALC—software for 40Ar/39Ar age calculations. *Computers Geosciences*, *28*(5), 605-619.

Kuiper, K. F., Deino, A., Hilgen, F. J., Krijgsman, W., Renne, P. R., & Wijbrans, A. J. (2008). Synchronizing rock clocks of Earth history. *science*, *320*(5875), 500-504.

Le Maitre, R. W., Bateman, P., Dudek, A., Keller, J., Lameyre, J., Le Bas, M. J., ... & Woolley, A. R. (1989). A classification of igneous rocks and glossary of terms. Recommendations of the IUGS Sub commission on the Systematics of Igneous rocks. *London: Blackwell Scientific Publications*.

McDonough, W. F., & Sun, S. S. (1995). The composition of the Earth. *Chemical geology*, *120*(3-4), 223-253.

McGuire, A. V., & Stern, R. J. (1993). Granulite xenoliths from western Saudi Arabia: the lower crust of the late Precambrian Arabian-Nubian Shield. *Contributions to Mineralogy and Petrology*, *114*(3), 395-408.

McKenzie, D. A. N., & O'nions, R. K. (1991). Partial melt distributions from inversion of rare earth element concentrations. *Journal of Petrology*, *32*(5), 1021-1091.

Min, K., Mundil, R., Renne, P. R., & Ludwig, K. R. (2000). A test for systematic errors in 40Ar/39Ar geochronology through comparison with U/Pb analysis of a 1.1-Ga rhyolite. *Geochimica et Cosmochimica Acta*, *64*(1), 73-98.

Moufti, M. R., & Hashad, M. H. (2005). Volcanic hazards assessment of Saudi Arabian Harrats: geochemical and isotopic studies of selected areas of active Makkah-Madinah-Nafud (MMN) volcanic rocks. *Final project Report (LGP-5-27)*, *679*.

Moufti, M. R., Matsah, M. I., Soliman, M. A., & Moghazi, A. M. (2010). Arabian plume dynamics beneath Al-Madinah Al-Munawwarah region and its related geohazards. King Abdulaziz City for Science and Technology, Saudi Arabia, Final project report. ARP-26-79) 382 p.

Moufti, M. R., Németh, K., Murcia, H., Al-Gorrry, S. F., & Shawali, J. (2013). Scientific basis of the geoheritage and geotouristic values of the 641 AD Al Madinah eruption site in the Al Madinah volcanic field, Kingdom of Saudi Arabia. The Open Geology Journal, 7, 31-44.

Moufti, M. R., Moghazi, A. M., & Ali, K. A. (2013). 40Ar/39Ar geochronology of the Neogene-Quaternary Harrat Al-Madinah intercontinental volcanic field, Saudi Arabia: implications for duration and migration of volcanic activity. *Journal of Asian Earth Sciences*, *62*, 253-268.

Murcia, H., Lindsay, J.M., Niedermann, S., Cronin, S.J., Smith, I.E., El-Masry, N.N., Moufti, M.R.H., Németh, K., 2013. The potential use of cosmogenic nuclides for dating in Harrat Rahat. VORISA Scientific Meeting extended abstract, pp. 24–28.

Murcia, H., Németh, K., El-Masry, N. N., Lindsay, J. M., Moufti, M. R. H., Wameyo, P., ... & Kereszturi, G. (2015). The Al-Du'aythah volcanic cones, Al-Madinah City: implications for volcanic hazards in northern Harrat Rahat, Kingdom of Saudi Arabia. Bulletin of Volcanology, 77(6), 54.

Murcia, H., Lindsay, J. M., Németh, K., Smith, I. E. M., Cronin, S. J., Moufti, M. R. H., ... & Niedermann, S. (2017). Geology and geochemistry of Late Quaternary volcanism in northern Harrat Rahat, Kingdom of Saudi Arabia: implications for eruption dynamics, regional stratigraphy and magma evolution. Geological Society, London, Special Publications, 446(1), 173-204.

Pallister, J. S., McCausland, W. A., Jonsson, S., Lu, Z., Zahran, H. M., El Hadidy, S., … Moufti, M. R. H. (2010). Broad accommodation of rift-related extension recorded by dyke intrusion in Saudi Arabia. Nature Geoscience, 3(10), 705–712. https://doi.org/10.1038/ngeo966

Pik, R., Marty, B., & Hilton, D. R. (2006). How many mantle plumes in Africa? The geochemical point of view. Chemical Geology, 226(3), 100-114.

Stein, M., & Hofmann, A. W. (1992). Fossil plume head beneath the Arabian lithosphere?. Earth and Planetary Science Letters, 114(1), 193-209.

Stern, R. J., & Johnson, P. (2010). Continental lithosphere of the Arabian Plate: a geologic, petrologic, and geophysical synthesis. Earth-Science Reviews, 101(1-2), 29-67.

Stuart, F.M., 2013. Comparing the composition of the earliest basalts erupted by the Iceland and Afar mantle plumes. Geophysical Research Abstracts 15. EGU, pp. 2013–13389

Sun, S. S., & McDonough, W. F. (1989). Chemical and isotopic systematics of oceanic basalts: implications for mantle composition and processes. *Geological Society, London, Special Publications*, *42*(1), 313-345.

Reilinger, R., & McClusky, S. (2011). Nubia–Arabia–Eurasia plate motions and the dynamics of Mediterranean and Middle East tectonics. Geophysical Journal International, 186(3), 971–979. https://doi.org/10.1111/j.1365-246X.2011.05133.x

Shaw, J. E., Baker, J. A., Menzies, M. A., Thirlwall, M. F., & Ibrahim, K. M. (2003). Petrogenesis of the largest intraplate volcanic field on the Arabian Plate (Jordan): a mixed lithosphere–asthenosphere source activated by lithospheric extension. Journal of Petrology, 44(9), 1657-1679.

Stern, & Johnson. (2010). Continental lithosphere of the Arabian Plate: A geologic, petrologic, and geophysical synthesis. Earth Science Reviews, 101(1), 29–67. https://doi.org/10.1016/j.earscirev.2010.01.002

Wahab, A. A., Maaty, M. A. A., Stuart, F. M., Awad, H., & Kafafy, A. (2014). The geology and geochronology of Al Wahbah maar crater, Harrat Kishb, Saudi Arabia. Quaternary Geochronology, 21, 70-76.

White, W. M. (2013). *Geochemistry*. Retrieved from https://ebookcentral.proquest.com

## 8- Appendices:

### A- Petrography:

Here I do a full petrographic description and mode for some lava flow samples collected from Harrat Ithnayn, western Saudi Arabia.

**1- Sample HI-5, Jabal Ithnayn (Qb6):**

**Mode:** 1) Groundmass (63%): mainly glass and lower abundance of plagioclase and olivine in the groundmass. 2) Vesicles ~5 %. 3) Phenocrysts (30%): Olivine is about 18%, Plagioclase ~10% and Clinopyroxene ~ 2% (Intergranular texture). Alteration is considerably low in this sample < 2%, mainly clays and calcite.

**Description:** This lava flow represents a Hypohyaline texture, meaning that it consists of more than 60 % glass. It is also Inequigranular, which means I see considerably different sizes of phenocrysts. Phenocrysts of Plagioclase (anhedral to subhedral) and Olivine (subhedral to euhedral) together forming a glomerocryst texture. Both minerals also form subophitic texture where plagioclases are embedded in Olivine phenocryst. Grain sizes vary from coarse-grained to fine-grained (0.2 - > 5 mm).

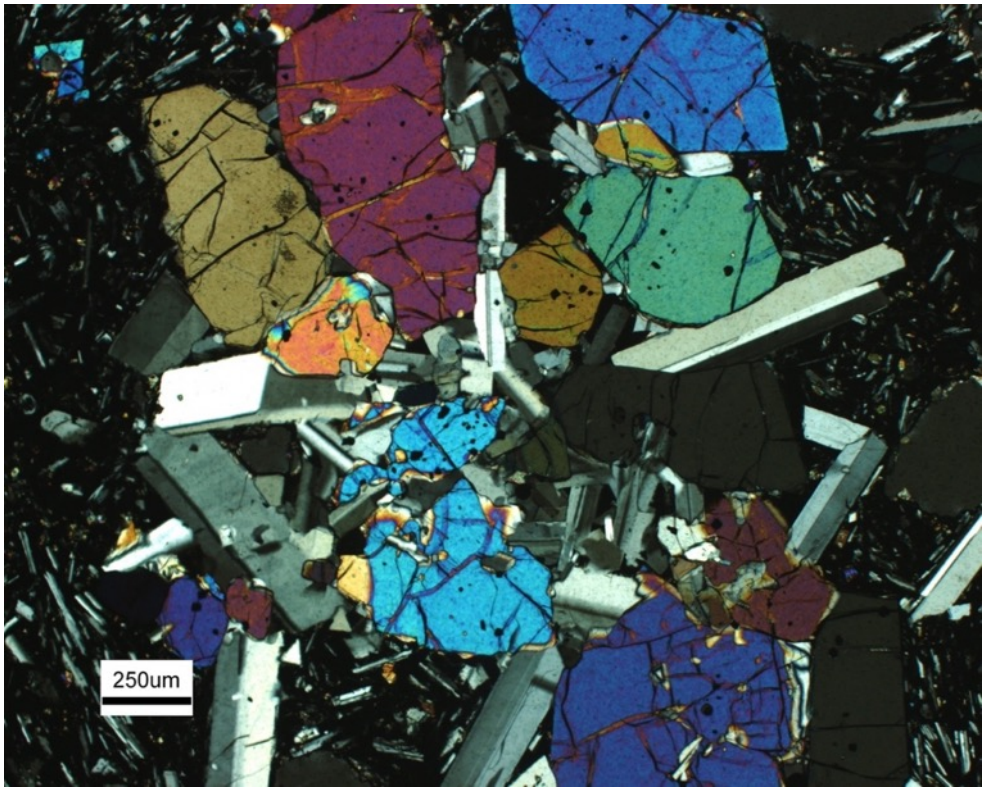


**Figure 1: Thin section photo of the lava flow sample collected at Harrat Ithnayn, western Saudi Arabia (HI-5), from the subunit (Qb6) of Abyad unit.**

**2- Sample HI-17, northwest Harrat Ithnayn (QTm2):**

**Mode:** 1) Groundmass (60%): higher abundances of plagioclase and olivine in the groundmass, glass is considerably low in this sample. 2) Vesicles are less than 5 %. 3) Phenocrysts (>35%): Olivine is about 13%, Plagioclase ~ 18 % and Clinopyroxene ~ 4% (Intergranular texture). No evidence of secondary mineral alteration of clays or calcites.

**Description:** This lava sample shows an Inequigranular texture, which means I see considerably different sizes of phenocrysts. Grain sizes vary from coarse-grained to fine-grained (0.2 - > 5 mm). Phenocrysts of Plagioclase (euhedral to subhedral) and Olivine (subhedral to euhedral). Thus, I can say that this sample shows porphyritic texture because of distinctly different in crystal sizes. Plagioclase phenocrysts exhibit glomerocryst texture. Both minerals also form subophitic texture where plagioclases are embedded in Olivine phenocryst.

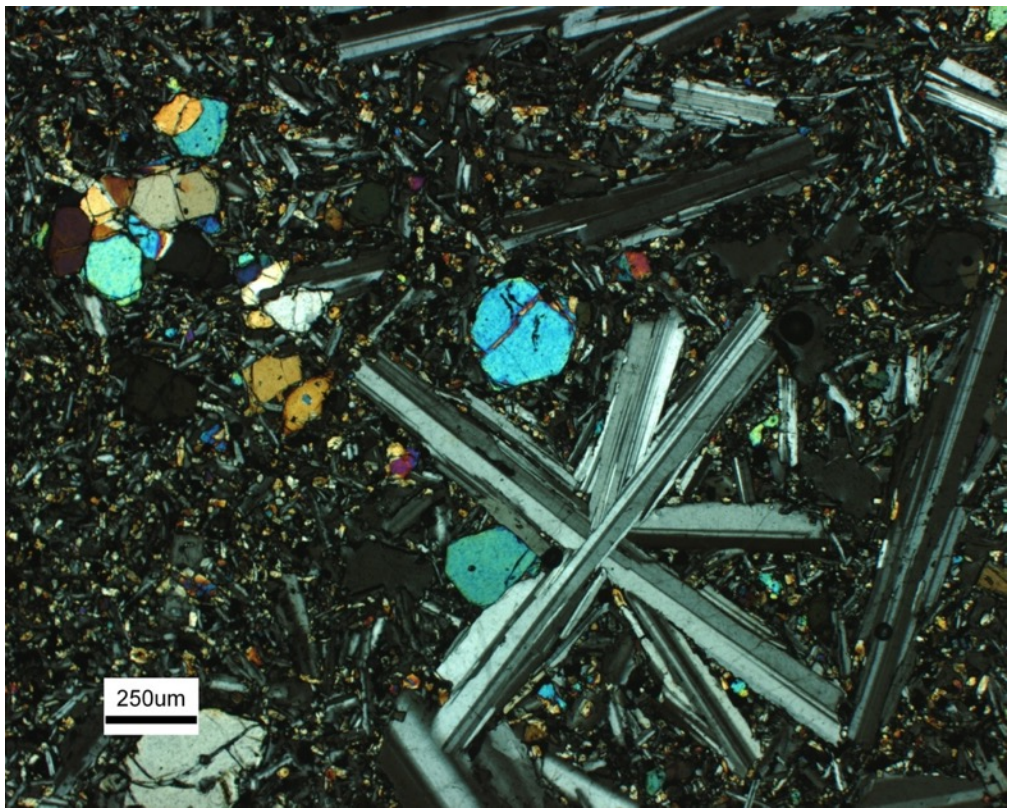


**Figure 2: Thin section photo of the lava flow sample collected at Harrat Ithnayn, western Saudi Arabia (HI-17), from the subunit (Qb6) of Mukrash unit.**

**3- Sample HI-12, near Al-Masa'a village (Qb5):**

**Mode:** 1) Groundmass (~70%): higher abundances of plagioclase and olivine in the groundmass ~ 45%, and relatively lower abundance of glass < 20 %. 2) Vesicles are less than 5 %. 3) Phenocrysts (>25%): Olivine is the most abundant by about 17%, Clinopyroxene ~ 5 % and plagioclase is less than 3 %. There is evidence of secondary mineral alteration of calcites, around some olivine phenocrysts.

**Description:** This lava sample exhibits a microcrystalline texture, meaning most of the phenocrysts in the sample are fine-grained (0.2 mm or less). The grain size of phenocrysts is mostly fine-grained, but there are olivine phenocrysts that are medium-grained (> 0.2 mm). Olivine and clinopyroxene are subhedral to euhedral, whereas plagioclase crystals are mainly anhedral. Based on crystal shape, this lava sample shows a hypidiomorphic texture (from euhedral to anherdral crystals).

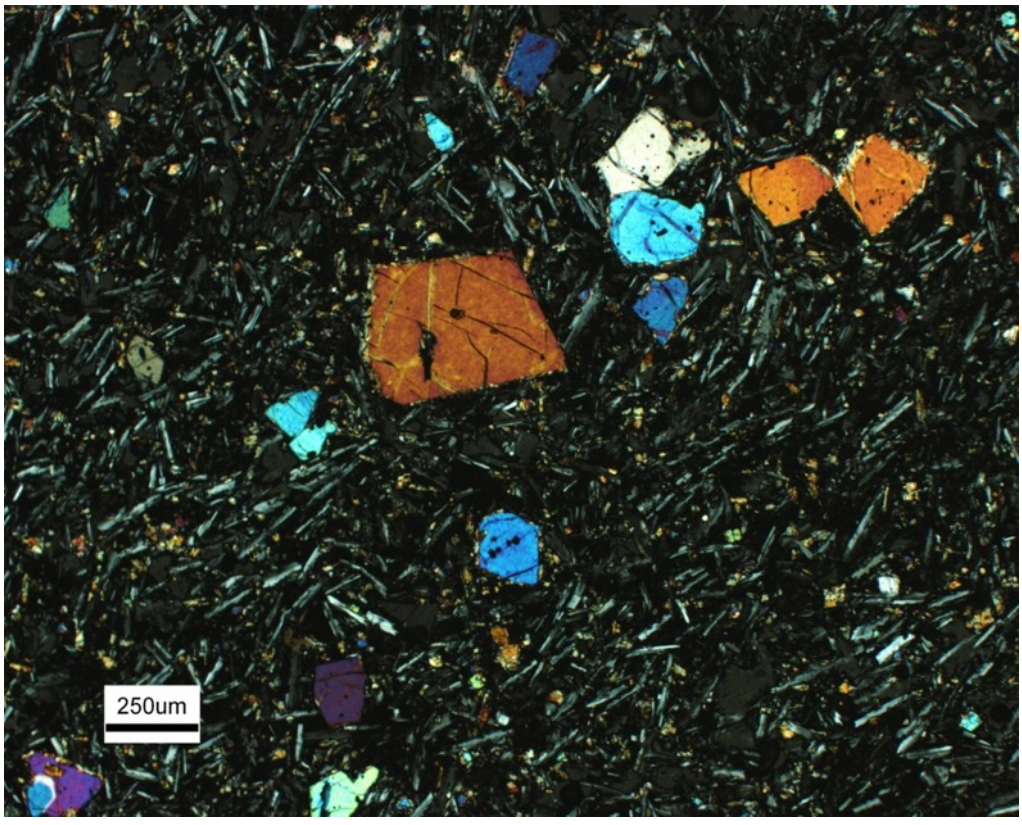


**Figure 3: Thin section photo of the lava flow sample collected at Harrat Ithnayn, western Saudi Arabia (HI-12), from the subunit (Qb5) of Abyad unit.**

**4- Sample HI-2, Jabal Hazam Khadra (Qb5):**

**Mode:** 1) Groundmass (45%): Olivine and plagioclase are the most abundant phases in the groundmass of this sample. Glass is relatively low ~ 15% 2) Vesicles are considerably abundant > 10%. 3) Phenocrysts (40%): Olivine is about 25%, Plagioclase ~ 7% and Clinopyroxene ~ 8%. Alteration is considerably high in this sample > 4%, mainly clays and calcites, especially around the vesicles.

**Description:** This lava flow exhibits a Inequigranular texture, which means I see considerably different sizes of phenocrysts, especially plagioclase. Grain sizes vary from coarse-grained to fine-grained (0.2 - > 5 mm). About the crystal shape, phenocrysts of plagioclase (anhedral to subhedral) and olivine (subhedral to euhedral), clinopyroxene (subhedral). This means that the sample shows a hypidiomorphic texture. Regarding the glass-crystal ratio, I say that this lava flow shows a Holocrystalline to Hypocrystalline, where apparently there is lower abundance of glass population.

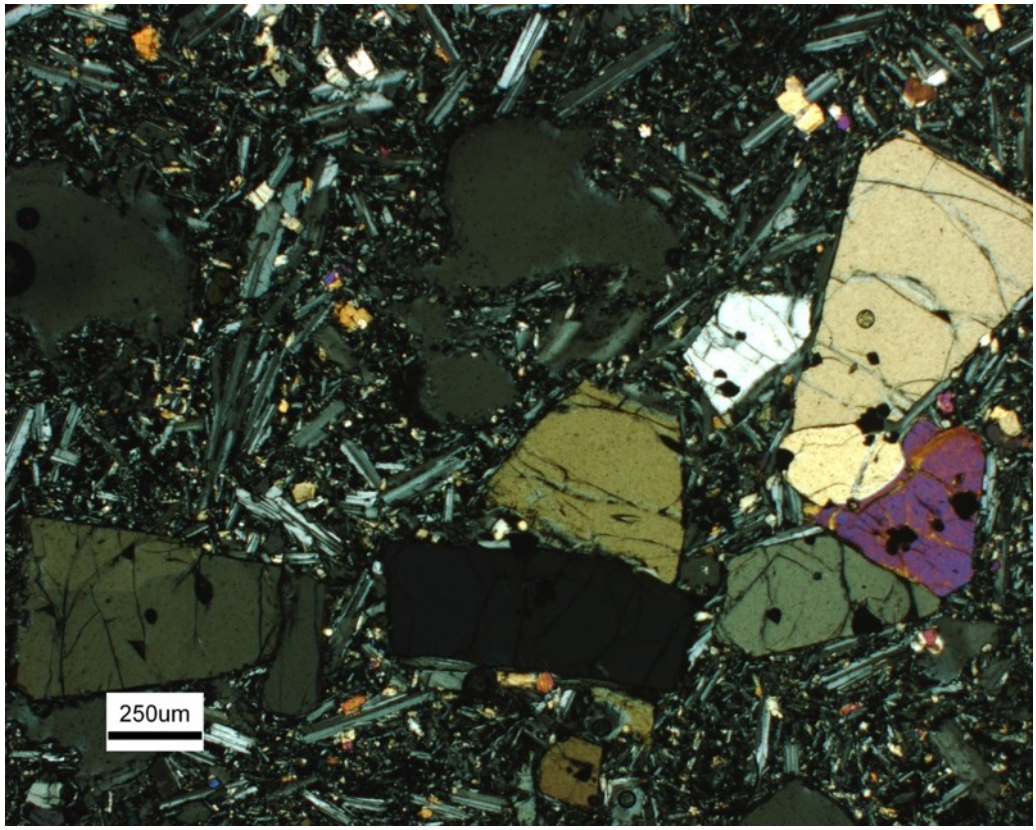


**Figure 4: Thin section photo of the lava flow sample collected at Harrat Ithnayn, western Saudi Arabia (HI-2), from the subunit (Qb5) of Abyad unit.**

## B- Geochemical data:

1) below is the geochemical data provided by Dr. Vic Camp who collected those data during their study at Harrat Khaybar and Ithnayn (Camp et al., 1991).

**Table 1**: Geochemical Data for lava flows, Harrat Ithnayn, Western Saudi Arabia (Camp et al., 1991) (major elements in wt.%, trace elements in µg/g)

| Sample ID | 4955 | 4123 | 4952 | 4859 | 4947 | 4948 | 4945 | 4958 | 4953 | 4957 |
|---|---|---|---|---|---|---|---|---|---|---|
| Unit | Tm2 | Tm2 | Tm2 | Tm2 | Qb4 | Qb4 | Qb4 | Qb4 | Qb4 | Qb4 |
| SiO2 | 47.29 | 48.31 | 49.32 | 50.01 | 45.89 | 46.32 | 48.24 | 48.64 | 49.16 | 49.43 |
| TiO2 | 1.83 | 2.09 | 1.66 | 1.71 | 1.49 | 1.74 | 1.43 | 1.55 | 1.72 | 2.14 |
| Al2O3 | 15.13 | 16.56 | 16.6 | 17.55 | 15.05 | 15.42 | 16.72 | 16.71 | 17.18 | 17.41 |
| FeO* | 10.32 | 10.41 | 11.05 | 10.26 | 10.23 | 9.88 | 9.71 | 10.42 | 9.29 | 9.51 |
| MnO | 0.18 | 0.17 | 0.18 | 0.18 | 0.18 | 0.18 | 0.17 | 0.18 | 0.17 | 0.17 |
| MgO | 11.12 | 6.69 | 7.55 | 7.24 | 11.62 | 10.49 | 7.15 | 6.97 | 7.85 | 7.06 |
| CaO | 10.5 | 11.99 | 10.76 | 10.94 | 10.33 | 9.35 | 12.03 | 11.34 | 8.82 | 7.7 |
| Na2O | 3.01 | 3.16 | 2.9 | 3.05 | 3.79 | 4.5 | 3.18 | 3.27 | 4.59 | 5.14 |
| K2O | 0.85 | 0.78 | 0.5 | 0.64 | 0.96 | 1.03 | 0.55 | 0.54 | 1.27 | 1.7 |
| P2O5 | 0.4 | 0.37 | 2.9 | 0.29 | 0.59 | 0.74 | 0.22 | 0.27 | 0.71 | 0.99 |
| Total | 100.63 | 100.53 | 100.81 | 100.87 | 100.13 | 99.65 | 99.4 | 99.89 | 100.76 | 101.25 |
| Mg# | 65.52 | 53.13 | 54.65 | 55.45 | 66.70 | 65.19 | 56.50 | 54.12 | 59.84 | 56.70 |
| µg/g | | | | | | | | | | |
| Ba | 229 | 191 | 156 | 216 | 412 | 419 | 190 | 212 | 416 | 504 |
| Ce | 0 | 44 | 0 | 0 | 0 | 0 | 0 | 0 | 0 | 0 |
| Cr | 392 | 141 | 195 | 177 | 392 | 333 | 200 | 172 | 242 | 155 |
| Cu | 63 | 87 | 76 | 50 | 68 | 62 | 85 | 92 | 57 | 40 |
| Ga | 17 | 23 | 22 | 18 | 16 | 18 | 19 | 18 | 17 | 17 |
| La | 0 | 12 | 0 | 0 | 0 | 0 | 0 | 0 | 0 | 0 |
| Li | 0 | 11 | 0 | 0 | 0 | 0 | 0 | 0 | 0 | 0 |
| Nb | 31 | 23 | 13 | 20 | 58 | 72 | 14 | 19 | 62 | 82 |
| Ni | 262 | 56 | 84 | 50 | 301 | 263 | 83 | 67 | 163 | 112 |
| Sc | 31 | 32 | 36 | 34 | 33 | 25 | 35 | 35 | 27 | 20 |
| Sr | 501 | 469 | 375 | 543 | 748 | 863 | 468 | 460 | 820 | 1102 |
| V | 219 | 260 | 254 | 224 | 196 | 196 | 237 | 263 | 183 | 161 |
| Y | 24 | 26 | 25 | 25 | 24 | 26 | 23 | 26 | 27 | 29 |
| Zn | 85 | 73 | 87 | 82 | 66 | 69 | 75 | 80 | 61 | 72 |
| Zr | 148 | 148 | 121 | 150 | 194 | 241 | 136 | 144 | 301 | 351 |
| Rb | 13 | 13 | 6 | 12 | 20 | 21 | 11 | 8 | 28 | 33 |

**Table 1**: *Continue* (Camp et al., 1991) (major elements in wt.%, trace elements in µg/g)

| Sample ID | 4862 | 4861 | 4950 | 4860 | 4946 | 4944 | 4124 | 4951 | 4857 | 4954 | 4121 |
|---|---|---|---|---|---|---|---|---|---|---|---|
| Unit | Qb4 | Qb4 | Qb5 | Ob5 | Qb5 | Qb5 | Qb5 | Qb6 | Qb6 | Qb6 | Qb6 |
| SiO2 | 49.56 | 50.04 | 48.24 | 46.65 | 48.34 | 48.84 | 49.94 | 48.9 | 49.63 | 49.81 | 50.27 |
| TiO2 | 2.14 | 1.91 | 1.92 | 1.89 | 1.56 | 1.58 | 1.94 | 1.85 | 1.59 | 1.69 | 1.61 |
| Al2O3 | 17.29 | 17.71 | 16.63 | 14.97 | 16.52 | 16.76 | 17.12 | 16.97 | 17.52 | 17.27 | 16.61 |
| FeO* | 9.76 | 9.4 | 9.69 | 9.72 | 10.21 | 9.7 | 9.85 | 9.61 | 9.68 | 9.16 | 9.92 |
| MnO | 0.17 | 0.17 | 0.17 | 0.18 | 0.17 | 0.17 | 0.17 | 0.17 | 0.17 | 0.17 | 0.18 |
| MgO | 7.03 | 7.43 | 8.41 | 11.07 | 7.37 | 7.71 | 6.31 | 7.8 | 7.25 | 8.27 | 6.63 |
| CaO | 7.73 | 7.69 | 8.3 | 9.81 | 10.99 | 10.42 | 10.57 | 7.91 | 11.2 | 8.81 | 11.04 |
| Na2O | 4.97 | 4.75 | 4.71 | 4.02 | 3.32 | 3.47 | 3.72 | 4.84 | 3.15 | 4.28 | 3.46 |
| K2O | 1.54 | 1.5 | 1.41 | 1.14 | 0.54 | 0.61 | 0.89 | 1.41 | 0.55 | 1.22 | 0.69 |
| P2O5 | 1.02 | 0.82 | 0.85 | 0.8 | 0.28 | 0.29 | 0.34 | 0.78 | 0.26 | 0.71 | 0.28 |
| Total | 101.21 | 101.42 | 100.33 | 100.25 | 99.3 | 99.55 | 100.85 | 100.24 | 101 | 101.39 | 100.69 |
| Mg# | 55.95 | 58.23 | 60.49 | 66.76 | 56.01 | 58.37 | 53.05 | 58.87 | 56.91 | 61.42 | 54.10 |
| µg/g | | | | | | | | | | | |
| Ba | 479 | 414 | 343 | 454 | 174 | 200 | 206 | 464 | 105 | 432 | 148 |
| Ce | 0 | 0 | 0 | 0 | 0 | 0 | 45 | 0 | 0 | 0 | 34 |
| Cr | 144 | 192 | 433 | 251 | 197 | 231 | 136 | 205 | 197 | 272 | 185 |
| Cu | 48 | 77 | 76 | 63 | 89 | 68 | 84 | 53 | 52 | 64 | 78 |
| Ga | 15 | 16 | 14 | 17 | 19 | 18 | 19 | 17 | 20 | 20 | 23 |
| La | 0 | 0 | 0 | 0 | 0 | 0 | 17 | 0 | 0 | 0 | 9 |
| Li | 0 | 0 | 0 | 0 | 0 | 0 | 11 | 0 | 0 | 0 | 9 |
| Nb | 82 | 73 | 64 | 72 | 21 | 21 | 33 | 64 | 18 | 59 | 19 |
| Ni | 149 | 177 | 290 | 170 | 80 | 110 | 54 | 171 | 79 | 171 | 51 |
| Sc | 23 | 22 | 27 | 24 | 32 | 34 | 36 | 23 | 36 | 27 | 34 |
| Sr | 1132 | 883 | 836 | 967 | 457 | 460 | 530 | 1025 | 421 | 823 | 405 |
| V | 145 | 154 | 187 | 172 | 239 | 223 | 261 | 144 | 252 | 176 | 267 |
| Y | 28 | 28 | 27 | 29 | 22 | 22 | 24 | 29 | 24 | 26 | 24 |
| Zn | 73 | 70 | 75 | 73 | 78 | 71 | 84 | 67 | 72 | 64 | 83 |
| Zr | 373 | 319 | 265 | 314 | 142 | 159 | 198 | 310 | 156 | 295 | 155 |
| Rb | 27 | 31 | 23 | 31 | 9 | 11 | 14 | 31 | 7 | 29 | 10 |

## 2) REEBOX model and Sensitivity analysis:

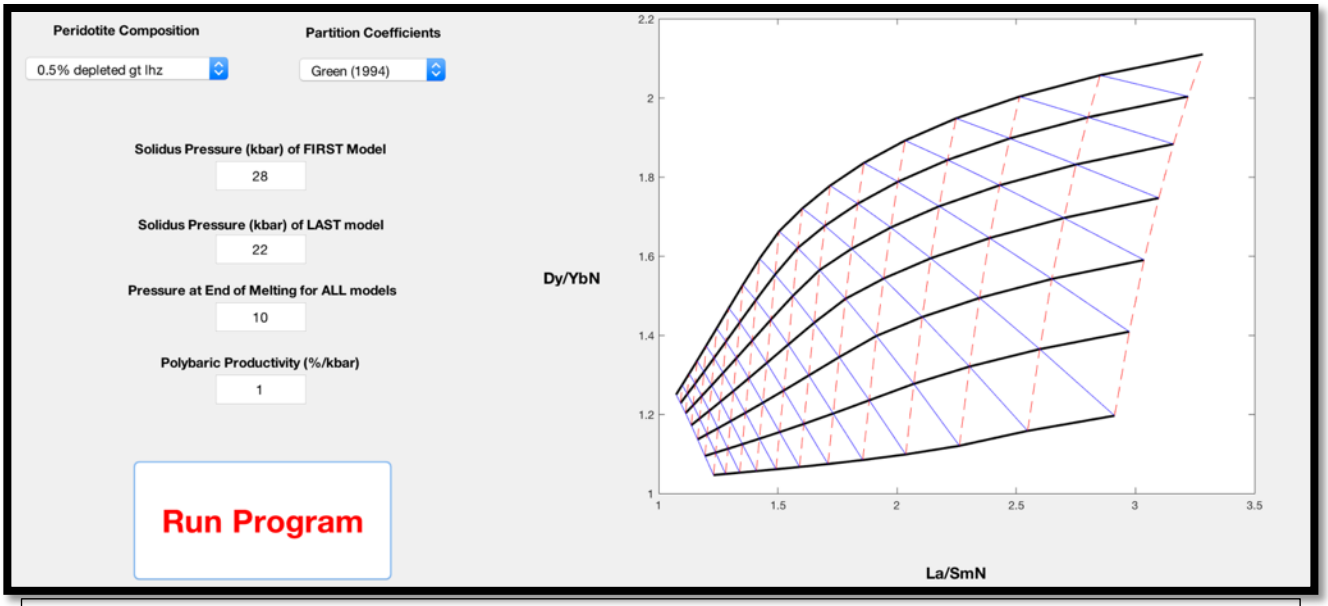


Figure 5: Screenshot of the input pop-up in the MATLAB script of the REEBOX model. This also shows the resulted output plot with the lines of the solidus pressures and melt fractions. Lines are described above.

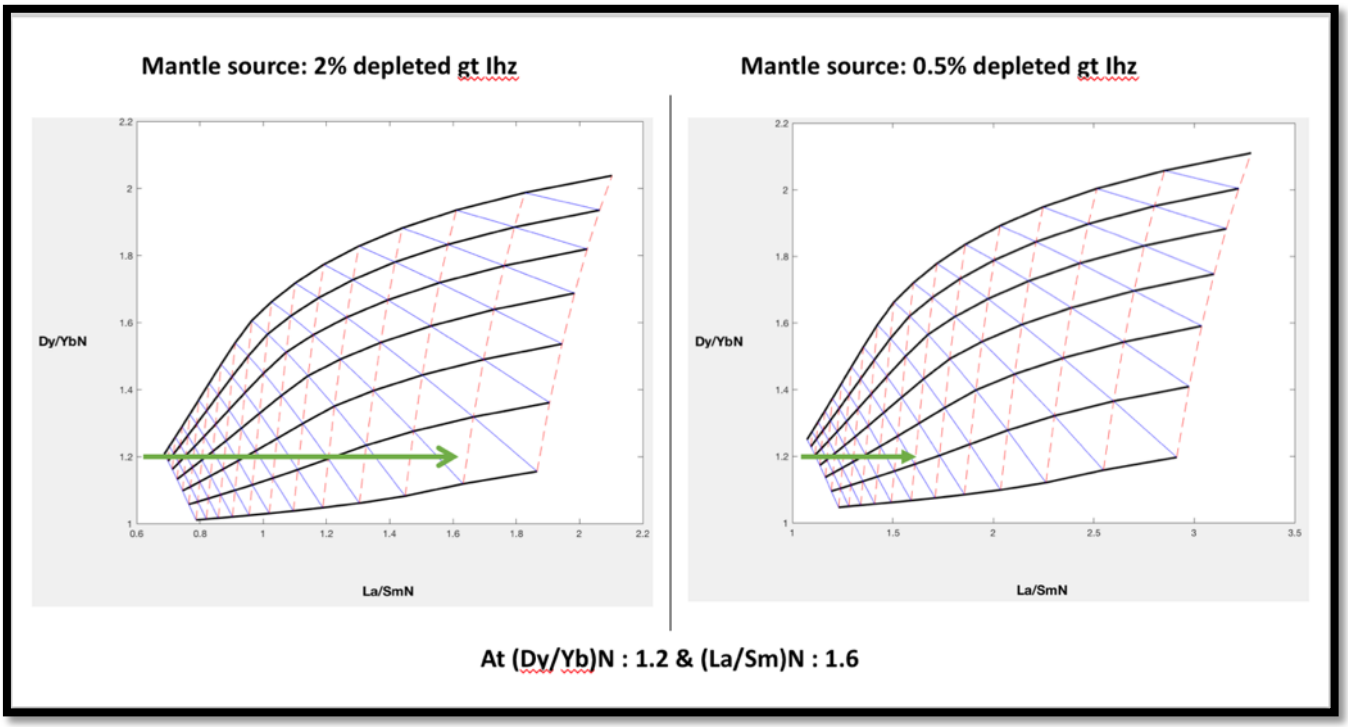


Figure 6: Screenshot of two different REEBOX model results. This shows how the wrong estimation of mantle source can produce a large range of error. We have here the same REE ratios, but with similar mantle sources resulted a difference in melt fraction by about 7%, and solidus pressure by about 8 Kbars.

3) Important bivariate diagrams:

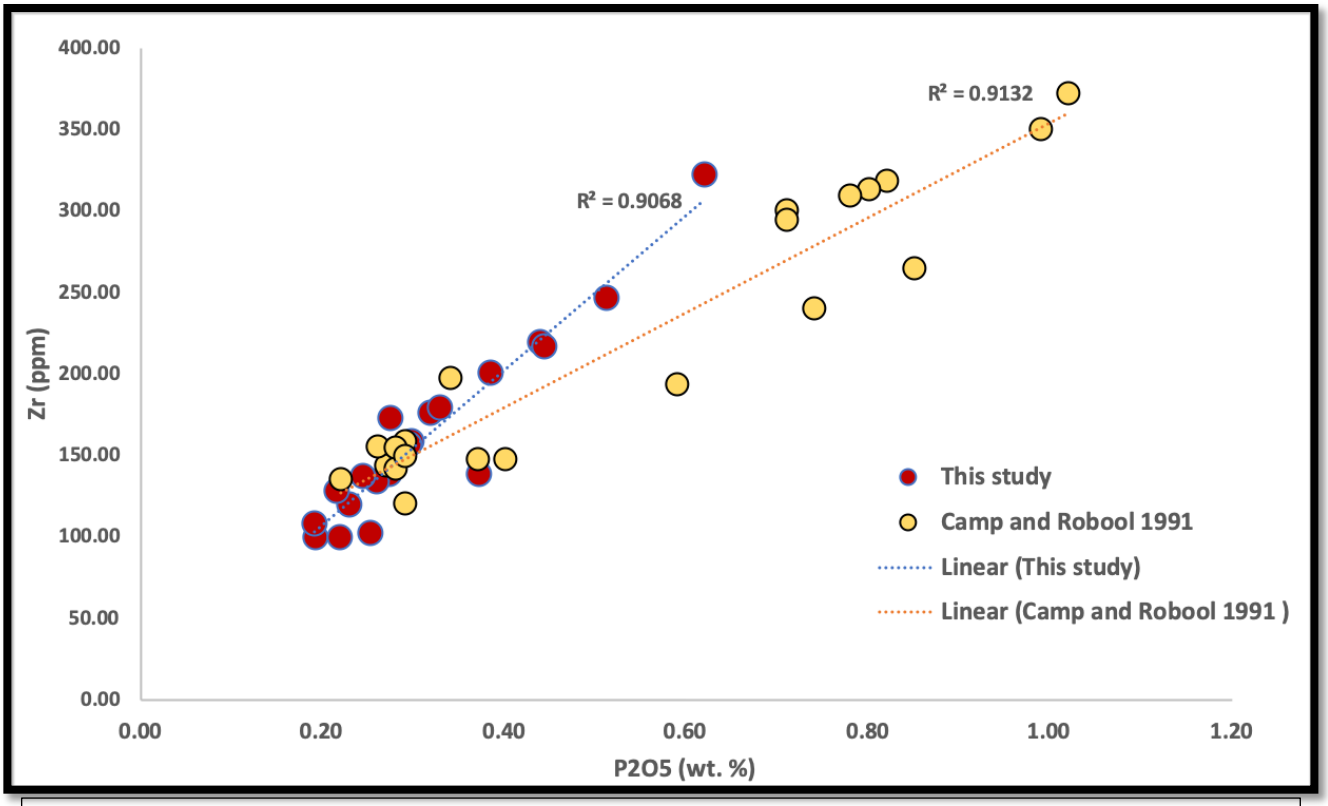


Figure 7: P2O5 (wt.%) vs. Zr (ppm) bivariate diagram. Red dots are samples of this study, yellow dots are samples of Camp et al. (1991) study. The linear correlation suggests that magmatic processes dominated by crystal fractionation. Since there is no high-evolved lavas at Harrat Ithnayn, another trend lined is not found, unlike what is seen at Harrat Khaybar with the Abyad comendite trend line.

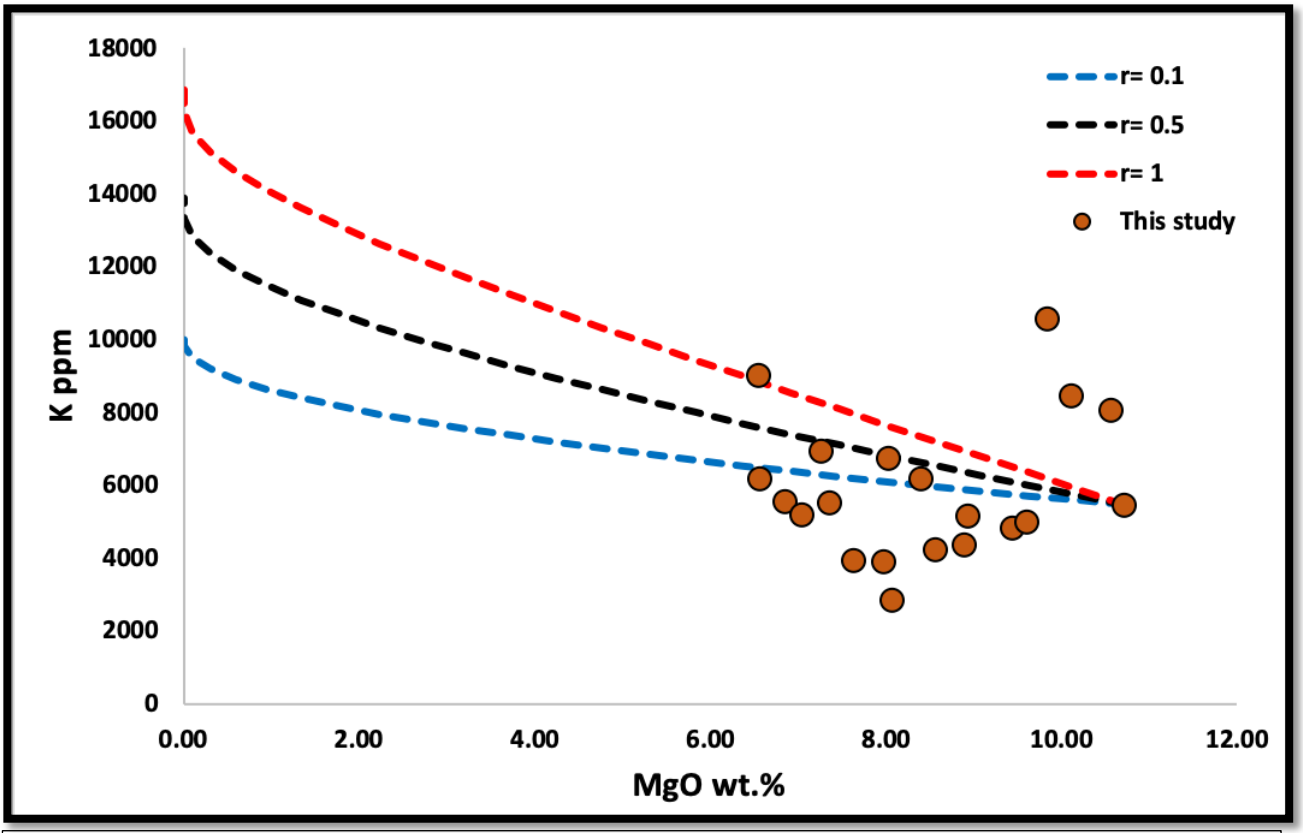


Figure 8: This is a scatter diagram of K ppm vs. MgO wt.% concentrations. Data shown here are only from this study, Camp and Robool (1991) are excluded because of the lack of trace element concentrations (i.e. Ba and Nb). Lines are the assimilation fractional crystallization (AFC) trends for mass ratio of assimilated to crystallized material ( r ) (blue: 0.1, black: 0.5, and red: 1). Background data of the average upper continental used in this model are from Kent et al. 2002.

**C- Geochronological data:**

1) Previous K/Ar age determination of the integrated volcanic unit of Khaybar and Ithnayn:

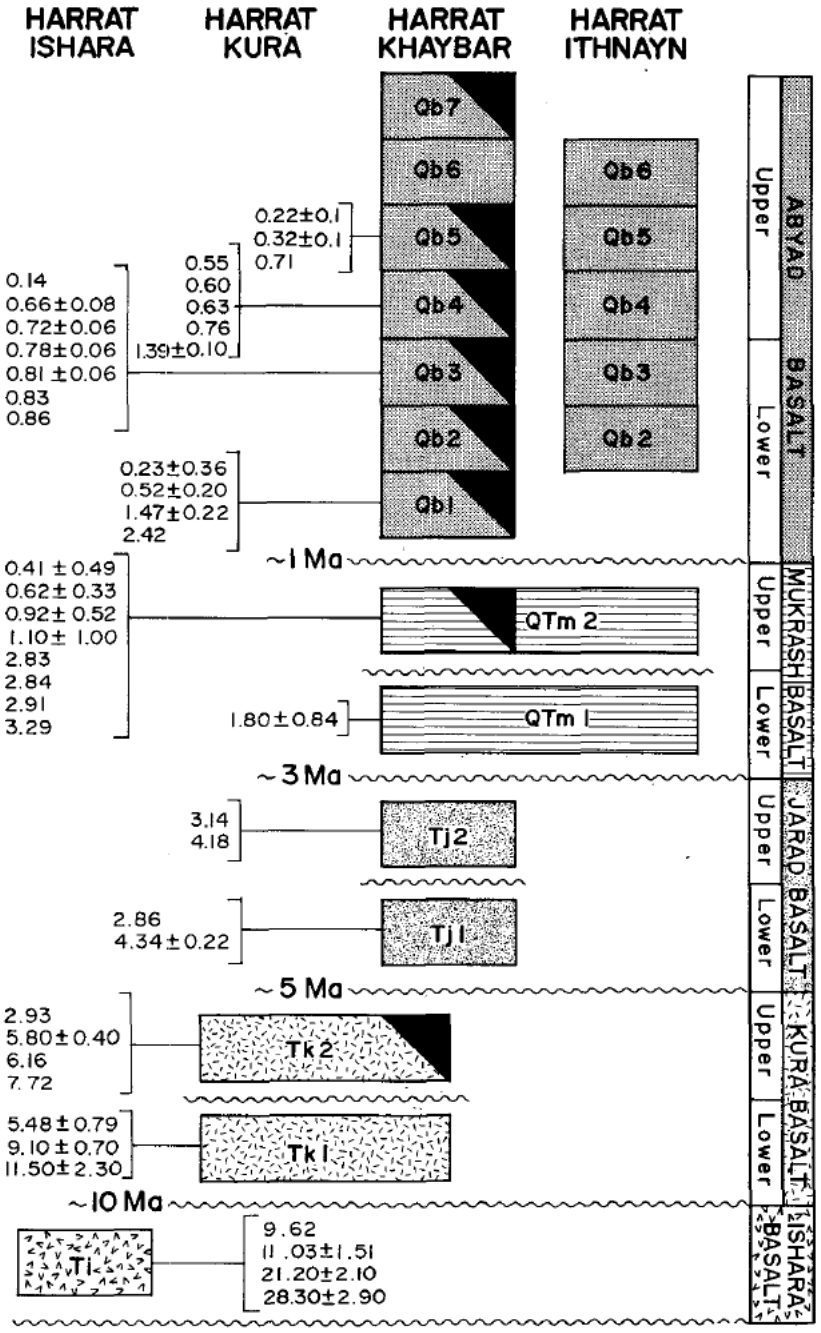


Figure 9: Stratigraphic classification and K/Ar age results from Camp and Robool (1991) study. Disconformities among these units were determined using the false-color band of LandSat imagery, degree of surface erosion, and field observations (Robool and Camp [a], 1991).

2) Plateau ages of all individual samples dated by $^{40}Ar$-$^{39}Ar$ method:

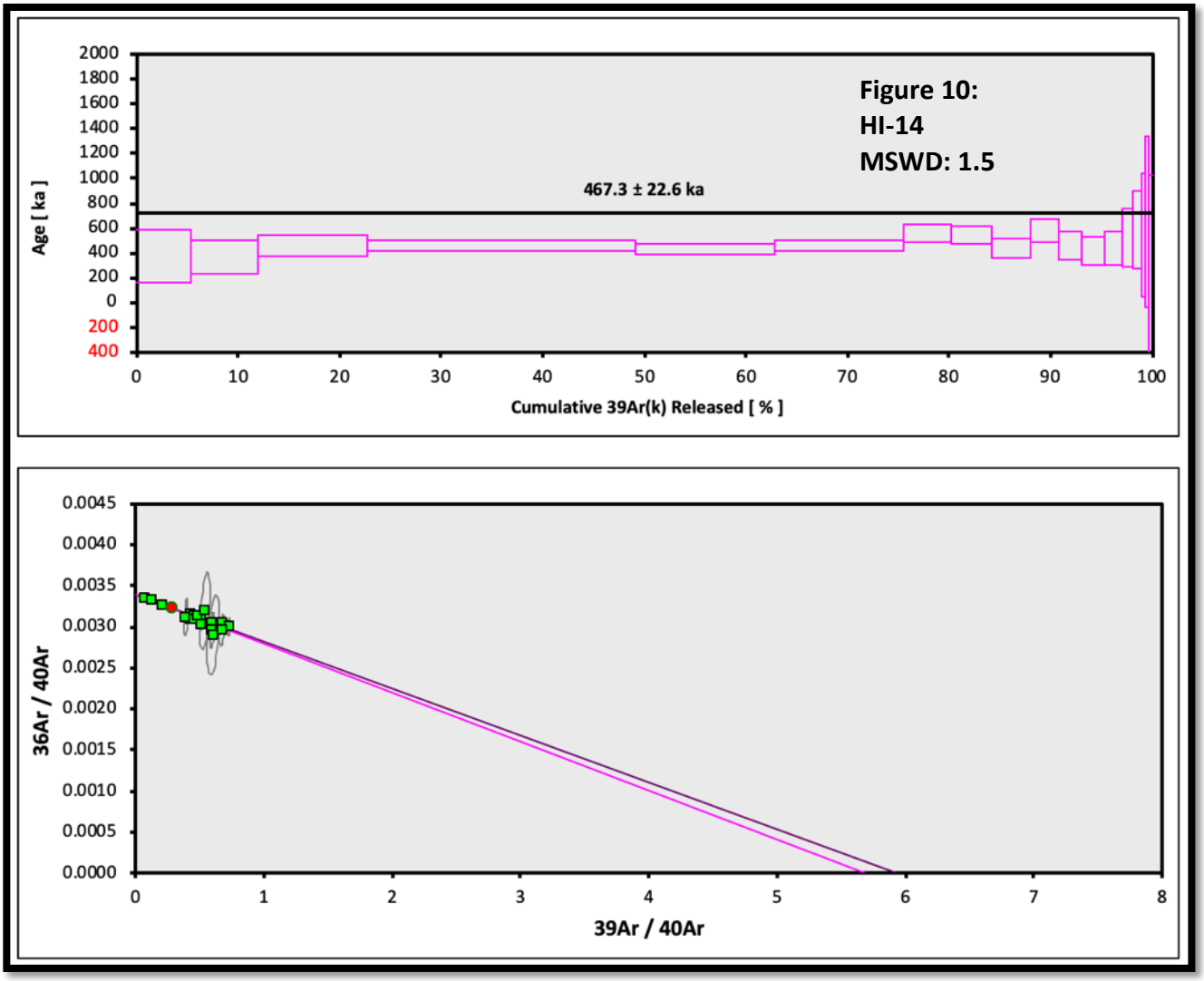

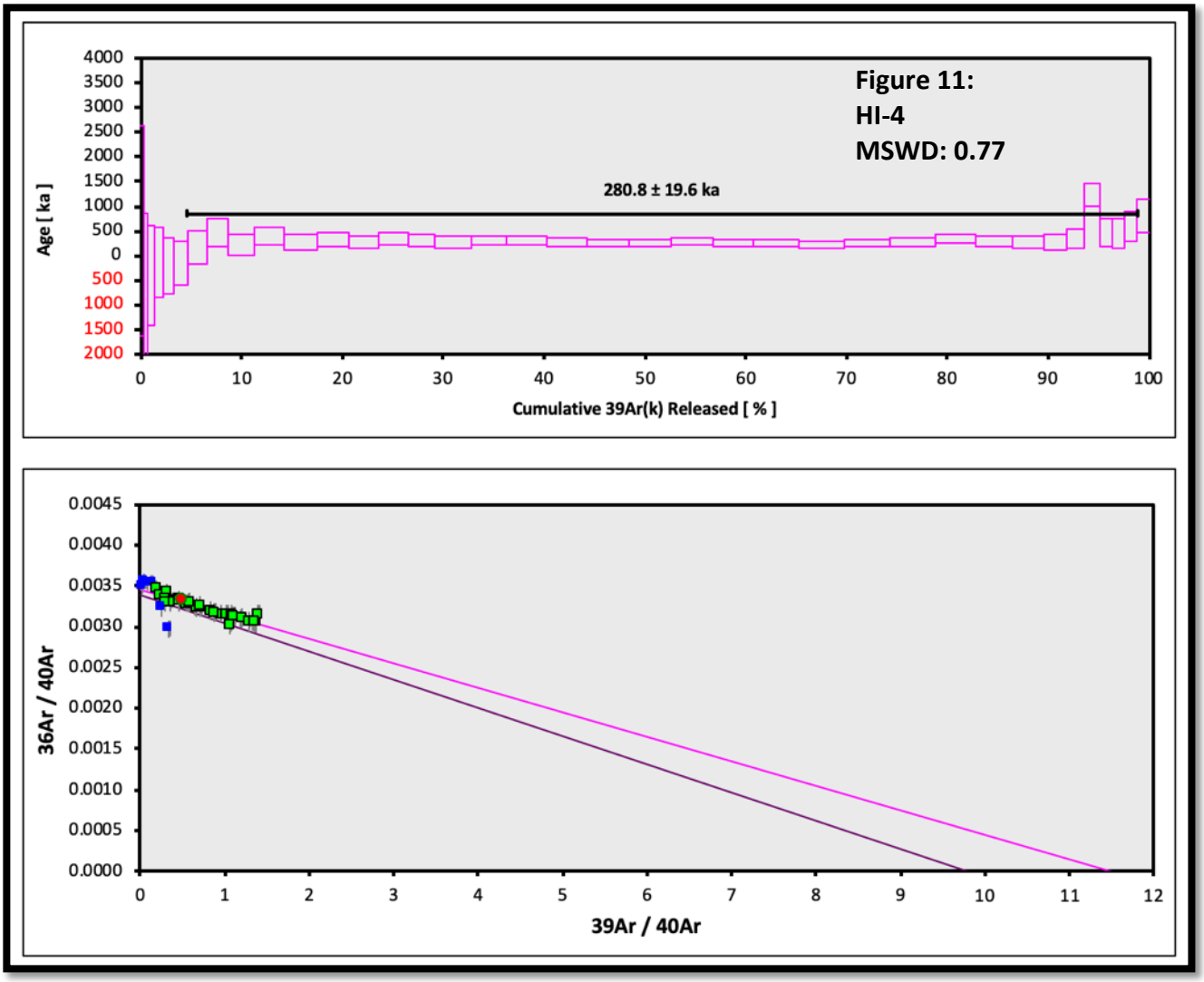
Figure 11:
HI-4
MSWD: 0.77
280.8 ± 19.6 ka
Age [ ka ]
Cumulative 39Ar(k) Released [ % ]
36Ar / 40Ar
39Ar / 40Ar

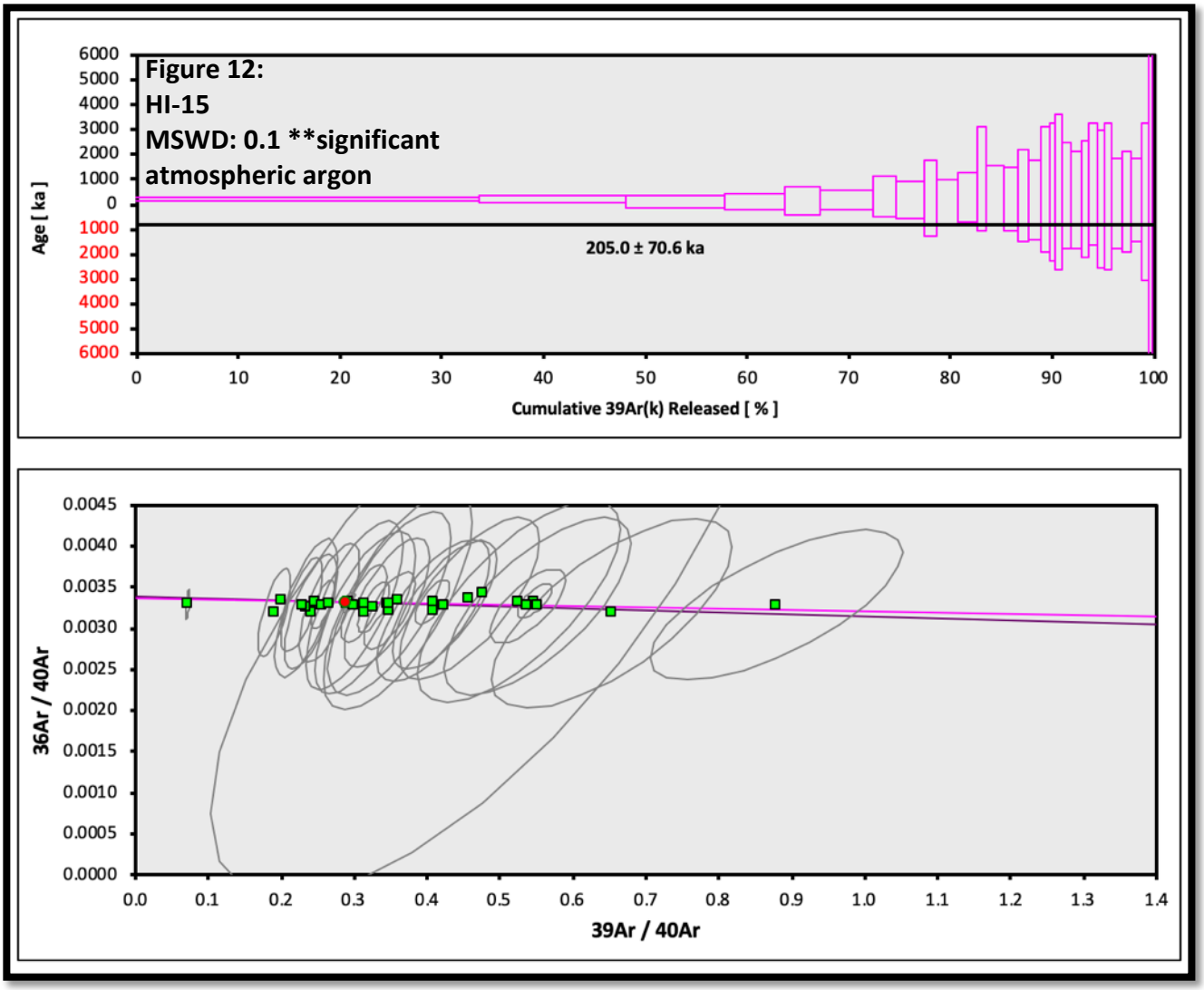
Figure 12:
HI-15
MSWD: 0.1 **significant
atmospheric argon
Age [ ka ]
6000
5000
4000
3000
2000
1000
0
1000
2000
3000
4000
5000
6000
205.0 ± 70.6 ka
0
10
20
30
40
50
60
70
80
90
100
Cumulative 39Ar(k) Released [ % ]
36Ar / 40Ar
0.0045
0.0040
0.0035
0.0030
0.0025
0.0020
0.0015
0.0010
0.0005
0.0000
0.0
0.1
0.2
0.3
0.4
0.5
0.6
0.7
0.8
0.9
1.0
1.1
1.2
1.3
1.4
39Ar / 40Ar

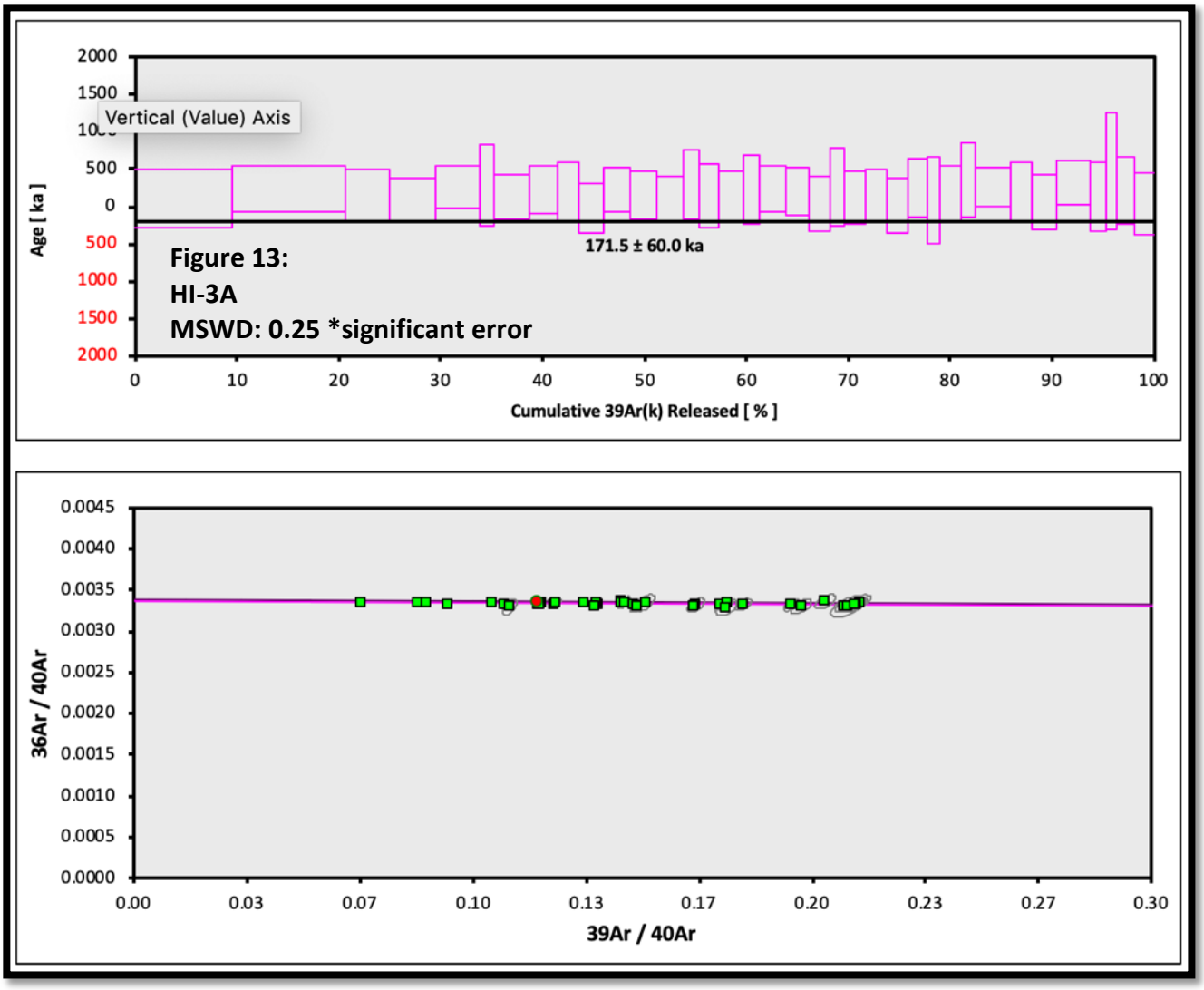


**Figure 13:**
**HI-3A**
**MSWD: 0.25 *significant error**

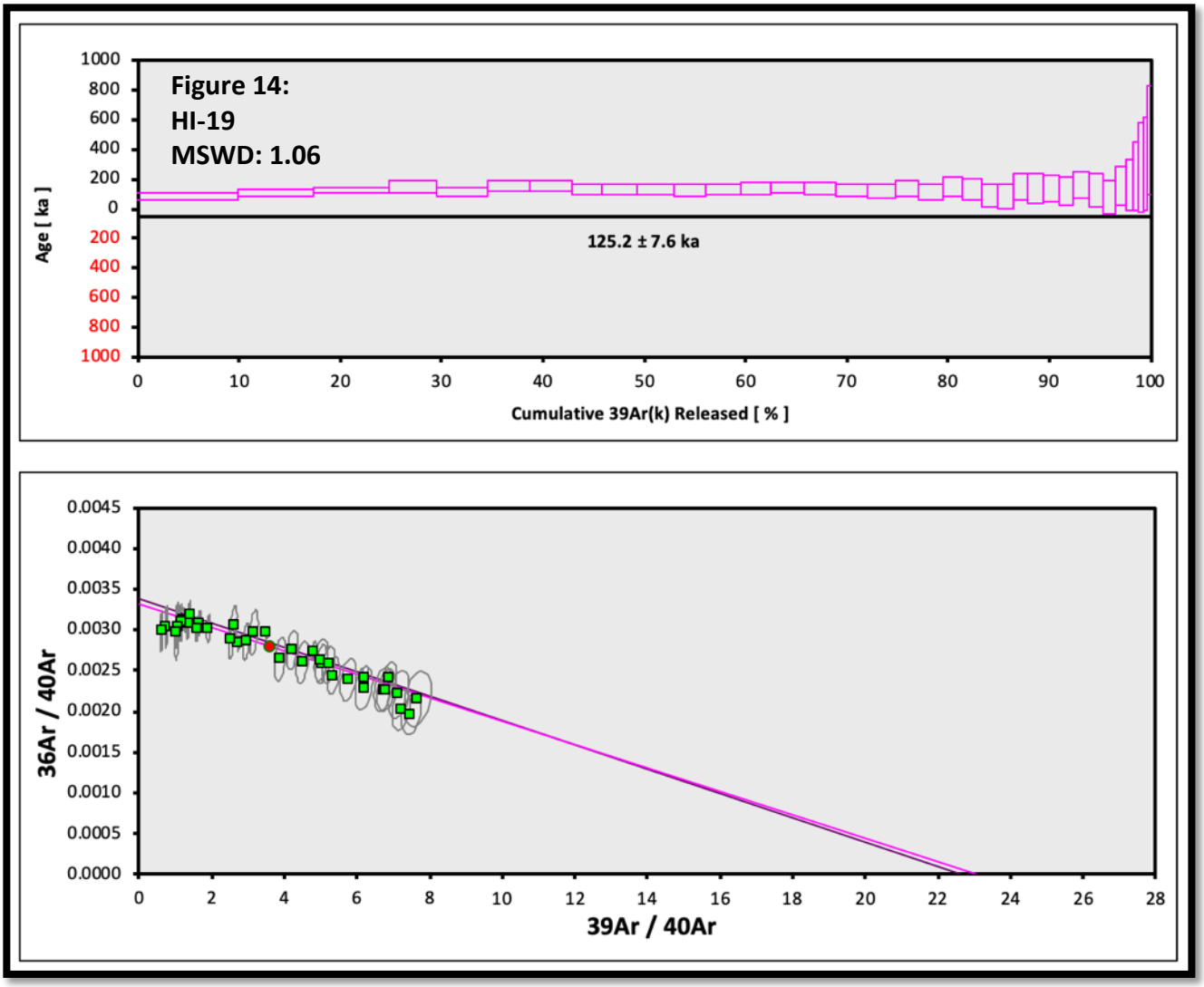
Figure 14:
HI-19
MSWD: 1.06
Age [ ka ]
1000
800
600
400
200
0
200
400
600
800
1000
125.2 ± 7.6 ka
0
10
20
30
40
50
60
70
80
90
100
Cumulative 39Ar(k) Released [ % ]
36Ar / 40Ar
0.0045
0.0040
0.0035
0.0030
0.0025
0.0020
0.0015
0.0010
0.0005
0.0000
0
2
4
6
8
10
12
14
16
18
20
22
24
26
28
39Ar / 40Ar

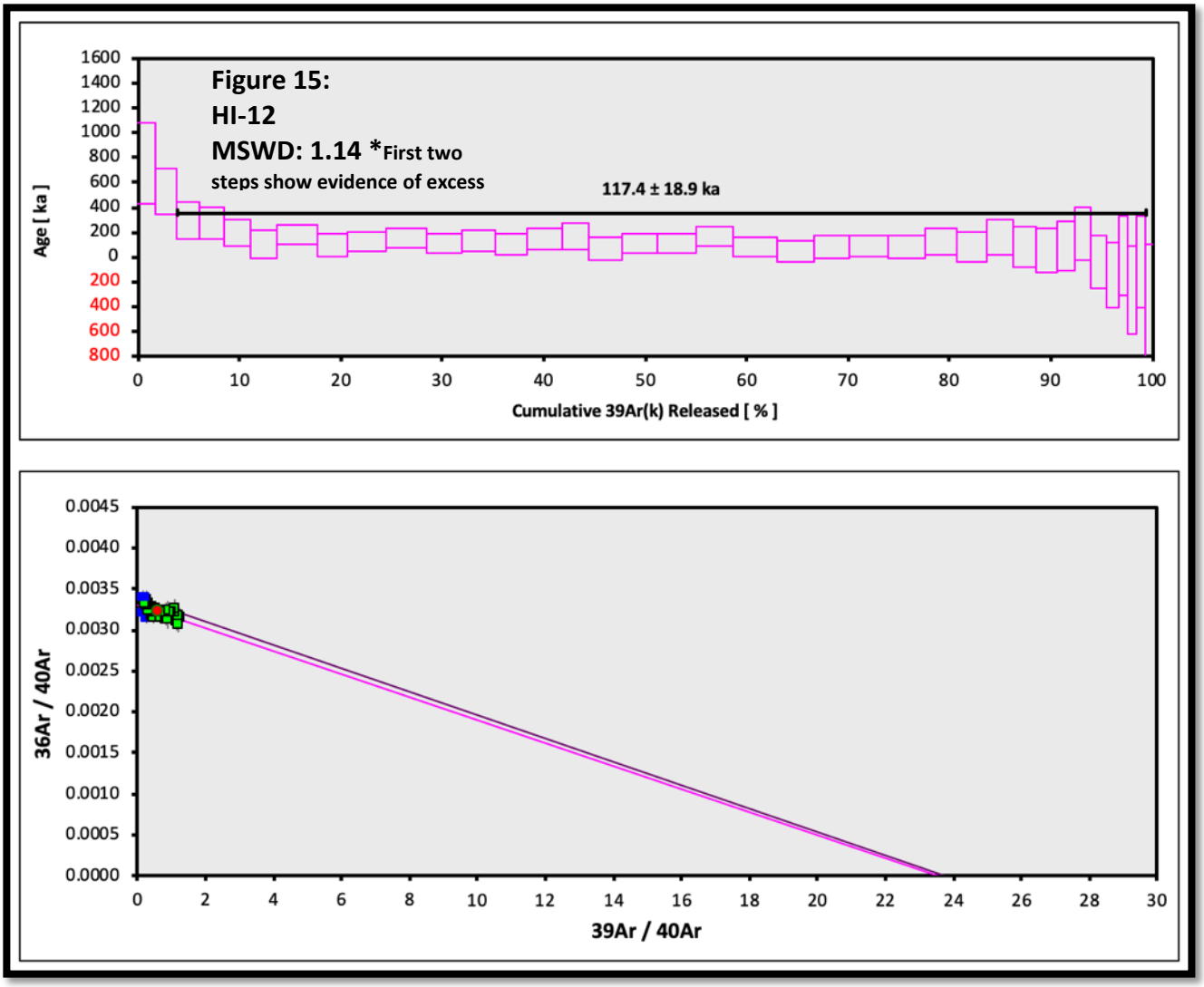
Figure 15:
HI-12
MSWD: 1.14 *First two steps show evidence of excess
117.4 ± 18.9 ka
Age [ ka ]
Cumulative 39Ar(k) Released [ % ]
36Ar / 40Ar
39Ar / 40Ar

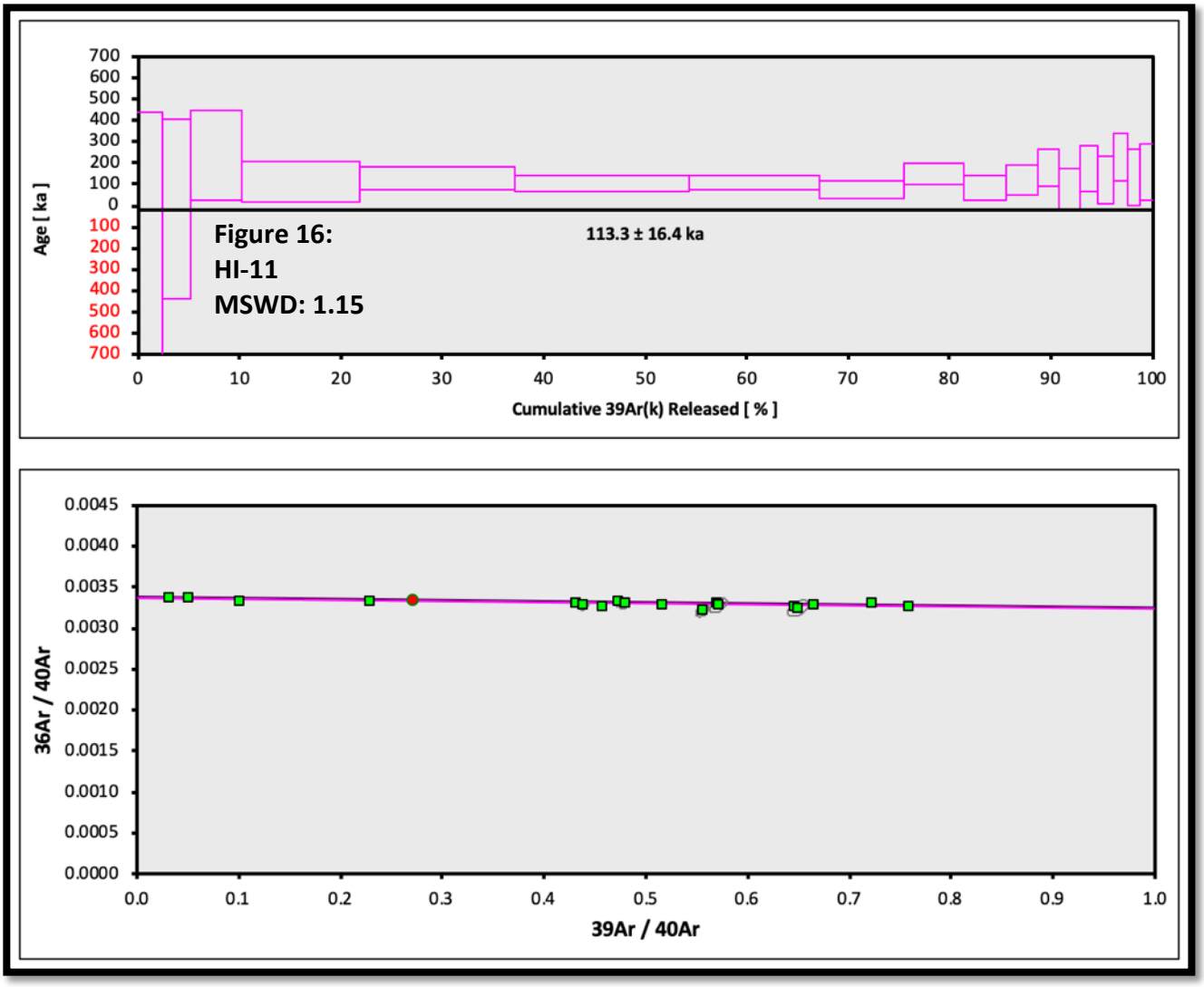


**Figure 16:**
**HI-11**
**MSWD: 1.15**

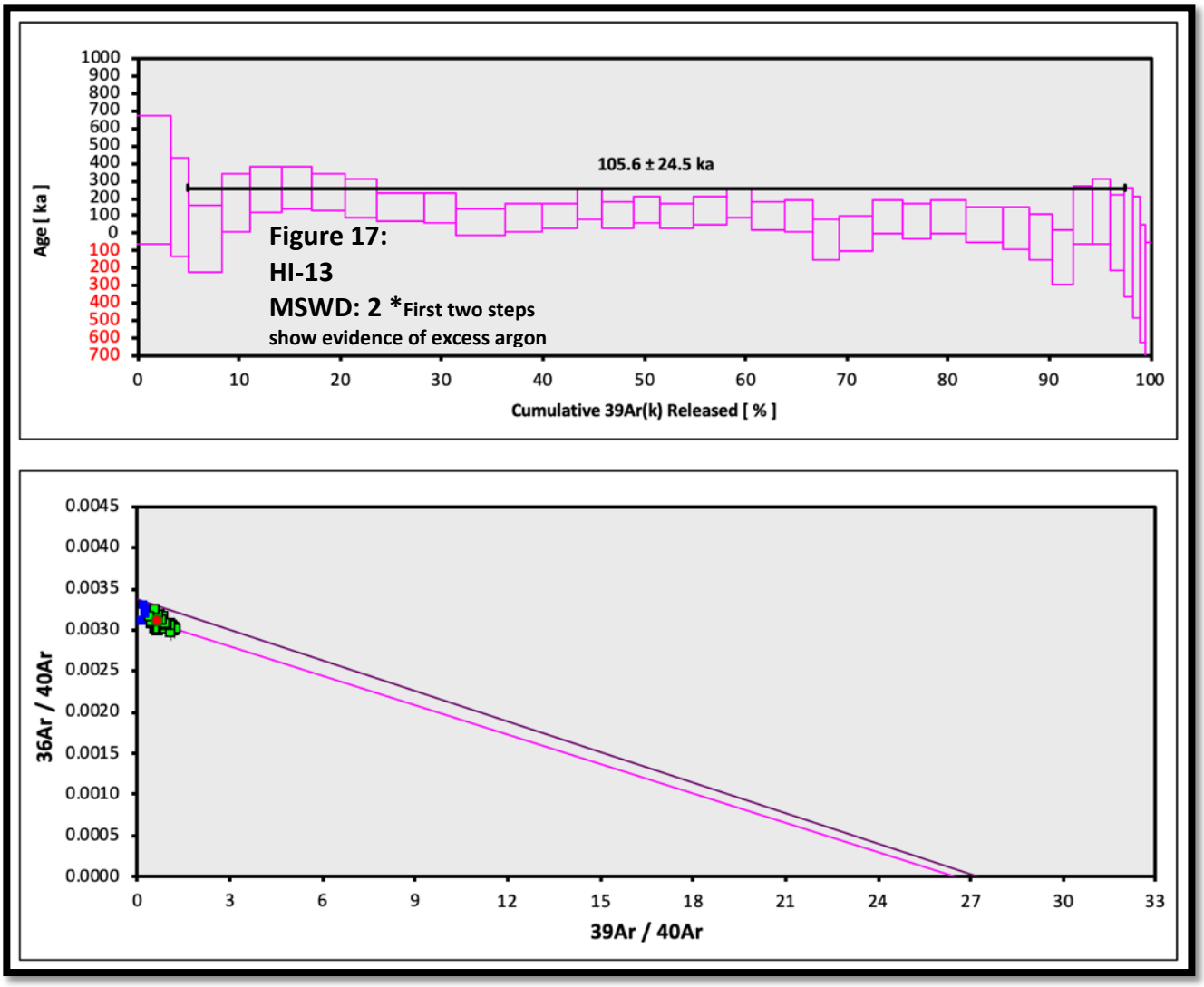


**Figure 17:**
**HI-13**
**MSWD: 2 *First two steps show evidence of excess argon**

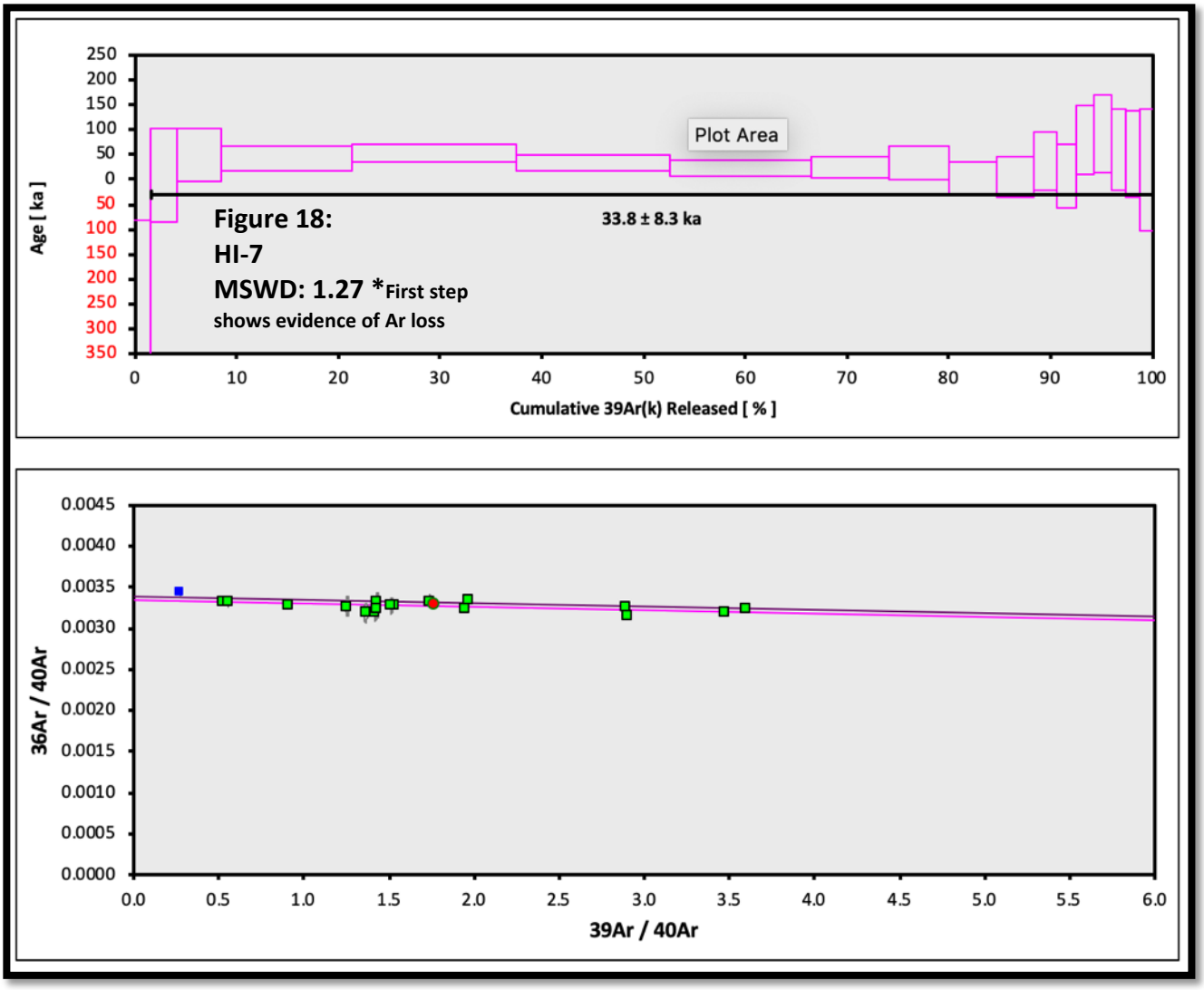


**Figure 18:**
**HI-7**
**MSWD: 1.27 *First step shows evidence of Ar loss**

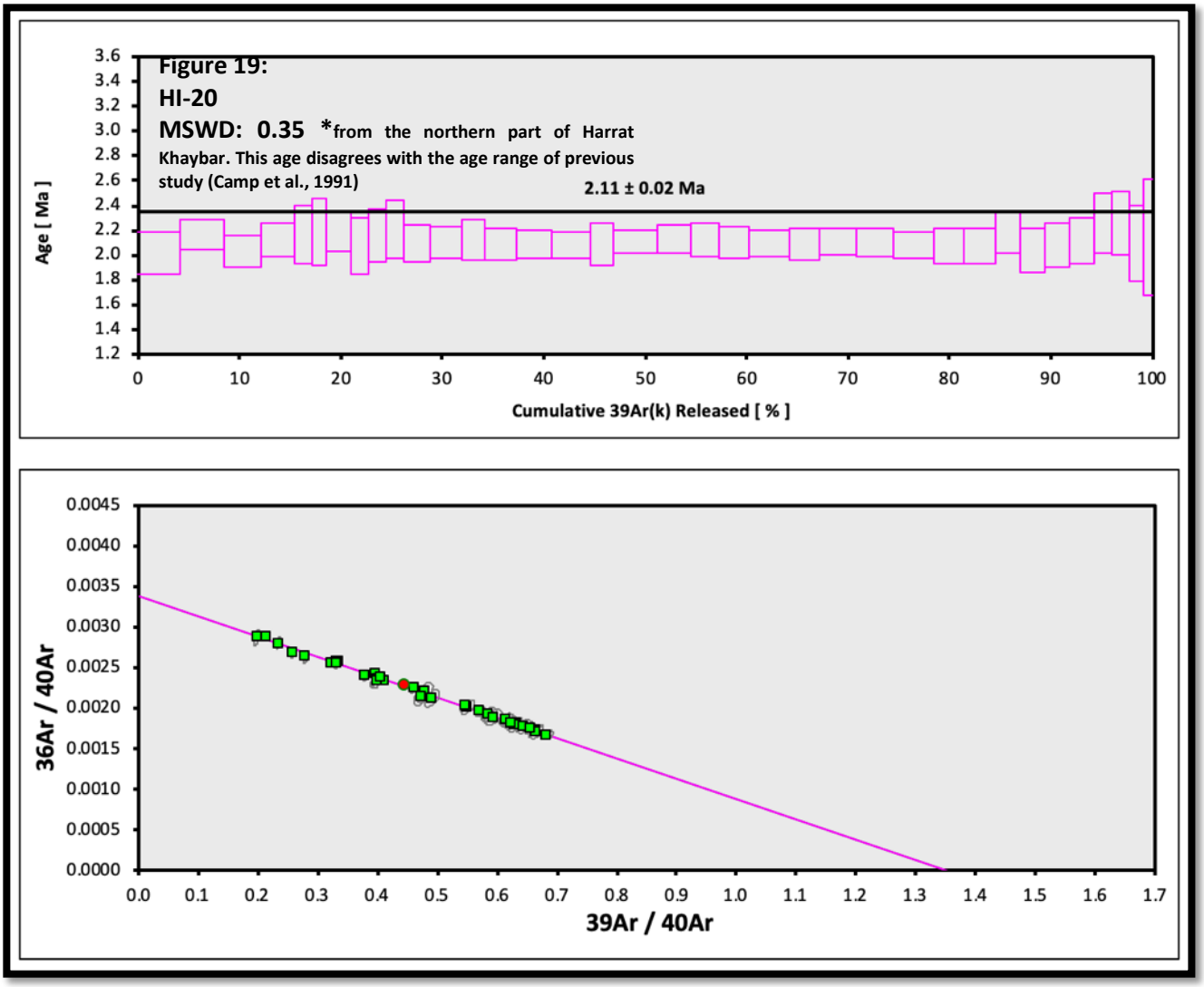
Figure 19:
HI-20
MSWD: 0.35 *from the northern part of Harrat Khaybar. This age disagrees with the age range of previous study (Camp et al., 1991)
2.11 ± 0.02 Ma
Age [ Ma ]
Cumulative 39Ar(k) Released [ % ]
36Ar / 40Ar
39Ar / 40Ar